A DISSIPATIVE WAVE PACKET APPROACH FOR UNIFIED NONLINEAR ACOUSTICS

by Kenneth D. Rolt

S.M., Ocean Engineering, M.I.T. (1991),
B.S.M.E., Massachusetts at Amherst (1984),
B.A., Journalism, Massachusetts at Amherst (1984).

A thesis submitted in partial fulfillment
of the requirements for the

Philosophiae Doctor

degree at the
MASSACHVSETTS INSTITVTE of TECHNOLOGY
Cambridge, MA 02139, U.S.A.

May, 1994.

Author _____
Department of Ocean Engineering
22 March 1994

Certified by _____
Professor Henrik Schmidt
Thesis Supervisor

Accepted by _____
Professor A. Douglas Carmichael
Chairman, Ocean Engineering Graduate Committee

A Dissipative Wave Packet Approach for Unified Nonlinear Acoustics

by **Kenneth D. Rolt**

keywords: *nonlinear acoustics, acoustic absorption, parametric sonar, sound-sound thermal effects, shock waves.*

ABSTRACT

Nonlinear acoustic waves are investigated from the viewpoint of a wavepacket. The wavepacket is defined as a portion of a wave that travels at an independent phase speed $c = c_0 + \beta u'$, where c_0 is the sound speed, β is a constant related to the propagation nonlinearity, and u' is the acoustic particle velocity. During travel the wave distorts during travel because of the nonlinearity, and undergoes absorption due to the effects of viscosity, heat conduction, and relaxation. Some of the most interesting phenomena associated with nonlinear acoustic waves are the result of the *combined* effects of nonlinear propagation (and the resulting distortion of the wave) and of absorption. These effects are especially at work in shock problems.

The mathematical approach begins with the notion of cumulative wave distortion, and its development from a nonlinear wave equation. Novel time domain expressions for acoustic absorption are then developed which are valid for both linear and nonlinear acoustic waves. These theoretical concepts, for nonlinear propagation and for absorption, are then combined into a propagation model which is then evaluated numerically in the spatial domain. Several specific and diverse examples are emphasized, including: pulse self-demodulation, oceanic parametric sonar, enhancement of ultrasound heating by sound-sound nonlinear interaction, and the formation and evolution of acoustic shocks without the need for the so-called *equal-area rule* in weak shock theory. Experimental data are used to verify both the theory and the computational results.

Thesis Committee

Professor Henrik Schmidt, MIT, Department of Ocean Engineering.

Dr. Yue Ping Guo, MIT, Department of Ocean Engineering.

Dr. Timothy Stanton, Woods Hole Oceanographic Institution,
Department of Ocean Engineering.

Mr. Kenneth Houston, Charles Stark Draper Laboratory.

ACKNOWLEDGEMENTS

This work, and my *Ph.D.* education, probably wouldn't have happened without the generous support of the Charles Stark Draper Lab (CSDL), via my MIT Research Assistant staff support as a *Draper Fellow*. I gratefully thank the Lab as a whole, and in particular, I thank both present and one-time staff members: Mr. John W. Irza, Mr. Ken Houston, and Mr. John Furze. I especially thank them for the support on the Nonlinear Acoustics short course, at the Spring 1993 Acoustical Society of America meeting in Ottawa, Canada, which allowed me to associate with, and learn from, many of the major players in the nonlinear acoustics community.

The thesis itself was written at MIT and at my home, and the analysis and experiments were performed entirely at MIT in the Departments of Ocean and Mechanical Engineering. I acknowledge and thank the following people for contributing, in various ways, to my doctoral education at MIT:

At the MIT Hyperthermia Center and Laboratory for Medical Ultrasonics, Dept. of Mechanical Engineering: Dr. Padmakar P. Lele for allowing me the use of his lab, and for his patience with my unorthodox graduate student *modus operandi*; and Dr. Brian Davis, Mr. Tony Pangan, and Mr. Charles Welch, respectively graduate students and engineer, all formerly of the Hyperthermia Center, for their assistance to me with the ultrasound experiments;

The members of my *Ph.D.* committee, Dr. Timothy Stanton from the Woods Hole Oceanographic Institution, Dr. Yue Ping Guo from the MIT Dept. of Ocean Engineering, and Mr. Ken Houston of CSDL;

A number of students, too many to list, in my now-former office, 5-007, were instrumental in many seminars, discussions, and in reading/criticizing material that I wrote. There's no substitute for having people like them around to sanity-check my work, and I am very grateful for having been associated with them. Joo-Thiam Goh and Brian Tracey were the principal conspirators, and I especially thank them, and wish that their impending theses are written, edited, and finally MIT-certified with dispatch.

Since I just mentioned the benefits of editorial criticism, I have to now remind the reader that I went to great lengths to write this as clearly as possible, and then to edit for content, clarity, and smoothness. But self-editing is almost worthless because the same faulty process is used to edit as it was to write. Hence I thank George H. Rolt, my father, who returns for another stint as the ghost editor, critic, and technical sounding board. Parental scrutiny appears once again.

Professor Henrik Schmidt of the MIT Ocean Engineering Department, my faculty advisor and committee chairman, recognized early on that "hands-off advising" worked best for my loose-cannon approach to graduate study at MIT. I suspect that Schmidt was a take-charge type himself when he was a graduate student, and he soon recognized the same flaw in me. I can't thank him enough for giving me considerable academic freedom over the past five years.

Now that this thesis is done and I'll graduate, my wife Christine Coughlin will really find out whether I'll live up to my "future potential" as I re-enter the working world. My gainful employment is her ultimate reward for, once again, putting up with me while I was at MIT. Thanks Christine!

~~~~~~~~

"IN PIOUS MEMORY OF THE FAMOUS DEAD
WHOSE REMAINS LAY BURIED IN OLD
ST.PAUL'S CATHEDRAL OR WHOSE MEMORIALS
PERISHED IN ITS DESTRUCTION

SIR PAYNE ROLT OF GUIENNE PRINCIPAL KING-AT-ARMS,
FATHER-IN-LAW OF JOHN-OF-GAUNT, AND OF CHAUCER 14TH CENT."

- In the crypt of St. Paul's Cathedral, London.

~~~~~~~~

"Publish and be damned." - Arthur Wellesley, Duke of Wellington, 1769-1852

Contents

List of Figures

List of Tables

Notation and List of Symbols

Notation symbols:

A	first coefficient in a Taylor series for $p(\rho)$.
A	a point of acoustic particle velocity on a sine wave.
A_o	an arbitrary amplitude for a function.
$A_{c.v.}$	control volume cross sectional area, m^2.
B	second coefficient in a Taylor series for $p(\rho)$.
C	third coefficient in a Taylor series for $p(\rho)$.
c_o	linear acoustics propagation speed (*i.e.* the sound speed), m/s.
$c_{effective}$	nonlinear acoustics effective propagation speed for a wave packet, m/s.
C_p	specific heat at constant pressure, Joule/(kg·K).
c_T	isothermal wave propagation speed, m/s.
C_v	specific heat at constant volume, Joule/(kg·K).
C.V.	control volume.
d	distance along x where a shock forms, m.
e	base of the Naperian log, e = 2.71828.....
E	a point of acoustic particle velocity on a sine wave.
f	frequency, Hz.
f	arbitrary function to solve the wave equation.
F	a point of acoustic particle velocity on a sine wave.
g	arbitrary function to solve the wave equation.
i	$\sqrt{-1}$.
j	node index for wave packet.
J	Joule, or N·m.
k	wavenumber, ω/c.
k	discretization step index.

k	complex wavenumber, $k = k_r + ik_i$.
K	Kelvin temperature (*e.g.* 273.16 K is 0.0 degrees Celsius).
k_r	real part of k.
k_i	imaginary part of k.
M	mass, kg.
n	an integer; *e.g.* 0, 1, 2 ...
p	total pressure, $p_o + p'$, Pascals (Pa) or N/m^2.
p'	acoustic pressure, Pa.
p_o	ambient pressure, Pa.
s	condensation, where $s \equiv \rho'/\rho_o$, dimensionless.
s_e	entropy, Joule/(kg·K).
t	time, seconds (s).
T	temperature, degrees Kelvin.
T_p	wave period, seconds.
u	acoustic particle velocity, m/s. Also see v'.
u_{loc}	acoustic particle velocity, m/s, in a local frame.
U_o	a specific acoustic particle velocity at x_o, m/s.
v	total particle velocity, $v_o + v'$, m/s.
v'	acoustic particle velocity, m/s. Also see u.
v_o	ambient particle velocity (*i.e.* the flow speed), m/s.
x	axis, or position on axis, meters (m).
x_o	a specific position on the x-axis (m).

Greek symbols:

ΔI	dissipation work flux, W/m^2.
Δt	a time span, s.
Δw	work, J/m^3.
Δx	thickness of a control volume slab along the x-axis, m.
ΔX	dissipationless distance to a shock on the x-axis, m.
α	absorption coefficient, m^{-1}.
β	coefficient of nonlinearity, $\beta \equiv 1 + B/(2A)$.
δ	a distance between two points on a wave, meters.
∇	Laplacian, a spatial derivative, units m^{-1}.

∇^2	second-order spatial derivative, units m^{-2}.
ε	dimensionless acoustic Mach number, $\varepsilon \equiv v'/c_o$.
ε	a shorthand parameter substitution used in Eq. (B.4).
γ	dimensionless ratio of specific heats, C_p/C_v.
κ	heat conduction coefficient, Watt/(m·K).
λ	wavelength, m.
η	shear viscosity, Pa·s.
η	transducer efficiency.
η_b	bulk viscosity, Pa·s.
ρ	total density, $\rho_o + \rho'$, kg/m^3.
ρ'	acoustic density, kg/m^3.
ρ_o	ambient density, kg/m^3.
τ	relaxation time, s.
τ	pulse duration, s.
ω	radian frequency, s^{-1}.

Mathematical and other symbols:

$\equiv$	equals by definition.
$\partial/\partial t$	partial derivative with respect to t.
$\partial/\partial x$	partial derivative with respect to x.
D/Dt	$\equiv \partial/\partial t + v\cdot\nabla$. Material time derivative for a C.V. moving at speed v.
<--->	implies that.
$\|_{x=a}$	equation notation for function evaluation at $x = a$.
|...|	absolute value.
$O\{s^n\}$	remaining terms of s with order integer-n and larger.
a : b	a is compared to b, usually on an order of magnitude basis.
$\binom{n}{2}$	short hand notation for $\frac{n!}{2!\ (n-2)!}$.
p_x	partial derivative of p with respect to x.

Abbreviations

BW	bandwidth.
broad band	a description of a signal where BW is not << f_c , (*e.g.* BW > 0.1 f_c).
c.	(Latin; *circa*) "approximately."
cc	cubic centimeter, $(cm)^3$.
cw	continuous wave.
e.g.	(L., *exempli gratia*) "for example."
et alia	(L., *et al.*) "and others."
f_c	center frequency.
FM	frequency modulation.
i.e.	(L., *id est*) "that is."
narrow band	a description of a signal where BW << f_c.
N.B.	(L., *Nota Bene*) "note well."
op. cit.	(L., *opere citato*) "in the work cited" or "in the work previously cited".
PE	polyethylene.
RTV	a silicone rubber, RTV-615 from General Electric Co.
w.r.t.	with respect to.

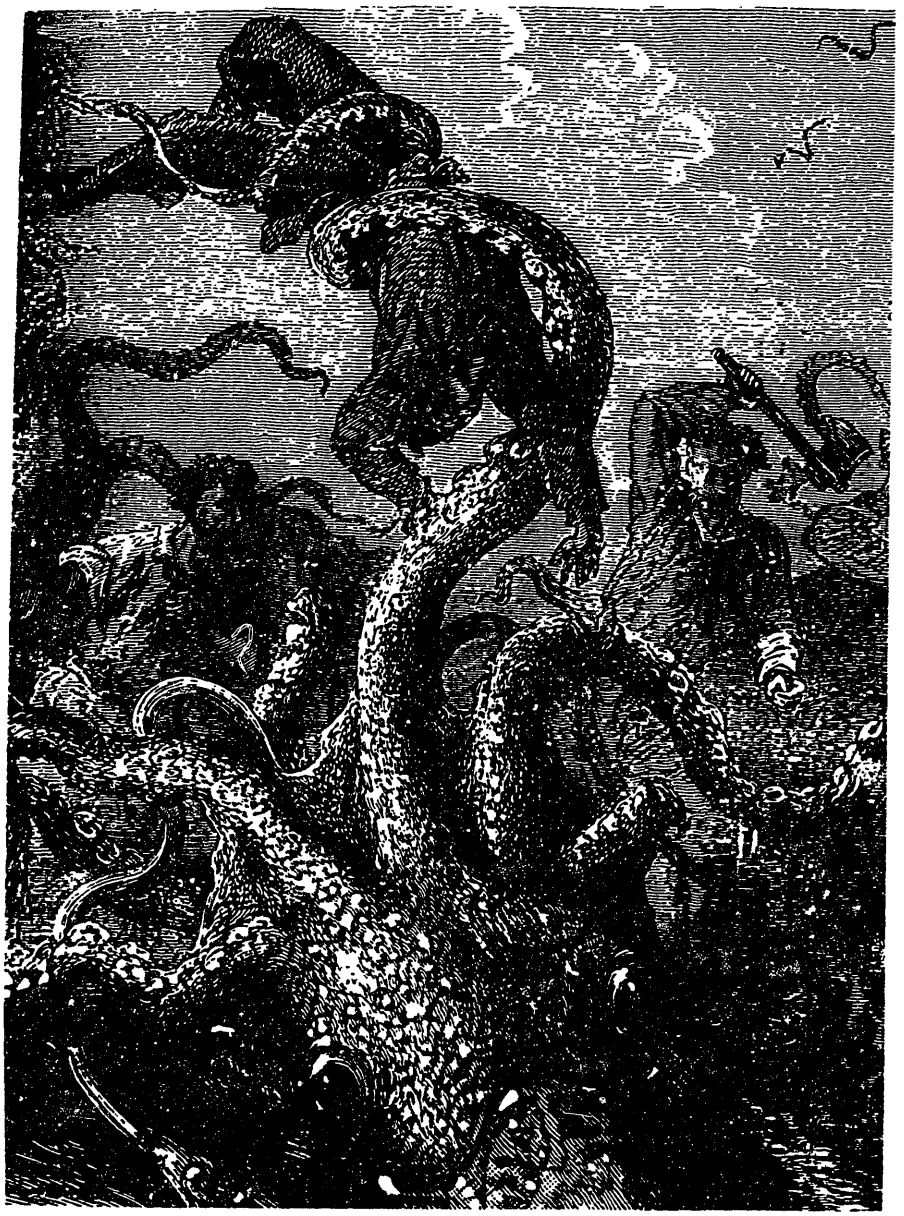

Chapter 1

Introduction

Two independent but related experiments conducted during the 1989-1991 period provided the initial motivation for pursuing this *Ph.D.* thesis in nonlinear acoustics. The first experiment was conducted by John Halsema (1992) as part of his MIT Ocean Engineer's thesis work; the second was performed by me.

Halsema's work, in collaboration with John W. Irza of the Charles Stark Draper Laboratory [CSDL], involved echo ranging with an assortment of acoustic waveforms generated by the nonlinear mixing of two acoustic signals; that is, by the use of a parametric sonar. I had the opportunity to work with Halsema and Irza at the *U.S.S. Constitution* pier, Charlestown Navy Yard, Boston and occasionally on the fine waters of Boston Harbor, during much of the test program. Halsema's work is fully described in his thesis. One of the nagging items that I pondered over, while Halsema was working on the hardware and interpreting his data, was that it would be handy to have a computational model that could predict, with some accuracy, the type of acoustic waveforms that he observed in the harbor testing. Modeling of this sort would require the calculation of nonlinear distortion, waveform mixing, and the full range of absorption components. At the time, no such model existed either at MIT or at CSDL. Not only that, but computational means that could model non-CW pulsed nonlinear waveform mixing was not then available anywhere. As of early 1993, such tools are emerging in the literature, but with certain assumptions made on absorption and validity at, or near, the shock formation distance. The work contained in this thesis, and as implemented

computationally, meets the requirements of modeling nonlinear sound waves, without undue restrictions on absorption, and is valid before, during, and after shock formation.

The second experiment, which I led, concerned the enhancement of acoustically generated heating by nonlinear acoustic means. The original idea was the basis for the final project/paper (see Appendix A) written for MIT course 6.562, *Ultrasound: Physics, Biophysics, and Technology*, during the Fall semester, 1988; the course was instructed jointly by MIT Professors P.P. Lele and F. Morgenthaler. The paper then led to 1989 and 1990 experiments in Dr. Lele's MIT Hyperthermia Laboratory, where it was demonstrated that simultaneous insonification by two confocal MHz-based sound sources gave more focal heat generation than the thermal superposition of each source separately. The 1990 experiment was intended to reproduce and confirm the results of the 1989 experiment. Apart from the positive results of the experiments, the future initiatives suggested from these experiments were: (1) the concept should be modeled computationally to fully investigate why the extra heat generation occurred, and (2) a full scale of experimental tests should be performed over a wide range of test conditions and within media such as water, salt water (which is chemically close to the composition of living animals), and animal tissue (steak, *e.g.*). The first of these two initiatives is met in this thesis.

Meanwhile, during this period I was busy with the usual MIT graduate student activities: courses, qualifying exams, and research in synthetic aperture sonar [SAS] imaging for my master's degree and thesis (Rolt, 1990). After fully wringing out SAS in my *S.M.* thesis and in the related publications that followed, the only significant contribution that I could see to further that subject (at the time) was to field a simple, inexpensive, operational SAS system. I concluded that until someone demonstrated a SAS system of hardware and processing, and showed images of sunken vessels, submerged acoustic mines *etc.*, the technology of unclassified SAS would never become as useful and as widespread as both SAR (synthetic aperture radar) and conventional sidescan sonar are today. The more I thought about this, the more I realized that the project would be almost entirely hardware-oriented, and therefore a hard-sell

to the MIT faculty for a *Ph.D.* topic. That's why this thesis is not about acoustic imaging with synthetic aperture sonar.

On the other hand, the substantial overlap of the computational model requirements between these two sets of experiments, an oceanic sonar one by Halsema, and a medical ultrasound-based one by me, offered a unique opportunity to pursue *Ph.D.* research in an acceptable area that would satisfy the needs of my sponsor [CSDL], fit into a category appropriate for my department at MIT [Ocean Engineering], and allow me to work on my own research area. That's how this research began.

1.1 What is Nonlinear Acoustics?

Nonlinear acoustics is most easily described by first defining linear acoustics. For the purposes of this thesis, linear acoustics supposes that the characteristic *shape* of a sound wave does not change as it travels (or propagates). During propagation, a dissipationless sound wave may have an amplitude that increases with distance (say in a convergent pipe, horn, or due to a converging acoustical lens), it may have a constant amplitude (a sound wave traveling inside a frictionless pipe), or it may have an amplitude which decays with distance due to geometrical divergent spreading. In all three cases, the amplitude of the wave may change, but the *overall shape* does not. This assumes that the waves are of the form $A_o \cdot f(x \pm c_o t)$, where A_o is the amplitude, f is the wave function shape (*e.g.* cosine), x is position, c_o is a constant sound speed and t is time. Sound waves having such characteristics are solutions to the linear dissipationless (*i.e.* lossless) wave equation.

Most simply put, and in the context of this thesis, lossless nonlinear waves have shapes which *do* change as the wave propagates. Lossless nonlinear acoustic waves are also sensitive to the initial amplitude of the wave. Hence, in contrast to the previous dissipation-free linear acoustic example, we now have a wave function f which is sensitive to amplitude, position, and time. In the linear case, the function f was independent of A_o, x, and t; in the nonlinear case, the function f depends precisely on these quantities. The shape-change

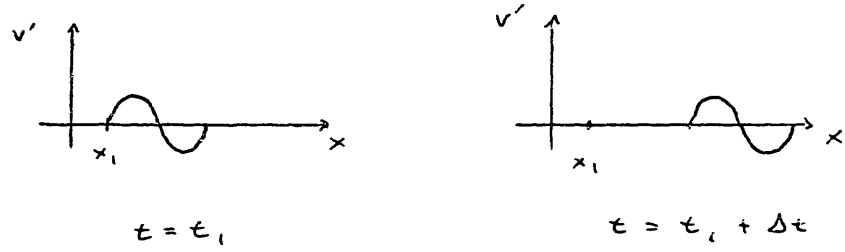

linear: $c = c_0$

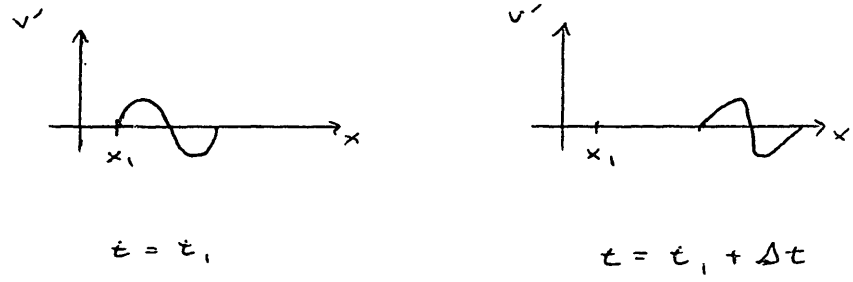

nonlinear: $c = c_0 + \beta v'$

Fig. 1-1 Linear versus nonlinear waves. In the absence of dissipation, the linear wave never changes shape (except in an amplitude scale due to geometric spreading), while nonlinear waves always change shape as they travel.

character of a nonlinear acoustic wave is both a property of the material in which the wave propagates, as well as a result of the convective parts of the nonlinear wave equation. Schematic illustrations for linear waves which don't change shape, and nonlinear waves which do change shape, are shown in Fig. 1-1.

The introduction of acoustic dissipation also causes the wave shape to change in both the linear and nonlinear acoustic cases; that is why the dissipation-free case was used to mark the distinction between linear and nonlinear acoustic waves.

1.2 Prior Work in Nonlinear Acoustics

The nonlinear acoustics literature, up to the late 1950s and early 1960s, is quite sparse. The classic papers written on the subject range from the 1755 work of Euler up to the 1930's work by Fay and Fubini. Blackstock (1969) wrote a very complete review of the antique work in nonlinear acoustics from this period. I will not review the material among the papers described by Blackstock; rather, I refer the interested reader to his excellent paper and to the related paper that was an outgrowth of Blackstock's *Ph.D.* thesis (Blackstock, 1962).

Though seldom mentioned in the literature, the mathematics considered and computationally used to model the focused explosive detonator for an atomic bomb, would have required substantial knowledge and understanding of many of the nonlinear acoustic principles brought to light much later on. It is entirely possible that considerable knowledge in nonlinear acoustics emerged from the *Manhattan Project* of World War II, especially considering the work by Bethe and Teller (1941), but only declassification of these documents will reveal the state of knowledge at the time.

Since the 1950s and 1960s, however, the field has expanded considerably, and the published literature in nonlinear acoustics since then is vast. The biannual meetings of the Acoustical Society of America have regular sessions devoted to various aspects of nonlinear acoustics. In addition, every two years or so, the International Symposium on Nonlinear Acoustics, or the ISNA

meeting[1], is usually held at, or near, a center for nonlinear acoustics research.

1.2.1 Prior Work in Nonlinear Acoustics at MIT

A number of papers in nonlinear acoustics have been produced at MIT, the first being a landmark paper by Professor R.D. Fay of the Electrical Engineering Dept. in 1931. Fay was later affiliated with the Underwater Acoustics Lab. of MIT during World War II. Fay renewed his interest in nonlinear and finite wave propagation in papers from 1956 and 1962. During the middle 1950s, K. Uno Ingard and his student D.C. Pridmore-Brown of the Physics Department studied the interaction and scattering of sound by sound (1955). This work was considered controversial; as recently as 1990, some of their results were still debated[2]. L. Wallace Dean III (1962), from the Physics Dept. and the Research Laboratory of Electronics, studied the interactions between sound waves. Dean also theoretically examined the problem Ingard had studied, for both beam-beam intersection, and beam-beam intersection in the presence of a hard object.

Two graduate students in the MIT Physics Department, L.N. Litzenberger (*S.M.* 1969, *Ph.D.* 1971) and L.P. Mix (*Ph.D.*, 1971), studied linear and nonlinear ion acoustic waves within ionized plasmas and within magnetic fields, both students being directed by Prof. G. Bekefi. Ion acoustic waves are, in the words of Litzenberger, "... quite similar to ordinary sound waves in neutral gases except that long-range Coulomb interactions between charged particles rather than short-range collision forces between molecules dominate the phenomenon."

S.W. Zavadil, an Ocean Engineering graduate student (O.E., 1976), created a computer code to model the nonlinear distortion of sinusoidal waves in viscous fluids, but he did not include relaxation nor heat conduction terms in the model, and his model was only valid for weak nonlinear waves; *i.e.* it would not handle shocks. He compared his model to that of Keck and Beyer (1960), and the agreement was very good.

Professor P.P. Lele of the Mechanical Engineering Dept, established a Laboratory for Medical Ultrasonics and Cancer Hyperthermia Center, and guided many graduate students throughout the last three decades. A number of the experiments done in the ultrasound/hyperthermia lab were related to nonlinear effects, principally including those by N. Senapati (1973) on cavitation and R. Handler (1976) on nonlinear sound absorption. Part of Handler's thesis was a section that estimated the harmonic generation for a focused sound beam using a model based on the work by Cook (1962). Handler was looking for an explanation for acoustically-induced thermal tissue damage. Handler concluded that the harmonic generation was an insufficient mechanism but cavitation might be sufficient.

J.A. Halsema's thesis (1992) and experiments, as mentioned at the beginning of this chapter, are both the most recent and apparently the first MIT-based foray into parametric sonar. Halsema used a .30-meter diameter piston transducer to radiate pulsed sound waves at roughly two frequencies: 184 kHz cw and a noise-like waveform in the range 169- to 179-kHz. By driving each of these frequency bands at large amplitude, he achieved nonlinear mixing of the two waves in the water, and created a difference frequency wave ranging from 5 to 15 kHz. These experiments were primarily performed in Boston Harbor, from the *U.S.S. Constitution* pier in Charlestown MA.

1.2.2 The State-of-the-Art in Nonlinear Acoustics

The state-of-the-art in nonlinear acoustics continues to unfold. As previously noted, every two or three years there is an International Symposium on Nonlinear Acoustics; the two most recent were hosted by the University of Texas, Austin (USA) in 1990 and the University of Bergen, Bergen (Norway) in 1993. The University of Texas/Applied Research Laboratory group in Austin, and the University of Bergen are recognized throughout the world as two of the principal research centers in nonlinear acoustics. In addition, nonlinear acoustics is playing a more important role in the use of ultrasound in medicine for therapeutic and diagnostic purposes, and it is intricately linked with the study of cavitation and sonoluminescence.

Today, there are principally four different approaches to the solution of nonlinear acoustics problems. The first, the oldest and most obvious, is the experimental approach. The second is the so-called phenomenological approach (in this thesis, I instead use the term wave packet approach, or WPA). The third is based on the use of Burgers' equation (Burgers, 1939) which Blackstock (1964) fully covers. Trivett and Van Buren (1981) created a computational model based on Burgers' equation that used Fourier decomposition to solve the propagation problem entirely in the frequency domain. They compared the results for a single frequency 300 Hz cw plane wave example with a phenomenologically-based computer model by Van Buren (1975) for the spectral level of the fundamental and a number of the harmonics, and the agreement was superb. Their model was limited, however, to a single cw waveform input, and *not* to a plurality of pulsed waves at different frequencies. Both models, Trivett and Van Buren (1981) and Van Buren (1975) used $\alpha_n(\omega_n) = \alpha_1(\omega_1)n^2$ where n=2,3, ... *etc.* and α_1 is the absorption coefficient for the fundamental frequency, to account for frequency-dependent absorption. This model accounts for sensible dissipation due to viscosity and heat conduction (in fresh water *e.g.*), but it does not account for relaxation absorption (in sea water or in air *e.g.*).

The fourth approach involves developing the wave equation in a parabolic form, and obtaining numerical solutions thereafter. This is the most popular computational method of record today, and is often the starting point for many papers authored by researchers at UTexas, Bergen and in the former Soviet Union (FUSSR). Presently there are at least two variants: one is a frequency-domain based method having origins in the FUSSR, and lately referred to as the *KZK equation*, initialed after the key theorists (Khokhlov, Zabolotskaya and Kuznetsov) who studied the problem during the late 1960s and early 1970s (see Zabolotskaya and Khokhlov, 1969; and Kuznetsov, 1971). The books by Beyer (1975), Rudenko and Soluyan (1977), and Novikov *et al.* (1987) each have sections which describe the mathematical development leading to the present form of the KZK equation. The other variant is the dissipationless Nonlinear Parabolic Equation, or *NPE*, of McDonald and Kuperman (1987) which is more amenable to time domain solutions. The NPE has the ability to model wave

propagation in the ocean in the presence of a sea surface, a seabed, and within a refracting water column. Thus it is useful for evaluation of broad propagation effects of linear and nonlinear waves as they are influenced by oceanic range- and depth-dependent features. What the NPE presently lacks, however, is a good absorption model. The NPE code includes an absorptive layer near the edges of the computational boundary to circumvent any numerical difficulties, but it does not include absorption (other than by weak shock theory, once shocks form) within the ocean waveguide itself[3]. This contrasts the statement made by Too and Ginsberg (1992)[4] , who claimed the NPE uses dissipation both for numerical purposes, as well as for ordinary sound attenuation. The only attenuation included in the present form of the McDonald and Kuperman NPE for propagation is due to weak shock theory. The separate work by Too and Ginsberg, an adaptation of the NPE code for special purposes such as the near field study of nonlinear sound radiation from sound sources, included a first-order approximate dissipation term.

A brief summary of other techniques used in solving nonlinear acoustics problems appears in *Physical Ultrasonics* by Beyer and Letcher (1969), including: Fubini's method (1935); the perturbation analysis for the viscous case; the analytical methods of Fay (1931), Mendousse (1953), and Rudnick (1958); hybrid analytical-numerical methods by Fox and Wallace (1954), and Cook (1962); the use of Burgers' equation, particularly on a method by Blackstock (1964); and finally on Blackstock's (1966) bridging of the separate-region solutions of Fubini and Fay. One further attack on the problem of nonlinear acoustics was by Stepanishen and Koenigs (1987), where they used a time-dependent Green's function approach. They were able to obtain a closed-form expression for the radiated field which was proportional to the second spatial derivative of the square of the pressure envelope, in agreement with a result obtained by Berktay in the 1960's, but they needed to assume that the absorption was restricted to that of the primary wave in the pulse. Hence, it was a clever attack on the problem, it was useful for trendwise calculation of the radiated field both on- and off-axis, but it was not very useful for real problems.

1.3 Technical Approach

The technical approach used in this work is a form of the *phenomenological approach*, a term borrowed from the work of Pestorius (1973), in modeling a sound wave which I refer to as a *Wave Packet Approach* (WPA). I refer to it as a Wave Packet Approach because it acts on small pieces of a wave pulse, wave packets, separately. This approach allows a *locally valid* wave equation to be applied that includes absorption and nonlinear effects. I regard the term phenomenological approach somewhat cumbersome, not only because it is hard to say, but also because semantically it suggests the model is based strictly on a physical phenomenon rather than being grounded in mathematics. Related methods by Fox and Wallace (1954), Cook (1962), Pestorius (1973), Van Buren and Breazeale (1968a, 1968b), Van Buren (1975), and Handler (1976) all lacked a number of features which are included here. These features are a space/time-domain dissipation and a formal justification for using the phenomenological approach to show that it really does correctly model acoustic wave propagation from a theoretical basis. The WPA, by its use of space/time domain dissipation, allows wave propagation before, during, and after the shock-formed region, and in principle it does so without the use of weak shock theory. The fundamental reason for the presence or absence of weak shock theory in a computational model, and the consequent advantages and disadvantages, will be fully described in a section at the end of Chapter 5.

A few of these key works are now described. Fox and Wallace (1954) used a graphical analysis, sans computer, as the starting point for their work. For a one-dimensional dissipationless medium, and starting with a pure tone sound wave, they divided the distance-to-shock into ten equal steps and proceeded to *partially* calculate the harmonic content (primary, plus first and second harmonics) of the wave, as it propagated from one step to the next. This allowed them to derive a growth factor for each harmonic, at each of the ten steps. An appropriate equivalent absorption factor (proportional to ω^2) was then introduced for each harmonic, at each step. The authors compared their model to experimental measurements made in water and in carbon tetrachloride, and the agreement was very good.

Cook (1962) used a similar procedure to that of Fox and Wallace, but used the Bessel-Fubini solution as the starting point, and did the modeling on a "high-speed computer." Blackstock has reviewed and showed the connection between the Fubini solution (before shock), and the solution of Fay's (saturated shock). Cook limited the numerical calculation to as many as 16 harmonics, assumed an ω^2 absorption dependence, and limited the propagation distance to 1/20-th of the shock formation distance. This sharply contrasted with the work of Fox and Wallace, who included only three harmonic terms, but made their calculations all the way to the dissipationless shock formation distance. Van Buren (1975) and Handler (1976) both used an approach based on the work by Cook.

Pestorius (1973) used the phenomenological approach as a basis for modeling high intensity noise-like waves propagating inside an air-filled tube, and he applied weak shock theory to account for the extinction of small wave perturbations by higher amplitude ones. A small dispersive component was added to the model to simulate the frictional interaction of the tube wall boundary with the pulse; this gave an absorption coefficient proportional to $\sqrt{\omega}$, and also added a considerable dispersive feature. He then compared his computational results with those from in-air pulse tube experimental data, and the agreement was very good, but it did slightly underestimate the absorption. An extension of Pestorius' work by Webster and Blackstock (1977) modeled the saturation of plane waves in air. Part of the work showed a comparison between experimental wave trace data and computed wave traces using the Pestorius algorithm.

1.4 A Brief on the Wave Packet Approach (WPA)

Starting with an initial acoustic wave pulse modeled at discrete x-node locations ... x_{j-1}, x_j, x_{j+1}, ... wave propagation is realized by mapping the acoustic pressure from a node location x_j to a new node location x_{j+k}, as shown in Fig. 1-2. Hence, each small segment of the wave, herein called a *wave packet*, moves to the j+k location on x at a speed $c_o + \beta v'$ (this relation will be derived on the basis of a wave equation in Chapter 2), where v' is the acoustic

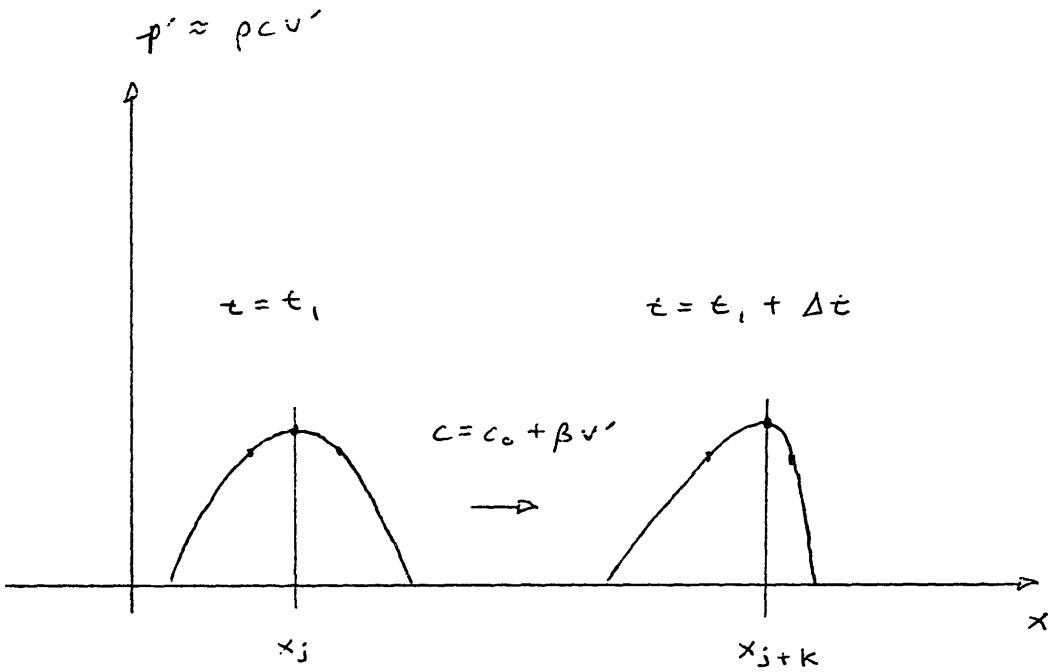

Fig. 1-2 Phenomenological Approach. In this approach, the wave is discretized by points, x_j, and each point moves on the x-axis at a different propagation phase speed determined by $c_j = c_o + \beta v_j$, where v_j is the local acoustic particle velocity, β is a constant related to the nonlinearity, and c_o is the sound speed for linear acoustics. In linear acoustics, all points x_j travel at c_o.

particle velocity, and where k is the nodal step size (usually $k >> j$) which is equivalent to the distance traveled along x by the wave during a certain time interval. This wave model assumes forward propagation only, as in a one-way parabolic equation. This type of propagation algorithm is common to those previously used by Fox and Wallace (1954), Cook (1962), and others since.

The missing items from Pestorius' work were: a justification for using the phenomenological approach (via a wave equation); sound wave absorption that included viscous, relaxation, and heat conduction losses (Pestorius used a dissipation term that was valid for wall friction, but he intentionally did not include the losses for the propagating wave outside the wall boundary layer of the tube walls; hence his algorithm is incomplete for modeling unbounded waves in planar, cylindrical, or spherical propagation); and a general discussion for why weak shock theory was able to qualitatively represent the behavior of noise-like shock wave propagation modeled without the ever-present unbounded dissipation mechanisms of viscosity, heat conduction and relaxation.

Other earlier uses of the phenomenological approach by Fox and Wallace (1954) and by Cook (1962) also lacked a rigorous wave equation justification. I originally planned to simply apply the phenomenological approach without worrying about whether it satisfied wave propagation notions including: conservation of mass, momentum, and energy (in the same manner as previous investigators). But as I progressed further, I decided that the lack of a formal justification would provide fertile ground for an officious professor attending the oral defense to ask a simple, yet hard-to-answer question. So I attempt to answer this question herein, and thus accomplish two things: to provide the justification absent from all previous phenomenological approaches, and to shortstop the question from being asked at my defense, by tackling it here.

The main distinction between the phenomenological approach used by others, and my so-called wave packet approach (WPA) is that space/time domain absorption, of the three significant dissipation types, is included. This contrasts with other means of solving the nonlinear wave equation by

integro-differential methods, finite differences, or finite elements. These methods usually lump the dissipation into a thermoviscous term that is really only valid at a single frequency (often, the fundamental frequency in the problem under scrutiny). The precise details of the WPA used will be detailed in Chapter 4, after a case has been made for the nonlinear wave equation in Chapter 2, and after the dissipation terms for viscosity, relaxation and heat conduction have been derived in Chapter 3. These are the tools required before the WPA can be formally described.

1.5 Contributions Made by this Thesis

This thesis makes four significant contributions to the body of knowledge in nonlinear acoustics. The first is a computer-based time domain model for both linear and nonlinear acoustic waves. The central component in the code is a local nonlinear wave equation. This equation, written as a modification of the linear wave equation, provides the formal justification for using a wave packet approach (WPA).

The second major contribution is the formal development of time-domain expressions for viscous, relaxation, and heat-conduction sound absorption coefficients. These expressions collapse into near-exact agreement with those in the existing literature under the special circumstance of pure tones. In the case of a sine wave exhibiting cumulative distortion, it can be clearly shown that the absorption at any point along the wave is uniquely related to the wave curvature in either p'-x (space) or p'-t (time) format. Hence, this theory provides a neat way to describe the absorption of a sound wave having arbitrarily complex shape, and provides a useful alternative to Fourier analysis as a means of explaining acoustic absorption. The computational model is sufficiently general to cover propagation in air, fresh water, sea water, glycerine, or a tissue/rubber model having a relaxation-dominated ω^n dependence.

The third major contribution is the investigation of the intersection and interaction of sound beams as a means of increasing thermal deposition in the sound-sound intersection region. This work was carried out in two ways: one

by laboratory experiments, and second by the use of the aforementioned computer code.

The fourth major contribution is an extention to the topic of shock theory, a special case of nonlinear acoustics. Traditional ways of approaching the development of weak shocks (where $v' < c_0$) have used the so-called *equal-area rule* to circumvent multi-valued solutions. This approach traditionally arrives from a dissipationless propagation model. When the shock occurs, and the wave becomes mathematically multivalued, the equal-area rule is imposed, whereby the multivalued part of the wave self-quenches. Hence, even though there was no dissipation used in the model, the equal-area rule provides attenuation even though it is unphysically realized. The mathematical development to attain the equal-area rule comes from conservation of certain sensible quantities (mass, momentum and energy), but nowhere are the ordinary attenuation means considered. The approach taken in this thesis retains all of the usual attenuation mechanisms completely up to the point where the wave would otherwise become multivalued. The key feature herein is that the attenuation mechanisms *provide adequate means to prevent the wave shape from becoming multivalued.* The summary that can then be made is if no absorption is included in the propagation model, weak shock theory does a reasonable job of approximating the wave shape behavior and absorption at the shock. When absorption is correctly included in the propagation model, the strong second-order spatial gradient (from viscosity, relaxation, and heat conduction) at the shock location provides a doublet-like absorption function which attacks only the energy at the shock, and the need for weak shock theory disappears. There is, however, a strong reason related to computational time and resources, for simultaneously using both the space/time-domain absorption theory developed here and the equal-area rule.

Other contributions in this thesis are comparatively minor in relation to the four mentioned above. They apply to the specific application examples shown later in Chapter 5.

1.6 Thesis Organization

This thesis is divided into six major parts beginning with Chapter 1, the Introduction, the one you have just read. Certain citations, listed at the end of the each chapter, include the author(s) name(s), year, and specific information such as page numbers or comments. The full citation, including paper or book title, is then included in the Bibliography at the end of the thesis.

The notion of the nonlinear and linear wave equations are derived in Chapter 2, as a means of formally justifying both the phenomenological and WPA approaches to wave propagation. Chapter 3 handles the three principal absorption mechanisms intrinsic to waves in fluids: viscosity, relaxation, and heat conduction. In Chapter 3 there is an occasional interchange of the terms *time-domain* and *spatial-domain*. The main reason for the use of *time-domain* is to make the absorption used here distinct from the usual frequency-domain absorption universally used elsewhere. Absorption in a time-domain sense happens to be implemented here in a spatial-domain only because I use an x-label for the propagation axis rather than a time axis, and the choice of the x-labeling scheme is purely due to my preference for think of waves propagating in space rather than in time. Chapter 4 combines the ideas in Chapters 2 and 3 into a sensible computer model, and creates the WPA as a combination of the phenomenological approach and space/time absorption.

Chapter 5 presents the reader with the most practical consequences of this thesis, and the most fun, because it covers a wide range of nonlinear propagation problems. Some of these problems, where experimental comparison is available, provide a degree of confirmation that the model is correct.

Chapter 6 wraps up the thesis with discussion, conclusions, and some suggestions for future work. Several Appendices are included, followed by a full Bibliography for all the citations used in each chapter.

---

[1] see ISNA in the bibliography, various years.

[2] Westervelt, P.J. (1990). See this paper in *Frontiers of Nonlinear Acoustics, 12th ISNA*.

[3]In the NPE User's Manual, from the subroutine *damper*: "there is no damping incorporated in the ocean itself nor is any incorporated in the sedimentary bottom; that is, no damping is incorporated from the 'nsurface' at the ocean surface down to the 'nsedbot', the bottom of the sediment."

[4]From the paper by Too and Ginsberg: "McDonald and Kuperman introduced a linear damping term in NPE for two reasons. Damping is needed to account for dissipation due to viscosity, heat transfer, and relaxation. In addition, it was intended to prevent the reflection of sound waves from the bottom of the simulation grid." See Too and Ginsberg (1992), p. 60, for this quote and for the first-order dissipation term.

THE WELLESLEY COLLEGIUM

Julie E. Cumming, director

presents

EUROPEAN MUSIC

CIRCA 1492

Featuring

Settings of *L'homme armé* by Busnoys (d. 1492) and others
Isaac's lament on the death of Lorenzo the Magnificent (d. 1492)
Music commemorating the conquest of Granada (1492)

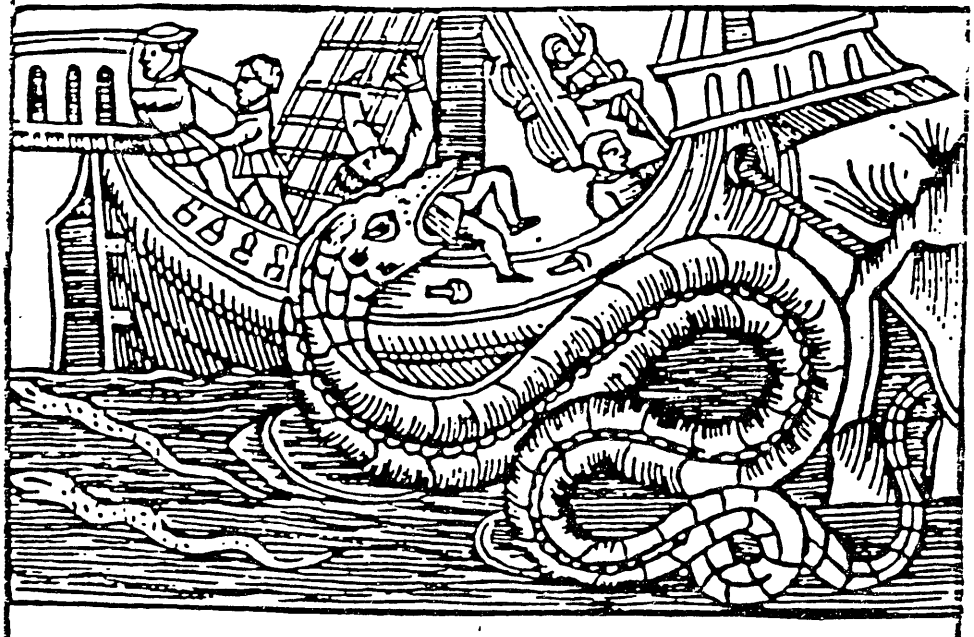

8:00 p.m. Saturday 25 April 1992
Houghton Memorial Chapel
Admission Free

Chapter 2

Nonlinear and Linear Acoustics

This chapter discusses the notions of nonlinear and linear acoustics. The development of each is a spinoff of the combined equations of mass, momentum, and state for a fluid in a small control volume. When these equations are combined, a wave equation results. A first-order term approximation results in the linear wave equation, while the retention of first- and second-order terms results in a nonlinear wave equation. The development of a nonlinear wave equation into one that reduces to a linear wave equation provides a justification for using the wave packet approach (WPA) in solving nonlinear acoustic wave propagation problems.

2.1 Introduction

One of the goals in this chapter is a mathematical justification of a WPA for nonlinear acoustic propagation. In the related work of Fox and Wallace (1954), Cook (1962), and Pestorious (1973), no attempt was made at a mathematical justification for using the approach beyond pointing to the excellent agreement with experiments, a realistically powerful but somewhat incomplete defense. I give explicit reasons for the agreement here, by reconciling the WPA with a nonlinear wave equation.

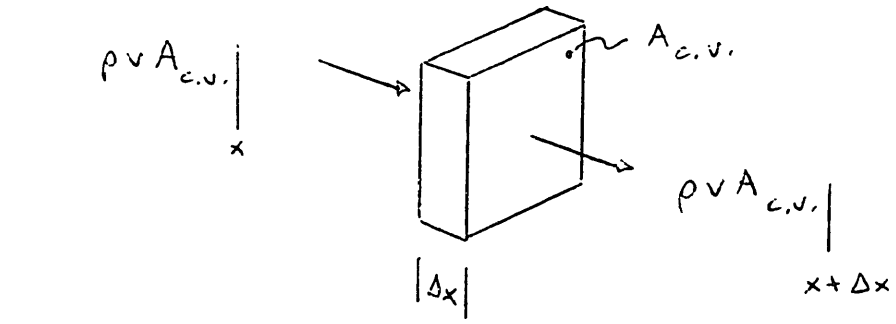

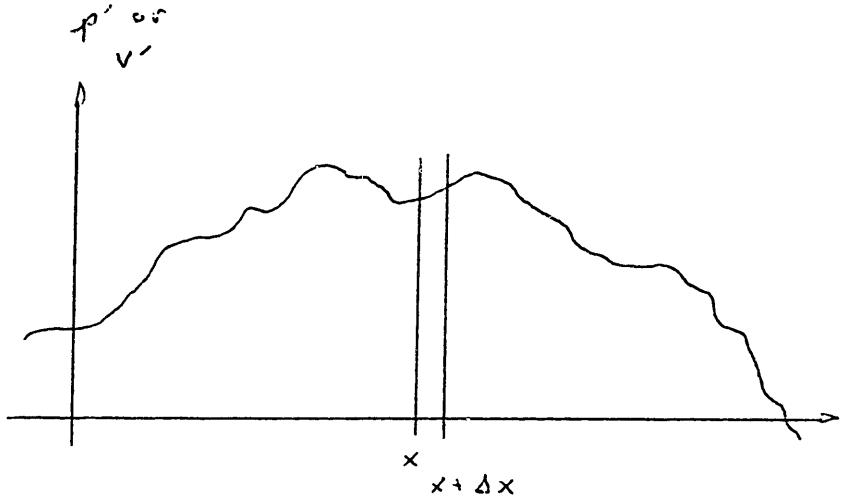

Fig. 2-1 Eulerian mass conservation.

Three principal characteristics are needed to justify the use of a WPA for nonlinear acoustics:

- first, when the wave amplitudes *are small*, linear acoustic waves are produced which don't change shape as they propagate. Thus a linear wave equation must be satisfied;
- second, that when the wave amplitudes *are not small*, the wave will change shape, or distort, as it propagates;
- third, that when a compression part of a wave advances in proximity with an adjacent rarefaction, a shock front is formed, which travels with roughly the average propagation speed of the compression and rarefaction fronts.

Since these three characteristics have been observed experimentally in real gases and liquids, they are regarded by all as the truth. The WPA will produce the first phenomenon as long as losses are included, and the second phenomenon with or without the inclusion of losses. Both of these features require the use of a nonlinear acoustic wave equation, which is one of the goals in this chapter. Weak shock theory, applied as a special case of the WPA, provides an excellent model of the third phenomenon; however, the detail as to *why* the weak shock method works is lacking. Providing the answers to the *why questions* is one of the basic premises in this thesis, leading to more insight into nonlinear acoustic phenomena.

2.2 Mass Balance

Consider the Eulerian control volume shown in Fig. 2-1. The fluid control volume has thickness Δx and cross section area $A_{c.v.}$, where $A_{c.v.}$ is perpendicular to the vector v'. The limits on the thickness Δx are that it be much smaller than any acoustic wavelength taking passage, but much larger than the molecular mean-free-path. The first limit presents no problem for an analysis such as follows here, while the second limit is a sensible one,

imposed by the entire notion of using a continuum-mechanics control volume approach.

To keep both the algebra and the corresponding mathematical bookkeeping manageable, the analysis is limited to one-dimension (1-D) along the x-axis. In many other acoustics and fluids works, the 1-D analysis gives the important features in relatively few pages. I do likewise here.

The important variables for this analysis are the pressure p, density ρ, and the particle velocity v. The variables p, ρ, and v are total quantities, and are respectively related to the acoustic quantities by the following relations:

total	=	ambient	+	acoustic	
p	=	p_o	+	p' ,	(2.1a)
ρ	=	ρ_o	+	ρ' ,	(2.1b)
v	=	v_o	+	v' .	(2.1c)

The ambient variables are assumed constant, and henceforth in this thesis the ambient flow v_o will be assumed zero.

Returning to the control volume (C.V.) shown in Fig. 2-1, the aim is to balance the mass. The mass flux passing through the C.V. is $\rho v A_{c.v.}$, which may then be separately evaluated on two sides of the C.V., once at x and again at $x + \Delta x$. The difference of the mass flux on each C.V. side (by subtraction) must equal the time rate-of-change of the mass enclosed inside the C.V. Formally, this is

$$\rho v A_{c.v.}|_x - \rho v A_{c.v.}|_{x+\Delta x} = \frac{\partial}{\partial t}(\rho A_{c.v.} \Delta x) \ . \tag{2.2}$$

Rearranging Eq. (2.2), and using the fundamental theorem of calculus for partial derivatives, the result is

$$\rho v_x + v\rho_x + \rho_t = 0 \ , \tag{2.3}$$

where x and t subscripted variables are a notation convention for partial derivatives. Note that

$$v\rho_x + \rho_t \equiv D\rho/Dt \ ,$$

where the material derivative

$$D/Dt \equiv \partial/\partial t + v\cdot\nabla \ .$$

Eq. (2.3) is a nonlinear equation for mass conservation. To make it more useful, the full variables for density ρ and velocity v may be expanded into their ambient (with subscript "o") and acoustic quantities (with prime ') via Eqs. (2.1 a-c):

$$(\rho_o + \rho')v'_x + v'\rho'_x + \rho'_t = 0 \ . \qquad (2.4)$$

To linearize Eq. (2.4), only the first-order acoustic quantities are retained because the assumption is made that products of two or more acoustic quantities (resulting in second-order or larger-order terms) give values that are numerically trivial as compared to the first-order terms. The result is

$$\rho_o v'_x + \rho'_t = 0 \ . \qquad (2.5)$$

Note that each of the two terms in Eq. (2.5) has only a single primed (acoustic) variable, and so it is called a first-order mass conservation equation.

2.3 Momentum Balance

The same type of approach used to balance the mass in the C.V. is used to balance the momentum. Fig. 2-2 shows the same C.V. as in Fig. 2-1 with momentum now under consideration. We consider the time rate-of-change of the momentum in the C.V., so we need not only the forces acting on the C.V. at its left and right surfaces, but also the momentum flux quantity $(\rho v)\cdot v$. On each side, at x and at $x + \Delta x$, these are respectively

$$pA_{c.v.} + \rho v^2 A_{c.v.} \ ;$$

$pA_{c.v.}$ is obviously force (pressure·area), and $\rho v^2 A_{c.v.}$ is the force flux due to the particles at speed v crossing into (or out of) the C.V. By the same type of procedure previously used for the mass, the difference of the forces *on* the sides of the C.V. must equal the time rate-of-change of the momentum *inside*

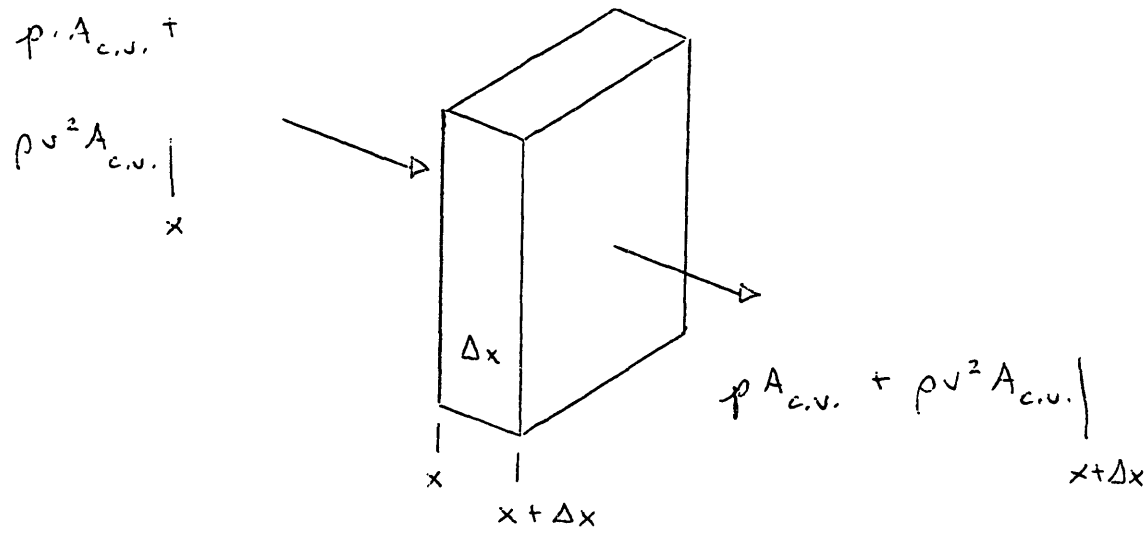

Fig. 2-2 Eulerian momentum conservation.

the C.V., or:

$$(pA_{c.v.} + \rho v^2 A_{c.v.})|_x - (pA_{c.v.} + \rho v^2 A_{c.v.})|_{x+\Delta x} = \frac{\partial}{\partial t}(\rho A_{c.v.}\, \Delta x\, v) \ , \qquad (2.6)$$

where the fluid is assumed lossless and irrotational. Rewritten in subscripted partial derivative form, Eq. (2.6) becomes

$$(\rho v)_t + (\rho v^2)_x + p_x = 0 \ . \qquad (2.7)$$

Expanding Eq. (2.7) into component terms yields:

$$\rho v_t + \rho v \cdot v_x + v\,\{\rho_t + (\rho v)_x\} + p_x = 0 \ . \qquad (2.8)$$

Eq. (2.8) is immediately simplified by recognizing that Eq. (2.4) makes the bracketed term, $\{\rho_t + (\rho v)_x\}$, equal to zero. Hence Eq. (2.8) becomes

$$\rho v_t + \rho v \cdot v_x + p_x = 0 \ . \qquad (2.9)$$

The density and particle velocity are then expanded into ambient plus acoustic variables:

$$-p'_x = (\rho_o + \rho')v'_t + (\rho_o + \rho')v' v'_x \ . \qquad (2.10)$$

Eq. (2.10) is a nonlinear momentum equation having first-, second- and third-order terms. The first-order approximation is the linear momentum equation given by

$$-p'_x = \rho_o v'_t \ . \qquad (2.11)$$

2.4 Equation of State: a Pressure-Density Relation

The mathematical relations for pressure-density (p-ρ) may be written in terms of a Taylor series expansion. Most authors[1] use series expansions of $p(\rho)$, rather[2] than series expansions of $\rho(p)$. It will be more convenient (later) to use the former approach, hence for now we write

$$p = p_o + \frac{A}{1!}s + \frac{B}{2!}s^2 + \frac{C}{3!}s^3 + O\{s^4\} \ , \qquad (2.12)$$

where $A \equiv \rho_o c_o^2$, and the condensation $s \equiv \rho'/\rho_o$. Then by rearranging Eq. (2.12), and substituting Eq. (2.1a)

$$p' = p - p_o = \rho_o c_o^2 \left[s + \frac{B}{2A} s^2 + \frac{C}{6A} s^3 + O[s^4] \right] . \qquad (2.13)$$

In the event that s^2, and higher-order terms in s, are considered small compared to the first-order term s, then we have a linear equation of state

$$p' = \rho_o c_o^2 \, s = c_o^2 \, \rho' . \qquad (2.14)$$

2.5 The Wave Equation: Linear & Nonlinear Forms

Now that we have the basic mass, momentum, and state equations to work with, wave equations may now be developed for both linear acoustics, and for nonlinear acoustics.

Linear Acoustic Wave Equation

The linear acoustic wave equation is derived from the linear equations of mass, momentum and state; these are respectively Eqs. (2.5), (2.11) and (2.14). The usual procedure is to take $\partial/\partial t$ on the mass equation (2.5), take $\partial/\partial x$ on the momentum equation (2.11), and add the results. This eliminates the cross partial derivative $\partial^2/(\partial t \partial x)$ terms. Then the acoustic density ρ' is eliminated by substitution of the equation of state, Eq. (2.14), so that the entire equation is in terms of the acoustic pressure p'. The result is

$$\frac{\partial^2 p'}{\partial x^2} = \frac{1}{c_o^2} \frac{\partial^2 p'}{\partial t^2} . \qquad (2.15)$$

Other manipulations are possible to write the wave equation in terms of ρ' or v' (see Jensen *et al.*, 1994), where each variable merely substitutes for p' in Eq. (2.15). Eq. (2.15) is in the general form of a standard 1-D linear wave equation which admits arbitrary solutions $f(x+c_o t)$ and $g(x-c_o t)$. Note that the shape of the wave never changes as the wave travels, and that every point and every

portion along the wave travels at the same speed c_o, independent of the pressure amplitude of the wave.

Nonlinear Acoustic Wave Equation

The procedure for deriving the nonlinear wave equation is the same as the linear case, but there are many more terms to deal with. What follows is considerable algebra, but it is shown here for completeness as it is seldom written out fully. Starting with the nonlinear mass equation, Eq. (2.4), take $\partial/\partial t$, with the result

$$-\rho'_{tt} = \underline{\rho_o v'_{tx}} + \rho'_x v'_t + \rho' v'_{tx} + \rho'_t v'_x + v'\rho'_{tx} \,. \tag{2.16}$$

Then take $\partial/\partial x$ on the nonlinear momentum equation (2.10), with the result

$$p'_{xx} = -\underline{\rho_o v'_{xt}} - \rho'_x v'_t - \rho' v'_{xt} - (\rho_o + \rho')(v'_x)^2 - (\rho_o + \rho')v' v'_{xx} - \rho'_x v' v'_x \,. \tag{2.17}$$

Adding Eqs. (2.16) and (2.17) eliminates the underlined terms in each equation. The result is

$$\rho'_{tt} = p'_{xx} + (\rho_o + \rho')(v'_x)^2 + (\rho_o + \rho')v' v'_{xx} + \rho'_x v' v'_x - \rho'_t v'_x - v'\rho'_{tx} \,. \tag{2.18}$$

Eq. (2.18) appears formidable, but there are a few modifications that may be made to make it more closely resemble a familiar wave equation. First, we need to rewrite the entire equation singularly in terms of p', or ρ'. Because of the way the equations have been developed thus far, it will be easier to eliminate p'. This is done by using the last of the three equations, the equation of state (2.13) which is repeated here,

$$p' = \rho_o c_o^2 \left[s + \frac{B}{2A} s^2 + \frac{C}{6A} s^3 + O(s^4) \right] ,$$

with $s \equiv \rho'/\rho_o$. To eliminate p' from Eq. (2.18), we need to take a second-order

spatial derivative on the equation of state. The result is

$$p'_{xx} = c_o^2 \{ \rho'_{xx} + \frac{B}{A\rho_o}[(\rho'_x)^2 + \rho'\rho'_{xx}] + \frac{C}{2A\rho_o^2}[2\rho'(\rho'_x)^2 + (\rho')^2\rho'_{xx}] + O\{s^4\} \}. \quad (2.19)$$

In Eq. (2.19) we see that there are three ρ'_{xx} terms; rewriting Eq. (2.19) with these terms grouped together we have

$$p'_{xx} = \rho'_{xx} c_o^2 \{ 1 + \frac{B}{A}(\frac{v'}{c_o}) + \frac{C}{2A}(\frac{v'}{c_o})^2 \} + c_o^2 \{\frac{B}{A\rho_o}(\rho'_x)^2 + \frac{C}{A\rho_o^2}\rho'(\rho'_x)^2\} + O\{s^4\}. \quad (2.20)$$

Eq. (2.20) was written by combining Eq. (2.13) with the impedance relation:

$$p' = \rho_o c_o^2 [s + \frac{B}{2A}s^2 + \frac{C}{6A}s^3 + O\{s^4\}] \approx \rho_o c_o v',$$

and by noting that

$$\frac{\rho'}{\rho_o} \approx \frac{v'}{c_o} \cdot \frac{1}{[1 + \frac{B}{2A}s + \frac{C}{6A}s^2 + O(s^3)]} \approx \frac{v'}{c_o}. \quad (2.21)$$

Now that we have what we want (p'_{xx}) from the equation of state, we can substitute Eq. (2.20) into Eq. (2.18), thus eliminating the acoustic pressure variable p' as we had intended:

$$\rho'_{tt} = \underbrace{\rho'_{xx} c_o^2 \{ 1 + \frac{B}{A}(\frac{v'}{c_o}) + \frac{C}{2A}(\frac{v'}{c_o})^2 \cdots\}}_{1} + \underbrace{c_o^2 \{\frac{B}{A\rho_o}(\rho'_x)^2 + \frac{C}{A\rho_o^2}\rho'(\rho'_x)^2\}}_{1}$$

$$+ \underbrace{\rho_o(v'_x)^2}_{2} + \underbrace{\rho'(v'_x)^2}_{3} + \underbrace{\rho_o v' v'_{xx}}_{4} + \underbrace{\rho' v' v'_{xx}}_{5} + \underbrace{\rho'_x v' v'_x}_{6} - \underbrace{\rho'_t v'_x}_{7} - \underbrace{v'\rho'_{tx}}_{8}. \quad (2.22)$$

One assumption made in writing Eq. (2.22) is that the $O\{s^4\}$ term, a fourth-order product of acoustic variables, has been omitted due to smallness. Eq. (2.22) may be further simplified by additional assumptions, so we must deal with the

overlined and underlined terms which are all second- and third-order products of acoustic variables. The first term, labeled 1, can be discarded because the accompanying term in the braces {···} is considerably larger. This is shown by rewriting the brace term as

$$\{ \frac{B}{A}\rho_o + \frac{C}{A}\rho' \} (\frac{\rho_x'}{\rho_o})^2 \ .$$

The term inside the braces may be evaluated as follows. For either fresh or sea water, B/A is about 5, and C/A is about 35; hence if $\rho_o >> 7\rho'$ then the $(C/A)\rho'$ term may be discarded. For air, B/A is about 0.4 and C/A is about 0.24; hence if $\rho_o >> .63\rho'$ then the $(C/A)\rho'$ term may be discarded. Because $\rho_o >> \rho'$ even for a large amplitude sound in water or air, the $(C/A)\rho'$ term is safely ignored[3], so we can safely discard term 1 in Eq. (2.22).

Terms 3 and 5 in Eq. (2.22) are discarded not only because they are third-order products of acoustic variables, but because they are also much smaller than terms 2 and 4 respectively, again because $\rho_o >> \rho'$. Term 6 is discarded because it is a third-order product of acoustic variables, which we assume small compared with the first- and second-order terms. With terms 1, 3, 5, and 6 discarded, and discarding any other third-order products, we have

$$\rho_{tt}' = \rho_{xx}' c_o^2 \{ 1 + \frac{B}{A}(\frac{v'}{c_o}) \} + c_o^2 \frac{B}{A\rho_o}(\rho_x')^2 v + \rho_o (v_x')^2 + \rho_o v' v_{xx}' - \rho_t' v_x' - v' \rho_{tx}' \ . \qquad (2.23)$$

By using the relation given in Eq. (2.21), we can rewrite the derivatives of v' in Eq. (2.23) in the form of density ρ':

$$\rho_{tt}' = \rho_{xx}' c_o^2 \{ 1 + \frac{B}{A}(\frac{v'}{c_o}) \} + c_o^2 \frac{B}{A\rho_o}(\rho_x')^2 + (c_o^2/\rho_o)(\rho_x')^2 + \rho_{xx}' c_o^2 (\frac{v'}{c_o}) + \rho'(\frac{c_o}{\rho_o})^2 (\rho_x')^2 - \frac{c_o}{\rho_o}\rho_t'\rho_x' - \rho'(\frac{c_o}{\rho_o})\rho_{tx}' \ ,$$

or reorganized as

$$\rho'_{tt} = \rho'_{xx}\, c_o^2 \left\{ 1 + \left(\frac{B}{A} + 1\right)\left(\frac{v'}{c_o}\right) \right\} + (c_o^2/\rho_o)\left(\frac{B}{A} + 1\right)(\rho'_x)^2 - \frac{c_o}{\rho_o}\,\rho'_t\rho'_x - \rho'\left(\frac{c_o}{\rho_o}\right)\rho'_{tx} \ . \qquad (2.24)$$

Eq. (2.24) is further rewritten to convert the time derivatives on the right side to spatial derivatives, by using the wave space-time duality convention that

$$\partial/\partial t \ \text{<---->} \ -c_o \cdot \partial/\partial x \ .$$

This makes the right side of Eq. (2.24) entirely populated either by ρ'_{xx} terms, or by ρ'_x terms. Hence

$$\rho'_{tt} = \rho'_{xx}\, c_o^2 \left\{ 1 + \left(\frac{B}{A} + 2\right)\left(\frac{v'}{c_o}\right) \right\} + \underline{\underline{(c_o^2/\rho_o)\left(\frac{B}{A} + 2\right)(\rho'_x)^2}} \ . \qquad (2.25)$$

The double underlined term in Eq. (2.25) has entirely positive constants, and the single underlined term is both positive-valued and second-order due to the square exponent. We shall discard this term on the basis that it is second-order compared with the remaining effectively first-order terms.

More interesting however is the form of the rest of Eq. (2.25): it has the form of a linear wave equation if the brace term, *i.e.* $\{\cdots\}$, is considered to be a modification of c_o^2. Taking the brace term as a modification of c_o^2, then the non-underlined part of Eq. (2.25) is treated as a linear wave equation with first-order acoustic terms, and we discard the underlined terms which are fully second-order:

$$\rho'_{tt} = c^2_{effective}\, \rho'_{xx} \ , \qquad (2.26)$$

where

$$c^2_{effective} = c_o^2 \left\{ 1 + \left(\frac{B}{A} + 2\right)\frac{v'}{c_o} \right\} \ . \qquad (2.27)$$

Recalling that $\frac{v'}{c_o} \approx \frac{\rho'}{\rho_o}$ from Eq. (2.21), we can compare the magnitude of the brace components in Eq. (2.27):

$$1 \ : \ \left(\frac{B}{A} + 2\right)\frac{\rho'}{\rho_o} \ .$$

For air the term $B/A + 2 = 2.4$, and for water $B/A + 2 = 7$, so the largest value we can consider is 7, hence

$$1 : 7\frac{\rho'}{\rho_o} .$$

But previously we imposed a requirement that $\rho_o >> \rho'$; thus even $7\frac{\rho'}{\rho_o} << 1$ so the $B/A + 2$ term is much smaller than 1 in Eq. (2.27). Thus an approximation for the effective wave speed in the control volume is

$$c_{effective} = c_o + (\frac{B}{2A} + 1)\, v' . \qquad (2.28)$$

Note that the effective wave speed for the packet of fluid is greater, or lesser, than c_o depending on the sign (+ or -) of the particle velocity v'. The term, $B/(2A) + 1$, also allows us to identify where the nonlinear effects of propagation manifest themselves. In the absence of a material nonlinearity, B equals zero; likewise the higher-order coefficients in the p-ρ series expansion in Eq. (2.12) equal zero. The remaining term, $A \equiv \rho_o c_o^2$, would make the p-ρ relationship linear. Hence, with $B=0$, the remnant nonlinearity in Eq. (2.27) is due to the higher-order terms from the conservation of mass and momentum, *i.e.* the convection terms. Hence $B/(2A) + 1$ compares the nonlinearity of the fluid material, the "$B/(2A)$" part, to the convection nonlinearity imposed by the mathematics of mass and momentum conservation, or the "+1" part. In fresh or sea water $B/(2A)$ is approximately 2.5, so the fluid material provides 71% of the nonlinearity as compared to the convection terms. In air however, the situation is the opposite: $B/(2A)$ is approximately 0.2, so the fluid material provides only 17% of the nonlinearity as opposed to the mass-momentum convection contribution. This discussion is consistent with an independent discussion and analysis by Blackstock[4].

In Chapter 3, it will be shown that $B/A = \gamma - 1$, where γ is the ratio of specific heats, C_p/C_v. The use of $\gamma - 1$ is more common for propagation in gases, and allows Eq. (2.28) to be written as

$$c_{effective} = c_o + (\frac{\gamma + 1}{2})\, v' . \qquad (2.29)$$

B/A is called the *parameter of nonlinearity*, after Beyer (1960). Unfortunately, many other authors also use $\beta = 1 + B/(2A)$ as the parameter of nonlinearity in their works. I will use Beyer's original convention, and refer to β as the *coefficient of nonlinearity*, per Hamilton and Blackstock (1988), which lumps together the nonlinearity of both the material and the convection mathematics. Thus Eq. (2.27) is also written as

$$c_{effective} = c_0 + \beta v' \ . \tag{2.30}$$

In summary, Eq. (2.30) provides a quasi-linear representation of wave speed for a control volume, based on a nonlinear wave equation that was written to mimic a linear wave equation. Since this wave speed is only useful within any particular control volume where the particle velocity is nearly uniform, the wave must be divided into separate segments, or wave packets, in order to use Eq. (2.30). This also provides a neat framework for applying acoustical absorption to each wave packet separately, a topic which will be thoroughly derived and discussed in Chapter 3.

2.6 Justification for the Wave Packet Approach

The development of Eq. (2.30) presented here appears to be unique; fortunately it agrees with different derivations by Earnshaw (1858), Pierce[5], Blackstock (1993) and others. What it also provides is a mathematical justification for the wave packet approach WPA mentioned in the Introduction. In review, the WPA models wave propagation as a mapping from a node location x_j to a new location x_{j+k}, where each small segment of each wave, herein called a *wave packet*, moves to the j+k node location on x at a speed $c_0 + \beta v'$. The mathematics given in this chapter used the usual conservation of mass and momentum, and relied on a nonlinear equation of state to make a physical link between p and ρ. The outcome was that the effective speed of a portion of a wave, within the bounds of a small control volume, is also $c_0 + \beta v'$. *So using the WPA implies satisfaction of conservation of mass and momentum, and utilizes the correct modeling of the nonlinear components for both the material and the convection terms.* The WPA will

result in wave propagation with wave shape distortion due to the cumulative effects of the nonlinearity, so long as the propagation path is sufficiently discretized. Details on the discretization are left to Chapter 4.

The only major items absent from the WPA are energy conservation and dissipation. Likewise, it is worth pointing out that conservation of energy is not a requirement in deriving the wave equation, but it is almost always introduced thereafter. In the absence of dissipation, the local energy density must remain constant from the propagation step j to $j+k$ along x, and this can easily be accounted for in a computational model. Hence, like most acoustical approaches, we don't *derive* conservation of energy, we rather *impose* it upon our math model.

Real propagation always encounters dissipation effects, therefore the combined dissipation effects of viscosity, relaxation and thermal conduction must be included. These topics are the subject of the next chapter.

---

[1]Beyer, R.T. (1975), pp. 98-100.
[2]Novikov *et al.*, (1987), p. 10.
[3]Beyer, R.T. (1975), p. 100; and Beyer, R.T. (1972), p. 208.
[4]Blackstock, D.T. (1993), short course in Nonlinear Acoustics, pp. D 6-7.
[5]Pierce, A.D. (1989), p. 568.

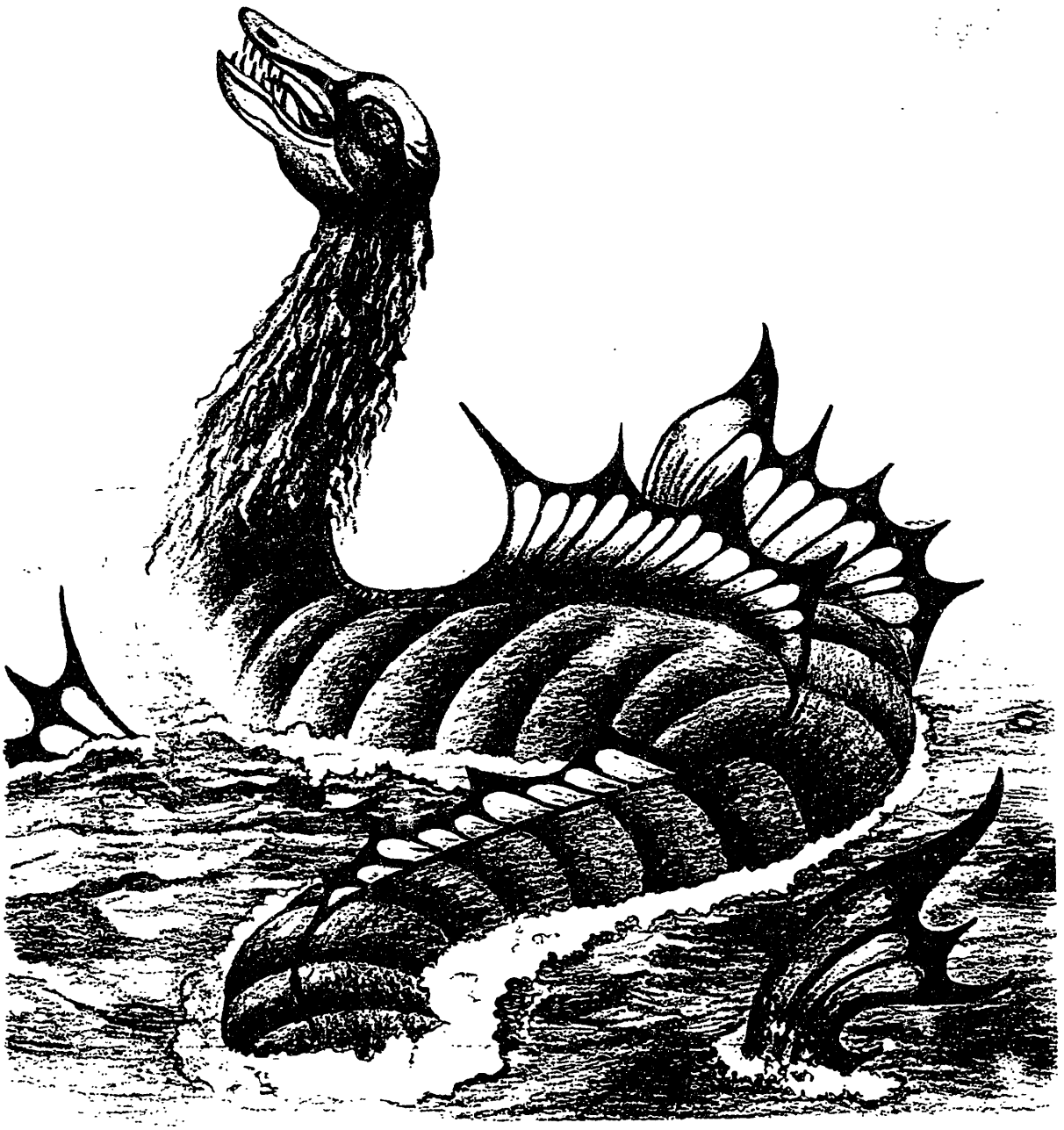

Chapter 3

Time Domain Absorption

This chapter studies the phenomena of acoustic absorption. Absorption of sound waves in fluids is mainly a consequence of a combination of three phenomena: viscosity, relaxation, and heat conduction [Radiative heat transfer from sound waves has been shown to be a weak effect[1]]. Each of these three absorption mechanisms is discussed in this chapter, with the goal of implementation in a time-domain computational framework.

It is worth noting here that most previous works dealing with acoustic absorption of nonlinear waves have adopted the use of terms like *excess absorption* or *nonlinear absorption.* These concepts are somewhat misleading because they suggest that there is some special form of absorption at work in a nonlinear acoustic wave, when in fact there isn't. This Chapter eventually will show that the absorption of a wave depends on its shape, specifically it depends on $\nabla^2 u$, because the absorption processes always attempt to straighten the wave. The association with *excess* or *nonlinear absorption* is an outgrowth of cumulative nonlinear distortion, and the apparent and mysterious increase in the attenuation coefficient for large amplitude problems which dates to the 1930's, and from the attempt by acousticians to explain why it occurs. These descriptions persist today. The simple fact is that nonlinear acoustic propagation means that the wave shape will change during propagation, and so the absorption character will also change.

3.1 Absorption Due to Viscosity

Classical theories of sound wave absorption assume an $e^{-\alpha x}$ amplitude dependence; that is, that the envelope of the wave decays with propagation distance. The same result is accomplished by assuming a complex propagation constant k, such that $k = k_r + ik_i$ where k_r and k_i are the real and imaginary parts of k. For a wave with $e^{-i(\omega t - kx)}$ dependence, this results in a propagating wave component $e^{-i(\omega t - k_r x)}$, multiplied by a decayed exponential part $e^{-\alpha x}$, where $\alpha = k_i$. The constant α for the classical viscous intensity attenuation for a pure tone wave[2] is given by

$$\alpha(\omega) = \left(\tfrac{4}{3}\eta + \eta_b\right)\frac{\omega^2}{\rho_o c^3} \quad , \tag{3.1}$$

where η and η_b are respectively the shear and bulk viscosities of the fluid.

One practical difficulty with using the classical theory is that it assumes a sinusoidal dependence of the wave, as witnessed by the ω^2-term in Eq. (3.1). In the strictest sense, this requires that the wave be continuous for all time, and hence would have a line spectrum at the single frequency ω. A sinusoidal sound pulse with base frequency ω would have a spectrum predominantly at ω, but would still have adjacent sideband energy. Two basic ways have been used to deal with this problem. The first, and the most common particularly in nonlinear acoustics, is to ignore the absorption at frequencies other than at ω, which is an assumption that the wave is narrow-band. The second way is to take the Fourier spectrum (using an FFT) at each propagation range, apply an appropriate $e^{-\alpha(\omega)\Delta x}$ weight in each frequency bin (which both reduces and tapers the frequency spectrum), and then take the inverse Fourier spectrum (using an IFFT) to establish the new wave shape; Δx is the distance the wave travels between each FFT-IFFT step. This procedure requires many FFT-IFFT steps. Similar spectral estimation procedures, *i.e.* pre-FFT, were used by Fox and Wallace (1954), and by Cook (1962). A fundamental difficulty with the FFT-IFFT approach is that, as the waveform steepens towards a shock, Gibbs ripple phenomena will be introduced into the time waveform after each IFFT step. This is one reason why the frequency domain approach for absorption in a

nonlinear propagation problem is often limited to problems not involving shocks.

The approach presented here avoids the frequency domain entirely and does not require a narrow band pulse. However, it does require the accurate calculation of acoustic absorption, so the classical equation for absorption based on a narrow band wave is insufficient. This motivated the search for, and the development of, time/space domain equivalent expressions for viscous, relaxation, and heat conduction absorption. The viscous absorption will be described first.

Consider now the plane wave illustrated by cross section in Fig. 3-1. The Figure shows the pressure p versus x-distance at a single time t_0 as if the pulse were frozen in time. The waveform is not necessarily sinusoidal, nor need it be periodic. The pressure amplitude is P_0 in a fixed reference frame, thin slab of the wave indicated by the x-thickness Δx, located at x_0. The instantaneous energy density within the slab is the sum of the instantaneous kinetic and potential energy densities[3] in the slab, and is given by

$$E = \frac{P_o^2}{\rho_o c^2} . \tag{3.2}$$

The instantaneous energy density units for Eq. (3.2) are equivalently

$$Pa \equiv \frac{N}{m^2} \equiv \frac{N \cdot m}{m^3} \equiv \frac{J}{m^3} .$$

The instantaneous energy density for the slab moves at the wave speed c. The energy flux for the slab is then

$$I_0 = E \cdot c . \tag{3.3}$$

The units for Eq. (3.3) are in Watts per square-meter, hence the symbol I_0 is used to denote an energy intensity. In the absence of any absorption, I_0 for the slab of the wave would be a constant as the wave propagates along the x-direction. We'll temporarily set Eq. (3.3) aside and return to it shortly.

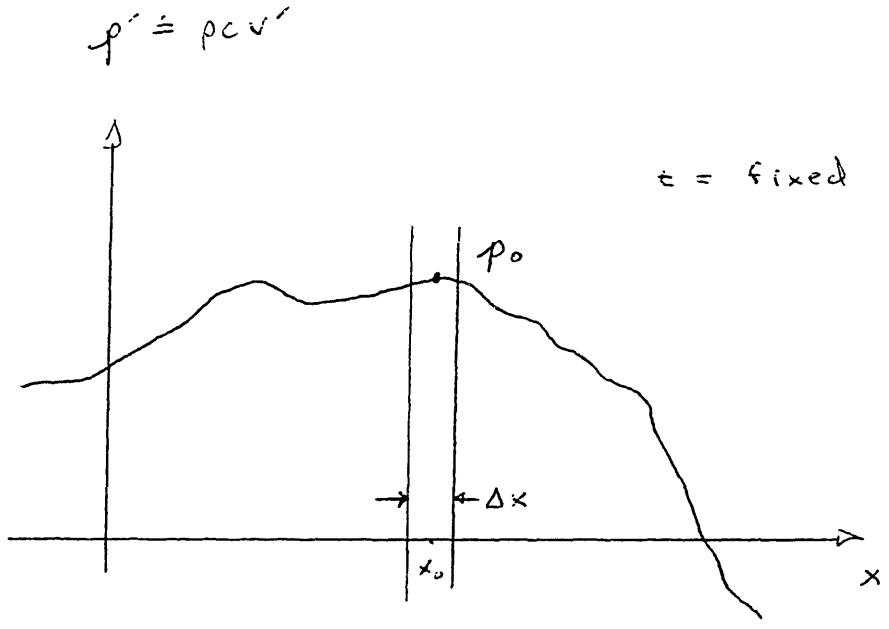

Fig. 3-1 Frozen acoustic waveform: p and v'.

Acoustic absorption is reconciled by considering the equation for momentum in the presence of viscous losses. This equation is given (in linearized form[3]) by

$$\rho_o \frac{\partial u}{\partial t} = -\nabla p + (\tfrac{4}{3}\eta + \eta_b)\nabla^2 u \,, \tag{3.4}$$

where u is the acoustic particle velocity (note: u and U_o are used in this chapter for particle velocity rather than v' which was used in Chapter 2; this is done to avoid confusion with the volume V which will be used later in this Chapter). The linearized version of this equation is used here to simplify the analysis and because the portions which are to be retained from Eq. (3.4) are due strictly to the viscous loss terms. This equation is called by such names as the momentum, the Newton, or the Navier-Stokes equation. It can be derived by considering the force balance across a slab-like element of fluid, such as shown in Fig. 3-1. A similar derivation, without viscous dissipation, was previously shown in Chapter 2.3. Eq. (3.4) is the linearized form of the momentum equation, with the inclusion of the viscous friction force opposing the fluid acceleration. The units of Eq. (3.4) are N/m^3, which is a force density. In the absence of viscosity (η and η_b both equal zero), Eq. (3.4) offers a balance of the *conservative* forces (or specifically, force densities). Thus

$$(\tfrac{4}{3}\eta + \eta_b)\nabla^2 u$$

is a *dissipation* force density acting on a slab of fluid. The work density on the fluid slab furnished by the viscosity is given by the product of the dissipation force density and the distance over which the force is applied, and evaluated at x_o:

$$\Delta w = \Delta x \cdot (\tfrac{4}{3}\eta + \eta_b)\, \left| (\nabla^2 u)|_{x_o} \right| \,, \tag{3.5}$$

where Δw is the work density, and Δx is the distance along x. An implicit assumption in Eq. (3.5) is that the particle velocity u is constant (U_o) as it travels across the slab Δx. The vertical brackets for the absolute value, $|\cdots|$, indicate the magnitude because organized work (energy) removed from the fluid by viscosity is always positive, independent of the direction of the

particle velocity, and redistributed into disorganized thermal vibration (heat). The use of the absolute value will later be removed for very deliberate reasons, the main one being, in the words of Prof. Henrik Schmidt, that they don't really occur in nature. The use of the absolute value, for now, gives us some mathematical latitude, and later on in this chapter, we will find we really don't need it.

To illustrate, assume that the particle velocity u is given by

$$u = U_{max} \cdot \sin(\omega t - kx) .$$

Substituting this into Eq. (3.5), and recognizing that the work must be positive (because viscosity is insensitive to particle velocity direction), the work density is then

$$\Delta w = \Delta x \cdot (\tfrac{4}{3}\eta + \eta_b) \cdot k^2 \cdot |U_{max} \cdot \sin(\omega t - kx)| .$$

One more item to note is that, in calculating the work density Δw, there is only one acoustic phase present in each slab, and it has particle velocity magnitude $U_o = P_o/\rho_o c$. The single acoustic phase having magnitude U_o is merely another way of saying that the trigonometric argument, $\omega t_o - kx_o$, is a constant at the location x_o, at time t_o and that

$$U_o = |U_{max} \cdot \sin(\omega t_o - kx_o)| .$$

Hence, the work Δw would then be

$$\Delta w = \Delta x \cdot (\tfrac{4}{3}\eta + \eta_b) \cdot k^2 \cdot U_o .$$

Returning now to the general case where the form of u is unspecified, the work Δw is deposited into the fluid slab as heat, so the slab experiences an increase in temperature; work Δw is in units of $N \cdot m/m^3$, or $Joules/m^3$, and has the same units as the energy density, Eq. (3.2). The dissipation work flux ΔI, which is an intensity loss of the fluid slab, is the product of the work Δw and the particle speed U_o of fluid in the slab which does the work:

$$\Delta I = U_o \cdot \Delta w = U_o \cdot \Delta x \cdot (\tfrac{4}{3}\eta + \eta_b) \left|(\nabla^2 u)_{|x_o}\right| . \qquad (3.6)$$

The units for Eq. (3.6) are, like Eq. (3.3), W/m^2. Eq. (3.6) is the incremental intensity loss for the fluid slab, as the particle velocity u travels across the Δx-thick slab. To find the total slab intensity loss of energy for the entire propagation distance, the incremental intensity loss must be summed from the starting point on x (which is taken as x=0) to the end point on x where all the acoustic energy has been dissipated (or more specifically, transformed into heat). To accomplish this, the incremental slab thickness Δx is replaced by the differential dx, and the summation is made by the use of a continuous integral. The integral, as written, represents the accumulating intensity loss of the slab of interest as we *follow* the slab wave packet during propagation from x=0 to x=∞. Hence time evolves from t=0 to t=∞.

$$I_{total} = (\tfrac{4}{3}\eta + \eta_b) \int_0^\infty U_o \cdot \left|(\nabla^2 u)_{|x_o}\right| dx .$$

This result is very general, and hence for most purposes, it is practically useless because it requires that the shape and amplitude of the wave be fully known throughout the propagation path. In the next Chapter on computational methods, where the findings from this chapter and Chapter 2 are implemented, it will be shown that propagation-absorption occurs piecewise. This means that for small-enough propagation steps, we can locally assume that the wave shape doesn't change and that the wave amplitude decays in some reasonable fashion. Making these assumptions, the general form is given by

$$I_{total} = U_o \cdot (\tfrac{4}{3}\eta + \eta_b) \cdot \left|(\nabla^2 u)_{|x_o}\right| \cdot \int_0^\infty e^{-\alpha x} dx , \qquad (3.7)$$

and the rationale follows. First, the magnitude U_o of the particle velocity u is taken to be a constant in defining the viscous work, per Eq. (3.5). This is a reasonable assumption, because the increment Δx is small. Hence the magnitude of u in the slab, U_o, may be passed through the ∇^2 operator; a sinusoidal wave example of this was shown several paragraphs ago. This step allows the calculation of the work, and hence intensity loss, for a single slab of

the medium. This is the first mathematical limit that must be taken: to assume that U_o stays constant over Δx. But when the integration in Eq. (3.7) is performed, the magnitude U_o must decay as the wave propagates along x. So the $\nabla^2 u$ is exterior to the integral over x, because it is referenced to a single slab at $x = x_o$; however, there must be a suitable function used inside the integral to correctly account for the decaying amplitude of the wave. An obvious choice would be the decaying exponential function because this is consistent with both historical observations in acoustic experiments, and matches the convention of using a complex propagation constant k within the argument of a wave function $e^{-i(\omega t \pm kx)}$. Inserting the function into Eq. (3.7) allows further algebraic manipulation, and the integration may now be completed over sensible limits: in this case for $0 \le x \le \infty$, because the exponential decay doesn't provide complete attenuation of the wave energy until x reaches infinity. The result is

$$I_{total} = U_o \cdot \left(\tfrac{4}{3}\eta_l + \eta_b\right) \cdot \left|(\nabla^2 u)_{|x_o}\right| \cdot \frac{1}{\alpha} \,. \tag{3.8}$$

Eq. (3.8) is the summation of all the differential intensity losses of the wave packet (for the initial slab at x=0) for the full propagation distance traveled. This must also equal the wave intensity previously provided by Eq. (3.3) since the intensity, which is an energy flow, must be conserved. By setting Eq. (3.3) equal to Eq. (3.8), and rearranging terms, the decay variable α is:

$$\alpha(x_o) = \frac{\left(\tfrac{4}{3}\eta + \eta_b\right)}{\rho_o c\, |U_o|} \left| \nabla^2 u_{|x_o} \right| . \tag{3.9}$$

Eq. (3.9) is the most general form for viscous acoustic absorption because it holds for any realizable, continuous acoustic waveform over small paths. It shows that the viscous dissipation coefficient is spatially dependent. Under the special circumstance when the waveform is sinusoidal, Eq. (3.9) is then constant, and independent of space:

$$\alpha = \frac{\left(\tfrac{4}{3}\eta + \eta_b\right) \omega^2}{\rho_o c^3} , \tag{3.10}$$

which is the familiar result for the classical viscous *intensity* absorption coefficient based on Stokes' viscosity approach[1,2], and shown previously in Eq. (3.1). If Eq. (3.10) is divided by two, and $\eta_b=0$ per Stokes' assumption, the classical viscous *pressure* absorption coefficient results. Eq. (3.10) is included here only as a sanity check on the approach taken to find Eq. (3.9), which is an energy-intensity balance using the dissipation force density provided by the Navier-Stokes momentum equation. *The usefulness of Eq. (3.9) is that it provides a direct means of calculating viscous sound wave absorption in the spatial domain for a wave which is not necessarily a pure tone. This allows the correct absorption to be calculated, based on the physical grounds of the preceding analysis, of wide-band signals having any physically realizable waveform.* The spatial domain derivatives may easily rewritten for derivatives in the time domain, if the propagation direction variable is in t for time, instead of x for space.

Temkin (1981) used an energy-dissipation method similar to the one developed here, to arrive at Eq. (3.10), but his analysis assumed a pure tone wave.

3.2 Absorption Due to Relaxation

The notion of relaxation phenomena is well illustrated by Figure 3-2, after Kinsler *et al.*[3] For a fluid pressure $p = P_o$ at $t \geq 0$, the pressure ratio p/P_o goes to 1, while the ratio of the condensation $s \equiv \rho'/\rho_o$ to $P_o/(\rho_o c^2)$ requires a finite time to reach 1. The interval τ is called the *relaxation time*, at which the condensation ratio reaches 63.2% of its final value. Sea water and atmospheric air each have two[4] relaxation times, τ_1 and τ_2, for most practical acoustical problems of interest. Fresh water has no significant relaxation time.

Kinsler *et al.* describe[3] the acoustic pressure as

$$p' = \rho_o c^2 \left(1 + \tau \frac{\partial}{\partial t}\right) s \,. \tag{3.11}$$

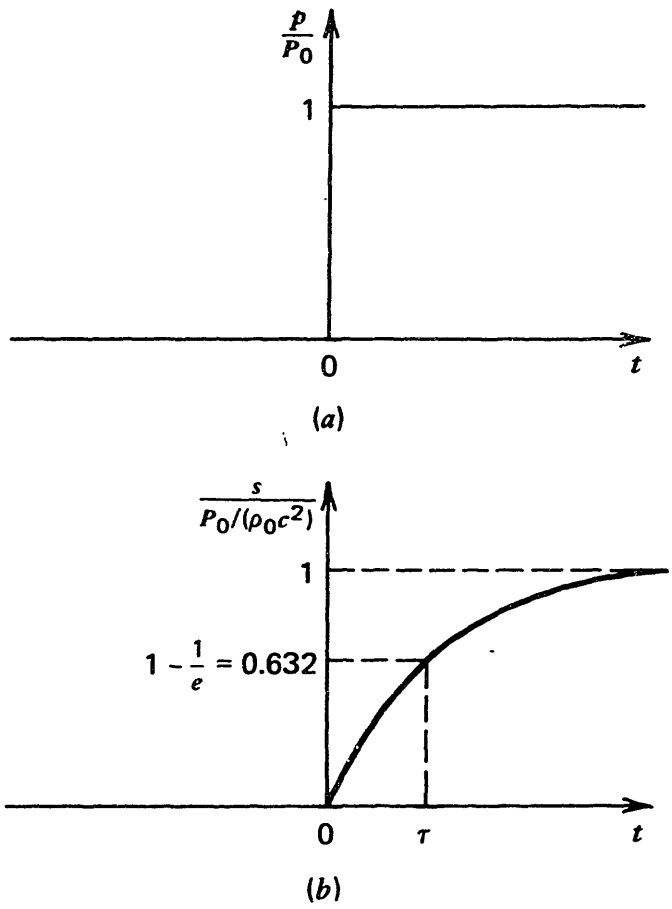

***Fig. 7.1.** Response of a relaxing fluid to a sudden increase in pressure.*

Fig. 3-2 Relaxation illustration; from Kinsler *et al.* (1982).

Eq. (3.11) may be substituted into the linearized momentum equation (3.4) used earlier in order to see how the relaxation process manifests itself in acoustic absorption. Making this substitution, ignoring the viscous terms (because they have already been dealt with in the previous section), and dropping the prime (') superscript on the acoustic variables for notational ease, the relaxation-modified momentum equation becomes

$$\rho_o \frac{\partial u}{\partial t} = -\nabla p - c^2 \tau \nabla \frac{\partial \rho}{\partial t} . \tag{3.12}$$

Eq. (3.12) strongly resembles Eq. (3.4), except that the viscous force density has been replaced by a relaxation force density, which is the right-most term. Using a similar procedure to that used in the previous section, the relaxation force density is isolated to calculate the work density due to the particle velocity within a Δx slab of fluid centered at x_o, where $u' = U_o$ and $p' = P_o$, per Fig. 3-1. The relaxation work (density) and the relaxation intensity loss come from the right-most term in Eq. (3.12) after successive multiplication by Δx and U_o.

Respectively, they are

$$\Delta w = \Delta x \cdot c^2 \tau \left| \left(\nabla \frac{\partial \rho}{\partial t} \right)_{x_o} \right| \tag{3.13}$$

and

$$\Delta I = U_o \cdot \Delta x \cdot c^2 \tau \left| \left(\nabla \frac{\partial \rho}{\partial t} \right)_{x_o} \right| . \tag{3.14}$$

We would like to substitute Eq. (3.11) into (3.14) but we need $\rho(p)$ rather than $p(\rho)$, so Eq. (3.11) is then rewritten for acoustic density as a function of pressure:

$$\rho' = \frac{p'}{c_o^2} - \frac{\tau}{c_o^2} \frac{\partial p'}{\partial t} + \frac{\tau^2}{c_o^2} \frac{\partial^2 p'}{\partial t^2} - \frac{\tau^3}{c_o^2} \frac{\partial^3 p'}{\partial t^3} + \frac{\tau^4}{c_o^2} \frac{\partial^4 p'}{\partial t^4} \cdots . \tag{3.15}$$

Eq. (3.15) is merely a rewritten form of Eq. (3.11), but now takes the form of an infinite series of partial derivatives. This poses no great problem because Eq.

(3.15) is merely a rewritten form of Eq. (3.11), an that equation is finite, bounded and convergent, so we know that Eq. (3.15) behaves the same way.

Adopting once again our notion of a Δx-thick continuum slab of fluid, we can always take the local p' versus x trace of the wave to be composed of a single effective local frequency component. This is tantamount to a local curve fit of a very small piece of a sine wave to the p'-x curve that exists for our Δx neighborhood. This allows us to replace any space derivative by ik and any time derivative by $-i\omega$. Making these substitutions, and by inserting Eq. (3.15) into (3.14):

$$\Delta I = U_o \cdot \Delta x \cdot \frac{\tau}{c_o} \omega^2 p' \left[(1 - \omega^2\tau^2 + \omega^4\tau^4 \cdots) + i\omega\tau(1 - \omega^2\tau^2 + \omega^4\tau^4 \cdots) \right] \quad (3.16)$$

Also note the two identical infinite series. Since their antecedents were convergent, these are as well and we can rewrite them as

$$1 - \omega^2\tau^2 + \omega^4\tau^4 \cdots = \frac{1}{1 + \omega^2\tau^2} . \quad (3.17)$$

Making this substitution and disregarding the imaginary part (which would lead to a phase term related to dispersion) we find

$$\Delta I = U_o \cdot \Delta x \cdot \frac{\tau}{c_o} \omega^2 p' \cdot \frac{1}{1 + \omega^2\tau^2} . \quad (3.18)$$

Eq. (3.18) is the relaxation intensity loss for a fluid slab of thickness Δx. To find the total relaxation intensity loss, a summation must be made over all slabs along x that the wave travels through. Like the previous section, we assume a non-changing wave shape and an exponential decay dependence to obtain a useful intensity loss expression. These are reasonable assumptions for small paths. Thus taking the sum of all such losses due to relaxation dissipation:

$$I_{total} = U_o \cdot \frac{\tau}{c_o} \omega^2 p' \cdot \frac{1}{1 + \omega^2\tau^2} \int_0^\infty e^{-\alpha x} \, dx . \quad (3.19)$$

Eq. (3.19) is then set equal to Eq. (3.3), in the same fashion as the previous section, and then solved for the intensity absorption coefficient due to relaxation:

$$\alpha = \frac{\tau}{c_o} \frac{\omega^2}{1 + \omega^2\tau^2} \quad . \tag{3.20}$$

By inspection Eq. (3.20) can be seen to have the correct behavior for values of $\omega\tau$ relative to 1. When is $\omega\tau << 1$, $\alpha(x) = \tau\omega^2/c_o$, thus having the same ω^2 dependence as viscosity and heat conduction losses. When $\omega\tau >> 1$, $\alpha(x) = 1/(\tau c_o)$, *i.e.* it becomes constant.

Eq. (3.20) provides an intensity value for α; for pressure, Eq. (3.20) must be divided by two, which then exactly agrees with the result from Kinsler *et al.*[5] The theoretical approach given here makes certain non-obvious assumptions about internal energy and specific heat, and the consequence is that the above equations correctly estimate the location in frequency of the relaxation 'knee' (going from ω^2-dependence to a constant), but drastically overestimate the absolute level of α. A frequency-based approach that *does* consider these parameters is given by Lindsay[7] (1960) which will not be repeated here because it is beyond the scope of my aims, and because it requires several pages of work to arrive at a relatively simple result: a coefficient, much smaller than 1, which reduces the levels of α given in Eq. (3.20).

Since we really seek a time-domain expression for the relaxation loss, we have to unwind the above analysis into a more useful form. We had previously supposed in our Δx-thick slab that only one effective frequency species existed, and so we replaced time and space derivatives by $-i\omega$ and ik respectively. By applying the reverse procedure we obtain:

$$\alpha(x_o) = \frac{1}{c\tau} \frac{\tau^2 c^2 \frac{\nabla^2 u}{u_o}}{1 + \tau^2 c^2 \frac{\nabla^2 u}{u_o}} \tag{3.21}$$

This procedure in writing Eq. (3.21) from (3.20), or deriving Eq. (3.21) directly for that matter, is only correct if the notion of a single local frequency

approximation holds. This doesn't cause any major hardship however because we use a separate Eq. (3.21) for each Δx-thick slab in the wave packet, and the shape of the wave will change during travel due to absorption. Hence the assumptions about the local frequency content and the wave shape being constant throughout travel from x=0 to x=∞ were merely used to find the form of $\alpha(x_o)$; when we actually implement $\alpha(x_o)$ we always do it in a sensible way, for small travel distances of the wave packet, and we always use a different local $\alpha(x_o)$ for each x_o along the wave. In this way, we don't violate the spirit of the local assumptions made, and the analysis still holds firm.

Note that in a fluid having two distinct relaxation times, τ_1 and τ_2, there would be two distinct expressions for α_1 and α_2, and fluids or fluid-like tissues may also have manifold relaxations with a different τ for each one.

A comment must now be made concerning the approach. The relaxation momentum in this section was treated independently from the viscous momentum in the previous section. The choice of deriving them separately was deliberate, for ease of reader understanding as well as the prevention of errors by the writer. The derivation of the viscous, the relaxation, and the (forthcoming) heat conduction absorption coefficients are also handled separately in most acoustics papers and texts; once derived, they may be lumped together to form effective dissipation coefficients. See Table 7.1 in Kinsler *et al.* for example comparison of viscous and thermal coefficients, and experimentally observed absorption coefficients among several gases and liquids.

3.3 Absorption Due to Heat Conduction

The previous two sections, 3.1 and 3.2, both used versions of the momentum equation to obtain absorption due to viscosity and relaxation, respectively. The approach towards viscous absorption, via Navier-Stokes, was intuitive because it came directly from the momentum equation. The approach for the relaxation was slightly less intuitive, but it was equally physical because a relation was found for momentum in terms of the relaxation behavior of the

fluid. A similar approach will be used once again here to develop the space/time domain absorption due to heat conduction, and it will involve writing the unsteady heat conduction equation in a modified form, so as to resemble momentum. The procedure thereafter is straight forward, and is similar to the procedures used in 3.1 and 3.2.

The starting point for this section comes from Kirchoff and Fourier, via Pierce[8]. Pierce writes the heat conduction equation as

$$\rho T \frac{Ds_e}{Dt} = \kappa \nabla^2 T , \tag{3.22}$$

where κ is the heat conduction coefficient, s_e is entropy , and T is temperature. Using several thermodynamic relations, Pierce then rewrites Eq. (3.22) as

$$\rho_o C_p \frac{\partial}{\partial t} (\rho' - p/c^2) = \kappa \nabla^2 (\rho' - p/c_T^2) , \tag{3.23}$$

where c_T is the isothermal wave propagation speed, and c is the ordinary linear acoustic sound speed. After some manipulation and elimination of higher-order terms on the left side, Eq. (3.23) leads to

$$\rho_o C_p \frac{\partial \rho'}{\partial t} \left(\frac{v'}{c_o} \frac{B}{A}\right) = \kappa (\gamma - 1) \nabla^2 \rho' , \tag{3.24}$$

where A and B are terms in a $p(\rho)$ expansion and v' is the acoustic particle velocity. For small v', the left hand side is close to zero as compared to the right hand side; this is consistent with the domination of conduction via the right side. If the acoustic process were purely adiabatic, with no heat conduction loss, then $\kappa = 0$, and the right side becomes zero and the left side dominates. Both of these conditions are stated by Pierce (1989, page 14). The interesting feature of Eq. (3.24) is the $\kappa(\gamma - 1)$ rather than just κ, which in effect alters the heat conduction coefficient to a lower value. We'll return to this comment momentarily.

Experimentally, for acoustic waves of interest in air, or in water, the measured sound speed is much closer to being adiabatic than isothermal. Newton's

(1686) calculation of the speed of sound in air was too slow by 16% (*i.e.* by a factor of $\sqrt{\gamma}$) because he unwittingly made an isothermal assumption; the discrepancy was not resolved until Laplace some 130 years later. Hence, propagation is substantially close to being adiabatic (without heat transfer) insofar as sound speed is concerned, but there is still a slight amount of energy given up to heat conduction. By assuming $\frac{Ds_e}{Dt} \approx \frac{\partial s_e}{\partial t}$ on the left side of Eq. (3.22) then we may rewrite

$$T\frac{Ds_e}{Dt} \quad \text{as} \quad C_p\frac{\partial T}{\partial t}$$

using the thermodynamic relation $C_p \equiv T(\partial s/\partial T)_p$. This assumption makes the left side of Eq. (3.22) *always exist*, as $\rho C_p \frac{\partial T}{\partial t}$, and is hence dominant relative to the right side. This means that the heat conduction must be weak or nonexistent (*i.e.* κ=0); assumptions like these would give the adiabatic sound speed but not the appropriate heat conduction loss. Hence, weak conduction is needed, so we incorporate a modified conductivity, $\kappa(\gamma\text{-}1)$, based on the arguments used to find Eq. (3.24). The result is

$$\rho_o C_p \frac{\partial \rho'}{\partial t} = \kappa(\gamma - 1)\nabla^2\rho' , \tag{3.25}$$

which bears strong similarity to

$$\rho_o C_p \frac{\partial T}{\partial t} = \kappa \nabla^2 T , \tag{3.26}$$

per White (1982) for unsteady heat conduction in a fluid or solid that *does not* undergo the passage of compressions or rarefactions. To account for the acoustic wave passage, the $\kappa(\gamma\text{-}1)$ must be used instead of κ. More detailed discussions for the passage of acoustic modes and thermal (entropy) modes are found in Pierce (1989) pages 13-14, 34-36, 522-523; and in Morse and Ingard (1968) pages 270-300.

The remaining task is to write the temperature of the fluid in a slab of Δx thickness in terms of the acoustic particle velocity u used previously, since

this would in turn provide a thermal conduction equivalent to the momentum equation and allow the development of time domain absorption due to thermal conduction. The following relations for ideal adiabatic gases are used (Van Wylen and Sonntag, 1978):

$$pV^{\gamma} = \text{constant}, \qquad \rho V = M, \tag{3.27}$$

where V is the volume and M is mass. Assuming the fluid changes from the ambient state (with subscript "o") to a new state due to an acoustic passage, and combining these two relations, the result is:

$$p/p_o = (\rho/\rho_o)^{\gamma} \ . \tag{3.28}$$

Eq. (3.28) is then combined with

$$pV/T = \text{constant}$$

to yield

$$T = T_o(\rho/\rho_o)^{\gamma-1} \ . \tag{3.29}$$

with $\rho = \rho_o + \rho'$. Eq. (3.29) is then substituted into Eq. (3.25), using the approximation from Eq. (2.21) that $\rho'/\rho_o \approx v'/c_o$. The result is

$$\rho_o \frac{\partial u}{\partial t} = \frac{\kappa}{C_p}(\gamma - 1)\ \nabla^2 u \ . \tag{3.30}$$

Eq. (3.30) is now precisely in the form of an equivalent dissipation momentum due to the influence of heat conduction. To proceed to the solutions for space/time domain and frequency domain absorption coefficients, one need only recognize that the right-hand side coefficient of Eq. (3.30), $(\gamma-1)\kappa/C_p$, is multiplied by $\nabla^2 u$. This is exactly the same as the viscous dissipation case where $(\frac{4}{3}\eta + \eta_b)\nabla^2 u$ was the dissipation momentum in Eq. (3.4). Since $(\gamma-1)\kappa/C_p$ and $(\frac{4}{3}\eta + \eta_b)$ are both respective sets of constants, we may substitute $(\gamma-1)\kappa/C_p$ for $(\frac{4}{3}\eta + \eta_b)$ in Eqs. (3.9) and (3.10) to find the viscous time- and frequency-dependent intensity absorption coefficients without having to perform all the intermediate steps again. Thus, in the space/time domain

$$\alpha(x_o) = \frac{\kappa}{C_p} \frac{(\gamma - 1)}{\rho_o c |U_o|} | \nabla^2 u |_{x_o} , \tag{3.31}$$

while in the frequency domain

$$\alpha = \frac{\kappa(\gamma - 1)}{C_p} \frac{\omega 2}{\rho_o c^3} . \tag{3.32}$$

Eqs. (3.31) and (3.32) are absorption coefficients for intensity, and so they must be divided by two for acoustic pressure use. After division by two, Eq. (3.32) agrees with the result given by Kinsler *et al.* (1982, p. 148).

A concluding remark for this section concerns the comparison of equivalent equations of state, written in two different ways: one with the nonlinear coefficients A, B, C *etc.* per Chap. 2.4, and the other using γ {corrected from Beyer (1975), p. 99, using Gradshteyn and Ryzhik (1965)}:

$$p = p_o [1 + \frac{A}{p_o} s + \frac{B}{p_o 2!} s^2 \cdots] , \tag{3.33}$$

and

$$p = p_o [1 + \gamma s + \frac{\gamma(\gamma - 1)}{2!} s^2 \cdots] . \tag{3.34}$$

Traditionally, Eq. (3.33) is used for liquids, while (3.34) is used for gases. However, Eq. (3.33) is equally valid for gases by comparing the coefficients to the corresponding ones in Eq. (3.34). The resulting conversion is $B/A = \gamma$-1, and so the heat conduction absorption coefficients given by Eqs. (3.31) and (3.32) may be written in terms of B/A rather than γ for use with liquids. Also note that in the hypothetical case where γ=1, the isothermal condition for an ideal gas, then B/A=0, which implies there is no material-related nonlinearity. As an added note, I include the following remark from Blackstock and Hamilton (1993, p. D-14):

> "WARNING: Do not make the mistake of taking the mathematical replacement too literally. The ratio of specific heats γ for liquids is not $1 + B/A$. In the case of water, for example, $\gamma = 1.0006$ whereas $1 + B/A \doteq 6$."

3.4 Why the Absorption Coefficient is Always Negative

In the first section in this Chapter, I liberally used an absolute value term for both $\nabla^2 u$ and for the acoustic particle velocity. This section explains why the mathematical artifice of the absolute value really isn't needed, and why the absorption coefficient α must always be negative from a mathematical sense to be consistent with the obvious observations that acoustic waves decay due to losses. The remarks made in this section apply to acoustic losses of all three types, viscous, heat conduction, and relaxation, because they each rely on the ratio of $\nabla^2 u$ to u.

Consider Fig. 3-3, which shows part of an acoustic wave, where the total pressure is plotted against spatial position x, all viewed at one instant of time. The places on the wave where the slope of the wave is constant, thus $\nabla^2 u = 0$, are clearly marked (*i.e.* where the curvature is changing sign and direction). In between each of these regions, the shape of the curve is either concave or convex; mathematically, this means that $\nabla^2 u$ is either positive or negative. If we consider drawing a *hypothetical straight line* from one point where $\nabla^2 u = 0$ to the next, then we can define a local particle velocity, u_{loc}, from this line. The interesting feature that emerges is that when $\nabla^2 u$ is positive, u_{loc} must be negative; when $\nabla^2 u$ is negative, u_{loc} must be positive. Hence the ratio of $\nabla^2 u$ to u_{loc} must always be negative. This means that we didn't really need the absolute values used previously in this Chapter, and explains why the absorption coefficient must be negative. Sensibly, we knew the absorption coefficient must be so, *because absorption processes always work to straighten out the wave.* One could also argue that the absorption coefficient may be positive, but behavior of absorption always gives rise to a decaying exponential and so there is always a negative sign which must be present. This is more of a semantic argument than a physical one however.

There is some subtlety present in Fig. 3-3 that you won't find anywhere else thus far, *i.e.* you won't find it in any other text or paper on acoustics. It is that the absorption coefficient really depends on two things: first $\nabla^2 u$, and second on the notion of a local particle velocity u_{loc}, where the local particle velocity (and hence local acoustic pressure) is defined relative to a local ambient

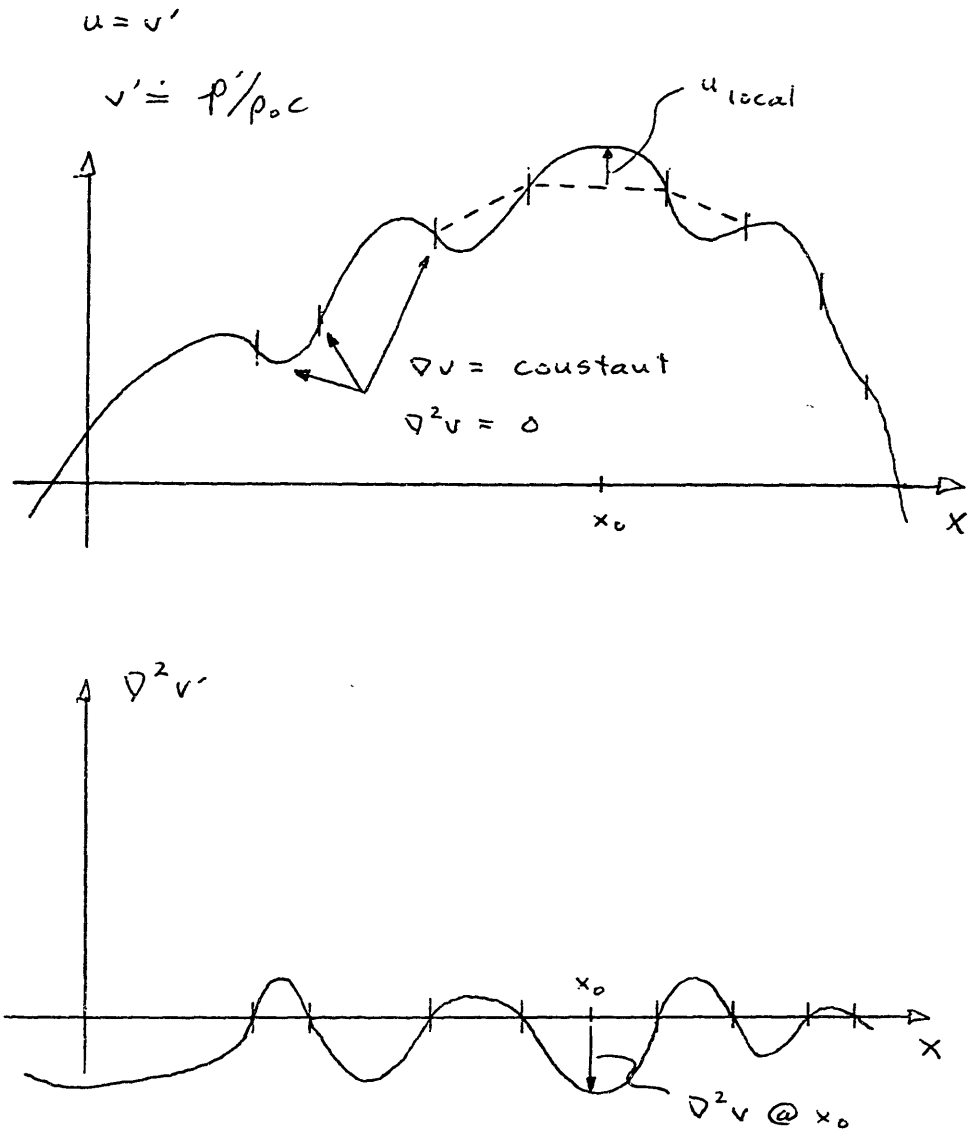

Fig. 3-3 $\nabla^2 u$ and u versus x; u_{loc} is defined in between $\nabla^2 u = 0$ locations.

pressure and *not* necessarily the ambient pressure extant in the problem. There is also an *assumption* made that u_{loc} is defined from some straight line connecting the pertinent $\nabla^2 u=0$ locations. This assumption is probably *close* to being correct, but there is no proof thus far. It turns out that this idea *must* occur for there to be a solid connection between the Fourier-based methods for correctly obtaining acoustical absorption in wide band or transient problems.

Having made these statements about the nature of acoustic dissipation, and the role of the ratio of $\nabla^2 u$ to u_{loc} in a wave packet slab Δx, the reader must be very careful in interpreting the notation in this chapter. The absorption coefficients are always functions of the neighborhood over which the calculation occurs. This means that the energy density, and hence local acoustic particle velocities, cannot be merely defined by using the ambient pressure as a reference. A local ambient must instead be defined. This is a major assumption that has been made in developing this entire chapter, and hence it provides part of the foundation for the entire thesis.

3.5 Absorption of Linear and Nonlinear Acoustic Waves

Now that the three major absorption mechanisms have been separately established for space/time domain use {Eqs. (3.9), (3.18) and (3.30)}, consider how these act on various types of waveforms.

We will first consider an acoustic sine wave, as shown in Fig. 3-4. From the preceding discussions, and for sufficiently low frequencies, all three absorption phenomena combine to give an α proportional to ω^2. Hence absorption, acting on a propagating sine wave, imparts a decaying envelope on the amplitude of the wave as it travels. However, the wave retains its sinusoidal appearance, so the absorption does nothing to alter the frequency content of the wave: an acoustic sine wave influenced by absorption is still a sine wave. This is illustrated by the absorption weighting function, also shown in Fig. 3-4.

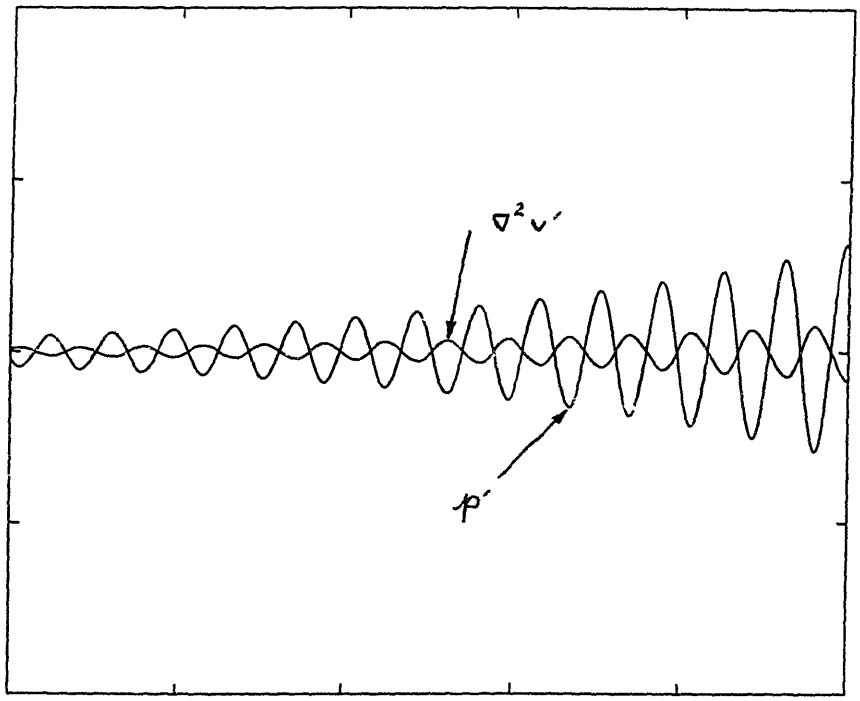

Fig. 3-4 Sine pressure wave (with decay taper) and accompanying $\nabla^2 u$.

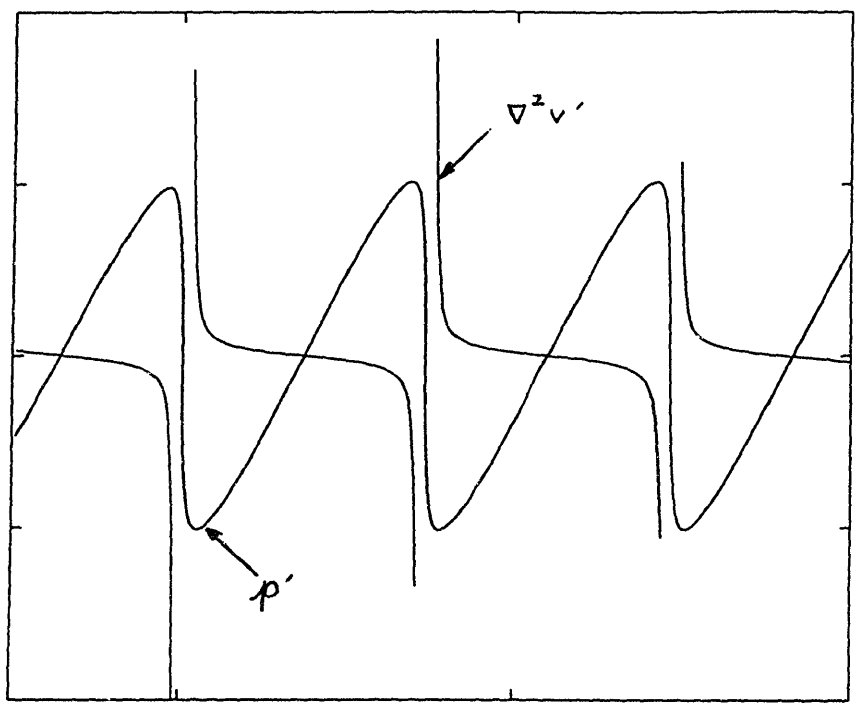

Fig. 3-5 Sawtooth pressure wave and accompanying $\nabla^2 u$.

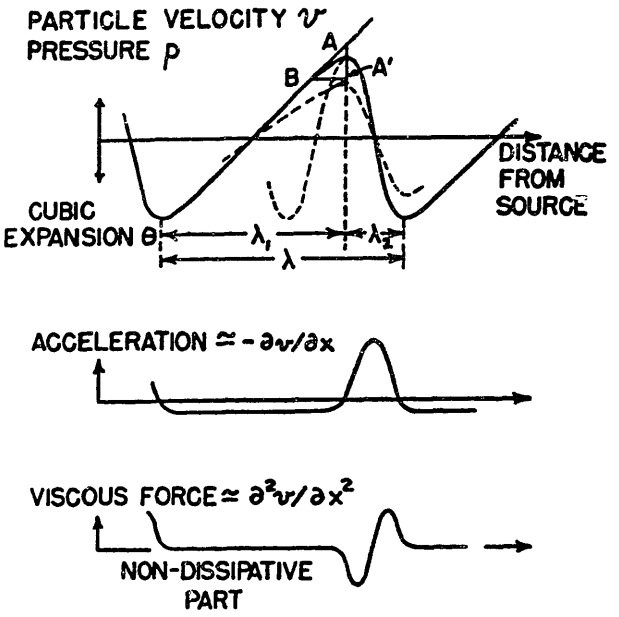

FIG. 1. Pressure, elastic force, and frictional force in a plane wave traveling along Ox. Completed to a full wave, the dissipative part would have the wavelength $2\lambda_2$.

Fig. 3-6 J.S. Mendousse's (1953) concept. Mendousse had the notion that the viscous dissipation acting on a nonlinear wave was proportional to $\nabla^2 u$. He also made the assumption that the absorption is virtually zero everywhere in a sawtooth wave except in the shock region, and he approximated this by fitting a portion of a high frequency sine wave in the region of each half shock.

Now consider an acoustic sawtooth wave, reminiscent of the teeth on a carpenter's sawblade, as depicted in Fig. 3-5. For convenience, the fundamental wavelength, or $c \cdot T_p$ where T_p is the wave period, is the same as the sine wave in Fig. 3-4, and the peak amplitudes in both Figures are the same. Since the wave is not composed of a single frequency, the simple sinusoidal absorption coefficient $\alpha(\omega)$ used for Fig. 3-4 cannot be used here; instead, the space/time domain absorption $\alpha(x_o)$ must be used, from section 3.1. The absorption weighting for the sawtooth wave is then a doublet function, with the spikes of the doublet acting on the maxima and minima in the sawtooth: the peak and the trough; elsewhere along the wave, the absorption is zero. Note that the wave pictured could be a linear acoustic wave (which won't undergo cumulative distortion during travel) or a nonlinear acoustic wave (which will distort with travel). The key is that they both have a sawtooth shape and so they will both experience doublet-like dissipation *near* the saw teeth peaks. The linear acoustic wave will of course rapidly be dissipated and the teeth will become rounded. The nonlinear acoustic version however, will try to maintain its sharp teeth state because the amplitude are high enough (via the $\beta v'$ term in the wave speed) to feed the shock. So the rate at which the shock is fed by the nonlinear distortion exactly balances and so the sawtooth shape is maintained, at least for a while. This is called a stable shock condition.

The idea of the doublet acting on the sawtooth wave is not new, since it was first proposed by Mendousse (1953). His illustration is repeated here as Fig. 3-6. The illustration also shows the difference between a true doublet acting on a perfect, sharp-cornered sawtooth wave per Fig. 3-5, and a realistic doublet-like $\nabla^2 u.$ acting on a sawtooth wave with dull rounded teeth.

Mendousse used, in his own words, a "simplified-picture theory" to obtain both the viscous dissipation region (at the doublet) and the non-dissipation region (everywhere else besides the doublet region). Mendousse's work lay dormant for over ten years before it received considerably more attention as the study of nonlinear acoustics became more popular (*i.e.* there was more funding). The space/time domain development of viscous absorption in section 3.1, as illustrated acting on a sine wave and a sawtooth wave, proves Mendousse's

hypothesis albeit in more rigorous fashion. Mendousse made the *assumption* of the viscous dissipation force and showed it in the Figure reproduced here; the work shown in section 3.1, in contrast, started with the Navier-Stokes equation, lifted the viscous force term from it, and proceeded into a balance of the stored energy density flux (or intensity) for the wave initially, and set it equal to the integral of the energy density flux loss due to dissipation. The result was a space/time domain form of the dissipation coefficient $\alpha(x_0)$. An extension of the same basic procedure also resulted in similar expressions for space/time domain absorption for relaxation and heat conduction phenomena. These components for heat conduction and relaxation could likewise be shown in a similar fashion as Mendousse's reproduced illustration in Fig. 3-6.

Lighthill (1956) wrote a monograph on the subject of the dissipation of nonlinear sound waves, but his treatment of viscous absorption and relaxation is written, like later works, in terms of ω rather than in the space/time domain. Blackstock (1988) discussed work by Carstensen (1982), where an operational definition of absorption was based on $\alpha = -\nabla \cdot \mathbf{I}/(2I)$, where I is the sound intensity and α is the total absorption in a nonlinear acoustic wave. These could be regarded as alternate ways to deal with absorption.

3.6 Absorption of Liquids, Solids and Bio-Materials

In the theory presented in preceding chapters, it was assumed that the three fundamental absorption characteristics apply to fluid materials such as liquids and gases, and hence the absorption always has an ω^2-dependence to it, except near a relaxation frequency. This is generally true. In other materials, like solids and biological materials, this isn't exactly correct. Many materials, including viscoelastic rubbers and animal tissue, exhibit absorption that has more of an ω-dependence, rather than a ω^2-dependence. These materials also have absorption characteristics for wave types other than the fluid compression-rarefaction one considered in this thesis. These other wave types include shear and interface waves.

I won't digress further on these matters other than to make the reader aware of them. Absorption dependent on ω could, in principle, be constructed by the use of multiple relaxation frequencies, by staggering them across the frequency axis. The staggering could be uniform, or it could be irregular. A uniform, and fairly close placement of relaxation frequencies would give an absorption curve resembling ω^n, where n is non-integer $0 < n < 2$. If the placement of these frequencies were far apart, then discrete steps in absorption would be seen, as in the case of sea water and in air.

I haven't taken the time to thoroughly dig into the literature on the absorption of rubbers and bio-materials in an attempt to quantify the known data (other than the papers by Goss *et al.*, 1978, 1980), and to see if any such steps occur. My guess is that they don't, because the composite nature of such materials leads to a blurring of the many relaxation frequencies, rendering an absorption vs. frequency plot relatively smooth, and with a tidy exponent of uniform n. The only other obvious test that could be made is to test such materials at both very high and very low frequencies, and look for a departure from ω^n.

After I had formulated the time-domain absorption coefficients in this chapter, I noted that none of the three could account for the approximate ω-dependence of most biological tissues, *except* for a cascade of relaxation frequencies. Sometime later, during the writing of this document, I read a preliminary draft of a presentation abstract by Li and Blackstock (1993) where they had modeled the absorption of finite-amplitude ultrasound (*i.e.* nonlinear ultrasound) in biomedical tissue by modeling the tissue as a medium with multiple relaxation frequencies. This is apparently not a new idea since I also found that Fry (1952) observed the ω-dependence could be explained by a spectrum of relaxation processes. A good summary of the linear dependence of absorption with frequency for biomaterials is given among several papers in the book *Ultrasonic Biophysics*, edited by Dunn and O'Brien Jr. (1976), which begins with the classic paper by Pohlman (1939).

A more recent view of relaxation dissipation, based on polymers, but generally applicable to other materials, is given by Hartmann *et al.* (1994). This paper

reviews the theoretical attempts to fit the observed measurements to various equivalent mechanical models involving springs and dampers (dashpots). The best fit occurs using the Havriliak-Negami (HN) model; Hartmann *et al.* also point out that the HN model equation "is equivalent to a particular distribution of relaxation times, that is, a continuous distribution of single relaxation time models or Maxwell models."

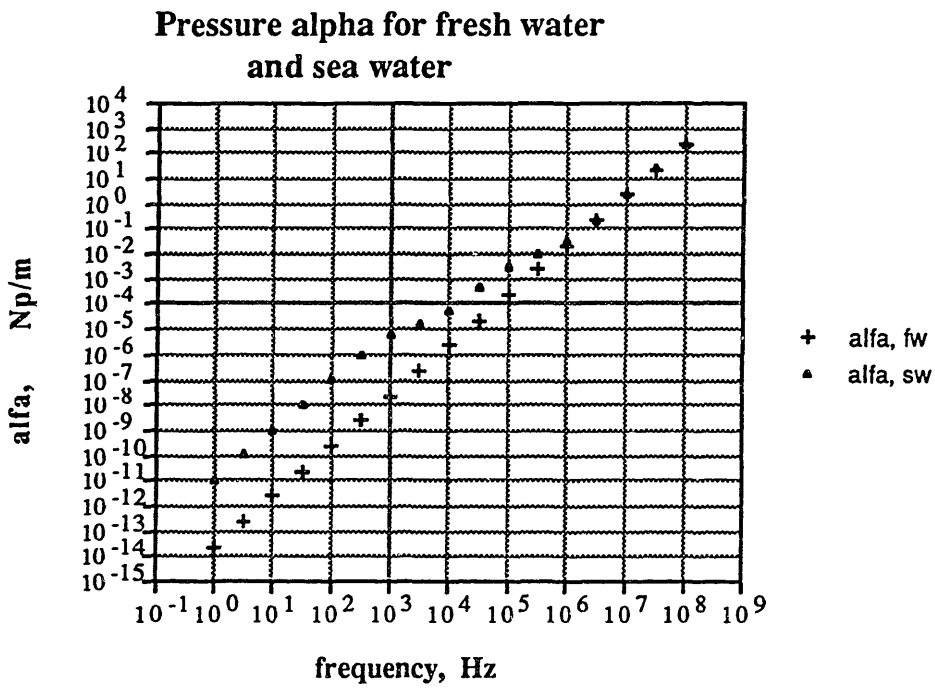

Fig. 3-7 Pressure absorption coefficient versus frequency for fresh water and sea water based on sinusoidal input wave of any amplitude.

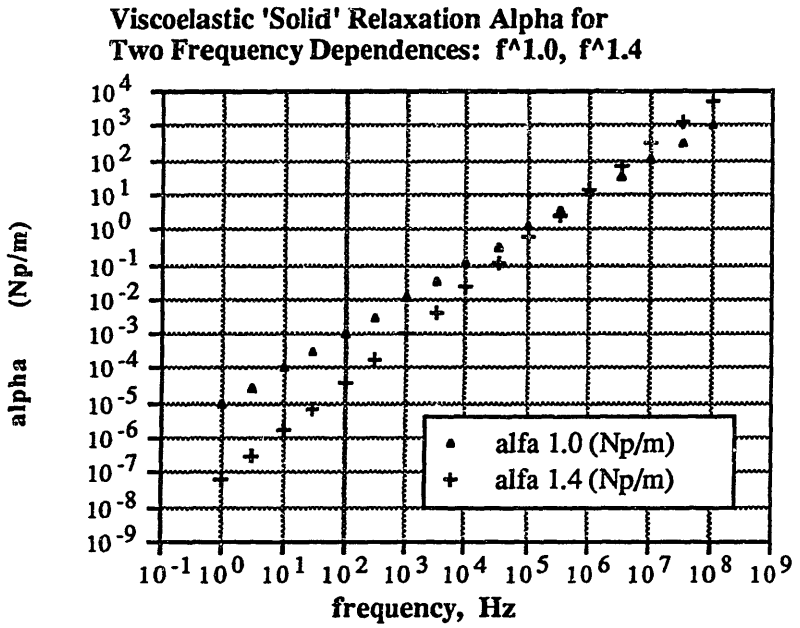

Fig. 3-8 Pressure absorption coefficient versus frequency for a viscoelastic fluid-like material having a relaxation-dominant ω^n dependence. This example shows two α for ω^1 and for $\omega^{1.4}$.

Lastly, Figs. 3-7 and 3-8 show the absorption coefficients calculated in the space/time domain (*i.e.* using the material in this Chapter) for several of the fluids and quasi-fluids used in this thesis. They were obtained directly by calculation based on viscosity, heat conduction, and relaxation parameters for sinusoidal waves.

---

[1]see Stokes, G.G. (1851), and Pierce, A.D. (1989), p. 13.

[2]Kinsler *et al.* (1982), p. 146-147, by including the bulk viscosity.

[3]Kinsler *et al.* (1982), Fig. 7.1 on p. 142.

[4]Mellen, R.H. *et al.* (1979) identify a third chemical relaxation involving magnesium and carbonic acid, that exists between the relaxation for $B(OH)_3$ and $MgSO_4$. This relaxation is not included in the model for this thesis, although it could be readily added.

---

[5]*op. cit.*, p. 145, eqn. (7.21).

[7]Lindsay, R.B. (1960), pp. 334-351, especially 347-349.

[8]Pierce, A.D. (1987). See pp. 13-14, Eq. (1-4.6), and pp. 34-36. Pierce used s for entropy, whereas in this thesis s_e is used to avoid confusion with the condensation s.

FLOWCHART for COMPUTATION

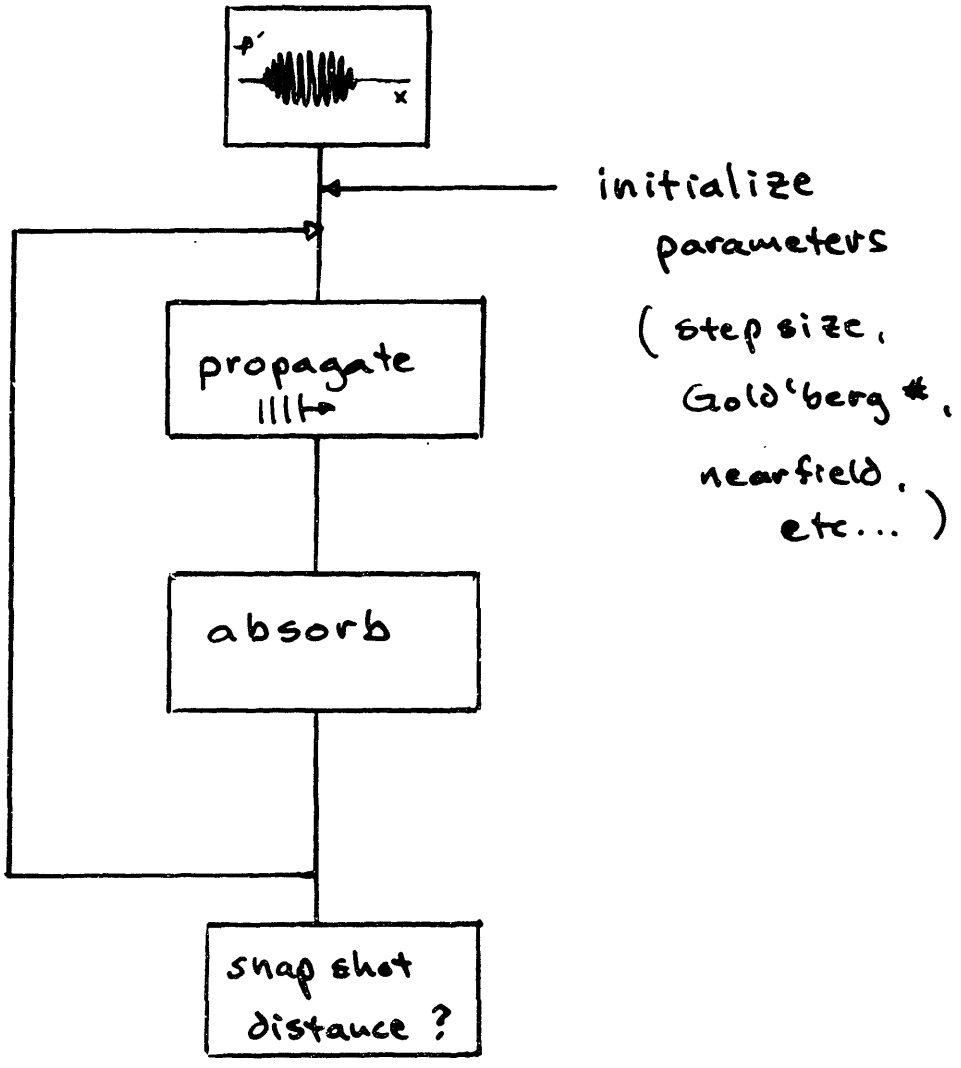

Chapter 4

Computational Approach

This chapter describes the computational approach used to model nonlinear propagation of acoustic waves and shocks. It treats a number of issues separately, and each of these is implemented in an ensemble in the computer code used to model the time-domain nonlinear propagation of acoustic waves in lossy fluids.

4.1 The Wave Packet Approach

In the derivation of the nonlinear wave equation shown in Chapter 2, the speed of any particular point on a wave was shown to be $c = c_0 + \beta v$. In essence this means that different points on the wave travel at different speeds, in an uncoupled manner. The coupling comes from the dissipation components shown in Chapter 3, because each particles' speed maps directly to acoustic pressure, and thereby can influence neighboring particles by the action (predominantly) of the $\nabla^2 v$ absorption terms. The notion of allowing wave parts, or particles, to travel at different speeds based on the nonlinear wave speed and of using this model in a computational algorithm was first done by Fox and Wallace (1954). Other investigators have also used the same basic technique, including Cook (1962), Van Buren and Breazeale (1968), Pestorius (1973) and others. These authors each used different approaches to inject dissipation into their models, although most used some version of a Fourier approach, and most avoided allowing solutions that would form shocks. Pestorius excluded dissipation in the fluid and included tube-wall boundary

dissipation, but again, like his predecessors, used a Fourier approach to apply it in the model. Pestorious referred to his propagation model as a *phenomenological approach*; other investigators may have also used this term. I have instead adopted the term *wave packet approach* (WPA) in this thesis because the approach combines the nonlinear propagation part used previously by these and other authors with space/time domain dissipation that allows quasi 1-D linear, nonlinear, and shock problems to be modeled.

The implementation of the WPA is simple. A finite duration, initial acoustic waveform is defined in the program by the use of a control file called *DECK*. This file contains information about the frequency, amplitude and duration of the pulse, as well as the type of fluid for the problem. The waveform is discretized into point sampling, with *npoints* (20 or greater) per base wavelength in the problem. The program automatically determines propagation step size, *deltax*, based on how strong the nonlinearity is and/or based on the fundamental absorption of a linear acoustic wave. The propagation step size automatically changes as the waveform propagates; *deltax* is smaller for a shock, and it increases as the shock diminishes and as the linear acoustic problem eventually prevails. For a typical nonlinear acoustic problem, *deltax* is set equal to 1/30-th of the dissipationless plane wave shock distance, which is on-par with Van Buren and Breazeale (1968), who used 1/20-th of the dissipationless plane wave shock formation distance. These are both conservative step sizes, since geometrical spreading (*i.e.* non plane wave) and absorption always extend the actual shock formation distance beyond the dissipationless plane wave estimate.

The program, *pulse.out*, reads the information from *DECK* and then proceeds. The two basic steps involved are propagate all points on the wave, and apply absorption on the whole wave. The wave distortion results largely from the nonlinear wave speed, and so each point on the wave (*i.e.* each Δx slab, or wave packet) moves at a slightly different speed than its neighbors. This causes the wave shape to slowly deform after each full wave, *deltax* step. Hence the self-distortion of an acoustic wave occurs cumulatively. After each step, $\nabla^2 v$ is calculated for each point on the wave based on a three-term Taylor series estimate (*e.g.* see Abramowitz and Stegun, 1972), after which the actual

dissipation for each point can be separately calculated, and applied. So long as both the self-distortion (from the nonlinear propagation) and dissipation occur gradually, by choosing a propagation step size small enough, then the actual combined nonlinear-dissipation effects present will manifest themselves in a smooth manner, and mimic the behavior of real acoustics.

Thus the WPA proceeds, computationally, by marching the wave pulse in discrete steps along the direction of sound propagation. A key question then is: what should the propagation step size be? This is answered by considering two limits: a limit distance based on the sound absorption for a linear acoustic wave, and the limit distance at which a shock forms for a nonlinear, but lossless, acoustic wave. These will be explored next.

4.2 Propagation Step Size per Linear Acoustic Absorption

The initial propagation step size from a linear acoustic absorptive wave viewpoint is determined from the consideration of the intensity loss in a wave as it travels. We start with

$$I(x) = I_0 - \Delta I , \tag{4.1}$$

which was a starting point for calculating the absorption coefficient in Chapter 3. $I(x)$ is the intensity of a slab in a wave packet at x, I_0 is the initial intensity of the slab in the wave packet, and ΔI is the incremental intensity loss. As in Chapter 3, we can take the initial intensity in the slab, I_0, and the downstream intensity $I(x)$ as having the same units, of the form

$$I_0 = \frac{p_0'^2}{\rho_0 c} = \rho_0 c\, v_0'^2 , \tag{4.2}$$

$$I(x) = I_{new} = \frac{p_{new}'^2}{\rho_0 c} = \rho_0 c\, v_{new}'^2 , \tag{4.3}$$

with v_0' as the initial particle velocity in the slab, and we define v'_{new} as the particle velocity in the same slab after the ΔI loss. For this discussion and for

notational simplicity, the loss in intensity, ΔI, can be considered to be due to viscosity only, and given by

$$\Delta I = \left(\frac{4}{3}\eta + \eta_b\right) \cdot v'_o \cdot \Delta x \cdot \nabla^2 v \,. \tag{4.4}$$

Losses due to heat conduction or due to relaxation will take a very similar form. Making these substitutions, we have

$$v'_{new} = v'_o \sqrt{1 - \underline{\left[\frac{4}{3}\eta + \eta_b\right] \Delta x \cdot \frac{\nabla^2 v}{\rho c v'_o}}} \,. \tag{4.5}$$

The term inside the radical is the part we need to concentrate on. Since absorption occurs incrementally, in small quantities, for each incrementally small propagation step Δx, then the underlined term above must be much less than one. Writing this and solving for the propagation distance step Δx we have

$$\Delta x << \frac{1}{\left[\frac{4}{3}\eta + \eta_b\right] \cdot \frac{\nabla^2 v}{\rho c v'_o}} \,. \tag{4.6}$$

If the wave is sinusoidal, the term $\left[\frac{4}{3}\eta + \eta_b\right] \nabla^2 v/(\rho c v'_o)$ is known as the viscous absorption coefficient for intensity; hence:

$$\Delta x << 1/\alpha_{intensity} \,,$$

or

$$\Delta x << 0.5/\alpha_{pressure} \,.$$

If the wave is not pure tone sinusoidal, but rather composed of several frequencies, the above restriction should then be applied for the highest frequency in the wave. This will ensure that the propagation step size Δx will always be small enough for any frequency in the problem. Hence, the requirement placed on the allowable size for the propagation of a linear

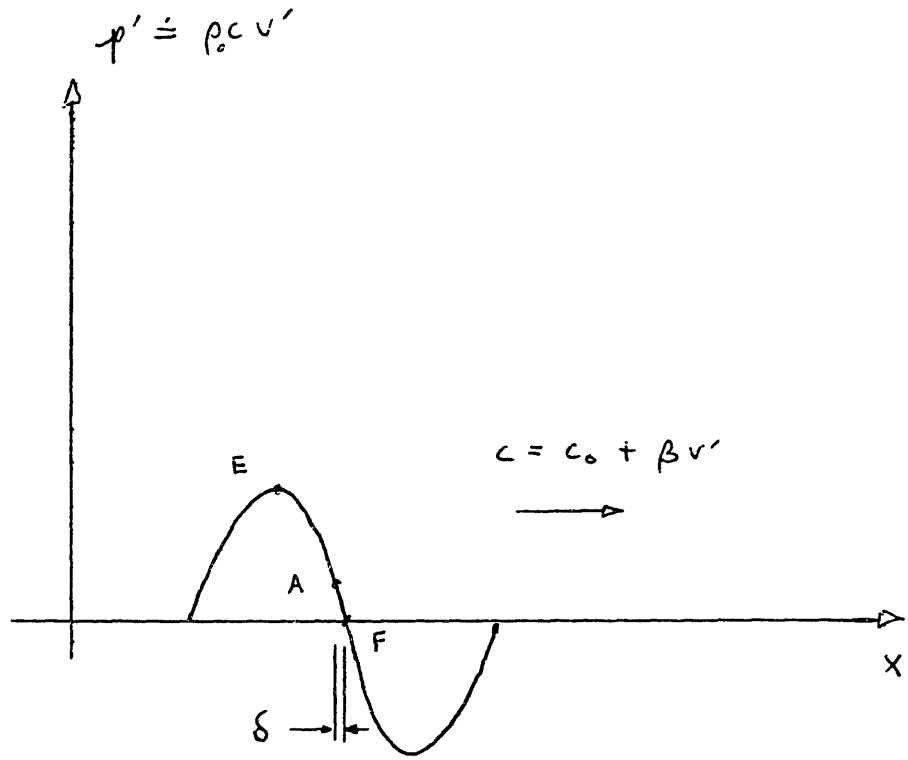

Fig. 4-1 Development of the distance to shock for a plane dissipationless sinusoid.

acoustic wave is that the step size should be much smaller than the inverse of the intensity or pressure attenuation coefficient for the highest frequency in the problem.

4.3 Propagation Path Step Size per Shock Distance Method

The second way to determine the initial propagation step size is to consider at what distance the wave will form a shock, *i.e.* the shock formation distance. Then we let the computational propagation step size be some small fraction of this number. The term shock refers to a near-vertical section in a p-t, or p-x waveform, where the near-vertical part has a slope magnitude that is substantially larger than any other part of the wave, either now or at any previous view of the waveform. Mathematically, shocks are often assumed to have a perfectly vertical segment (*i.e.* infinite slope) with the peak-to-peak thickness in x or t being identically zero. In practice and in this work, a shock has a large but finite slope, and a non-zero thickness across the shock as measured from the 95% to the 5% values of the peak-to-peak extent.

Other authors have described the shock formation distance from a number of distinct approaches. The two shown here seem the most appropriate to the WPA; the first was also identically shown in Stephens and Bate (pp. 485-486, 1966).

Consider the single pressure cycle of a dissipationless plane wave train shown in Fig. 4.1, in which there are two points labeled E (at a wave crest) and F (at a zero crossing). As the wave travels in the positive x-direction, the wave will distort and eventually a shock will form. If we define the distance from the wave location to the shock formation location as d, we can write the following:

$$\text{for E: } (d + \lambda/4)/\Delta t = c_0 + \beta v' , \tag{4.7}$$

and

$$\text{for F: } d/\Delta t = c_0 , \tag{4.8}$$

and recall that $\beta = B/(2A) + 1$. Solve each for d and then solve simultaneously:

$$\Delta t = \lambda/(4\beta v') \ . \tag{4.9}$$

Hence the distance to shock is

$$\Delta X = \lambda/(4\beta\varepsilon) = (\pi/2)/(\beta\varepsilon k) \ , \tag{4.10}$$

where the acoustic Mach number is given by $\varepsilon = v'/c_0$. Strictly speaking, this result gives the *distance to full saturation* across the shock front; *i.e.* a vertical discontinuity in acoustic pressure occurs fully from peak-to-peak (trough). Full saturation therefore means a full sawtooth wave. For an initially sinusoidal wave, the shock will actually form at the acoustic pressure zero crossing first; as the wave proceeds thereon, the shock will then occupy more of the peak-to-peak amplitude until full saturation occurs, and the sawtooth wave results. Note the the use of the word *saturation* implies that the spectrum of an initially sinusoidal wave (a delta function at the wave frequency ω) shifts until the resulting spectrum (of the sawtooth wave) is *filled* harmonically above ω.

A second wave to calculate the shock formation distance is to find the distance at which the shock *first* forms. For an initially sinusoidal wave, the shock will first form near a zero crossing in pressure. Consider two points of acoustic particle velocity on a sine wave, A and F, where A is very small and close to F, and F is again at zero acoustic velocity. Along x, the point spacing between A and F is δ, and we again assume that the shock begins to form at d somewhere on the x-axis.

$$\text{for A: } (d + \delta)/\Delta t = c_0 + \beta v' \ , \tag{4.11}$$

and

$$\text{for F: } d/\Delta t = c_0 \ , \tag{4.12}$$

and recall that $\beta = B/(2A) + 1$. Solve each for d and then solve simultaneously:

$$\Delta t = \delta/(\beta v') \ . \tag{4.13}$$

Since we began with a sine wave, the maximum slope (dv/dx) at the zero crossing is

$$\text{max slope} = k\, V_{max} = (v_A - v_B)/\delta = v_A/\delta \tag{4.14}$$

where $k = \omega/c_0$. If we note that v' in Eq. 4.13 is really v_A, we can substitute Eq. 4.14 into Eq. 4.13, then multiply by c_0 to find the distance to shock:

$$\Delta X = 1/(\beta\varepsilon k) , \tag{4.15}$$

which is exactly the same result given by Blackstock (1993) from a different approach. The distance ΔX is an underestimate because it ignores the effect of dissipation and geometric spreading which tend to retard shock formation. In fact, if there is sufficient dissipation due to the various acoustic losses, or sufficient spreading, or the sound pulse isn't that strong, or some combination thereof, a shock will never form. A useful estimate for whether a wave will form a shock, in the plane wave case, is given by the Gol'dberg number Γ [p. 120 in *Nonlinear Acoustics* by R.T. Beyer, (1975)], which is the dimensionless ratio of $1/\alpha$ for linear absorption to the shock formation distance ΔX, where α is the pressure absorption coefficient.

Generally speaking, if $\Gamma << 1$ then the wave will not form a shock and if Γ is small enough, the wave will behave in a linear acoustic manner. This situation is the one that applies to the most problems that acousticians study, but they seldom use this particular argument as justification. Instead, they rely only on the argument of a small acoustic Mach number $\varepsilon = v'/c$ which, they reason, is enough to discard the higher order terms in the wave equation. This is fallacious reasoning. If ε is small, then it is safe to discard higher order terms in the wave equation, but *only within the confines of the control volume specified for wave equation derivation.* Outside this control volume, if Γ is large enough, the *wave will distort and may even form a shock.* So even though the Mach number is small, the problem may still be nonlinear. The only safe way to determine if an acoustic problem is linear (if $\Gamma << 1$) or nonlinear is by a calculation of the Gol'dberg number, or by some equivalent calculation. Wave equation considerations are not enough.

On the other hand, if Γ is approximately 1 a shock will form. If $\Gamma >> 1$, then a shock will form and it will probably saturate.

The evaluation of the Gol'dberg number, and variations on it for planar (as shown here), cylindrical, or spherical geometries is discussed at length in

many papers and texts on nonlinear acoustics (especially by Blackstock) and so it will not be further reviewed. Computationally, it will always be safe to calculate the Gol'dberg number Γ for a plane wave and apply it to cylindrical or spherical problems because spreading always retards the formation of the shock since the wave intensity decreases with propagation. So the planar Gol'dberg number provides a conservative estimate of whether a shock will form, and the dissipationless shock distance ΔX provides a conservative shock distance estimate. Computationally, the sensible choice for the size of a discrete propagation step would then be some fraction of the smaller of either the Δx (from the linear acoustic approach in section 4.2), or the shock formation distance ΔX in this section.

4.4 Other Comments

Strictly speaking, the coefficient of nonlinearity β should be evaluated at every distinct discretization point along the wave. Hence the fluctuation of β along the wave will mimic the wave behavior; an example is a sinusoidal pressure wave, where β along the wave has a *small* sinusoidal deviation about the mean β value. A recent paper by Cotaras and Morfey (1993) offers separate polynomials to evaluate β for sea and fresh water, based on the relations for sound speed c of Chen, Millero *et al.* (see Cotaras and Morfey, 1993, for the full references of Chen, Millero *et al.*), so a pressure-, temperature- and salinity-sensitive β could be implemented. For now, however, fixed values for β in fresh water, sea water, air, glycerin and tissue-like fluids are used.

4,349,898

43.25.Lj SONIC WEAPON SYSTEM

William Drewes, Bronxville, New York, and Edward M. Vlicki, Elmwood Park, New Jersey, assignor to William Drewes
14 September 1982 (Class 367/138); filed 9 November 1978

This formidable weapon emits no ordinary sound, but rather a pumped beam of parametric sound which it generates and collimates in a highly imaginative manner. A further degree of sophistication is contributed by a laser 19 which, together with an interferometer and a frequency analyzer, measures the movement of the target 18. A jet engine 12 is aptly called the raw acoustic source. The sound it generates passes through a set of 11 tubes which are closed at their ends by synchronously rotating shutters, like siren blades, that supposedly transform the continuous spectrum of the jet noise into a line spectrum of 11 components spaced at octave intervals from 5 to

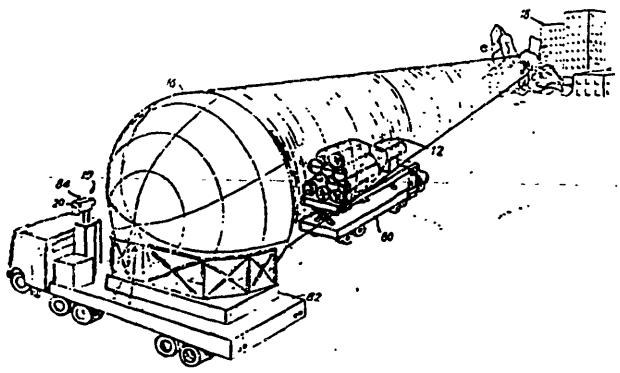

5120 Hz. The sound is collimated in a narrow beam by a 50-ft diam reflector 16, and directed toward the target. With acoustic intensities so high that the air behaves nonlinearly, the 5120-Hz component pumps the 2560-Hz component, which in turn pumps the 1280-Hz component, and so on. The components of interest are at 5, 10, and 20 Hz, which presumably are in the range of resonances of the structures to be destroyed. By virtue of the pumping phenomenon, these low-frequency components are confined in the same narrow beam as the highest (5120-Hz) component. Consequently, they propagate without spreading loss, and maintain an intensity sufficient to destroy large buildings at a range of 5000 ft. This thing could be quite annoying until someone finds a way to quiet it.—LB

Chapter 5

Applications and Phenomena

This chapter is devoted to specific applications in several areas of nonlinear acoustics. Each application uses the wave packet approach (WPA) propagation model described in Chapter 1 and justified in Chapter 2, each uses the absorption terms derived from the time domain viewpoint in Chapter 3, and each is implemented computationally using the methods shown in Chapter 4. The applications begin with parametric sonar and medical ultrasound heating; these two topics were the original motivators for the thesis.

The next two items considered are pulse self-demodulation, and shock waves. The self demodulation of a pulse, a description first provided by H.O. Berktay (1965), is a classic demonstration of nonlinear acoustics. Shock waves, the ultimate result of nonlinear acoustic steepening, are next considered. The main issue of exploration is the concept of the "equal-area rule" for handling the purely mathematical result of a multi-valued acoustic wave. Multi-valued acoustic waves cannot exist in the same way that a breaking surface hydrodynamic wave exists, and yet the lossless mathematical theory popular today permits such a solution. This unphysical result is handled by the the equal-area-rule of weak shock theory, which reshapes the wave to remove the multi-value part of the wave. This method also induces a form of energy dissipation even though the mathematics include none of the conventional absorption types (viscosity, heat conduction, relaxation). Why does this method give reasonable results as compared to experiments? What happens when the usual absorption phenomena are also included in the propagation

model? Is the equal-area-rule even necessary? These are important questions that have not, apparently, been investigated thoroughly.

5.1 Parametric Sonar

Parametric sonar, the notion of using nonlinear acoustic mixing in the water to form a difference frequency tone f_d, where $f_d = |f_2 - f_1|$, from two parent tones at f_1 and f_2, and where $f_d << f_1$ or f_2, was and probably still is the most useful application of nonlinear acoustics. The benefit is that a highly directive source is obtained at the difference frequency because the sonar main beam at f_1 and f_2 forms a virtual line array of f_d sources in the water that are phased to add constructively along the beam axis, and virtually nil elsewhere. So the parametric source is highly directive even though it issues from a real source (*i.e.* the sonar transducer) having a dimension (diameter *e.g.*) which is usually much smaller than a wavelength at λ_d ($c_o = \lambda_d f_d$). To obtain the same directionality at f_d would require a sonar transmitter with a much larger aperture, sometimes impractically so. The disadvantage of the parametric sonar is that it is notoriously inefficient, on the order of 35 to 70 dB below the level of the acoustic primaries f_1 and f_2. At the very best, the parametric sonar is on the order of 1% efficient, a number on-par with the best explosive and sparker sources. Parametric sources in general are described in the books by Novikov *et al.* (1987), in the NUSC book *Nonlinear Acoustics 1954 to 1983*, and among many other citations in the bibliography.

This section will specifically deal with replicating the parametric sonar work of Halsema (1992), work that was performed in Boston Harbor. The features of the actual experiment are shown in Table 5-1.

During the conversion efficiency test, the measurement hydrophone was placed 293 m from the source and two electrical signals were added, and then amplified to drive the single sonar transducer. One signal was pulsed cw at 184 kHz and the second was pulsed pseudorandom modulated sequence (PRMS) centered at 174 kHz with a 10 kHz bandwidth. These two signals were

Table 5-1 Parametric Sonar, Boston Harbor Experiment

sea water, sound speed c_o	1485 m/s, measured
transducer:	
diameter	.33 m
elec. input	75 W, each signal
$Q_{acoustic}$	13.7
efficiency η	.16 (off resonance)
DI	40.7 dB
pulse duration τ	51 ms
primary signals:	
SL	222 dB re μPa, 1 m each (*i.e.* p' = 126 kPa surface, each)
f_1	184 kHz cw
f_2	174 ± 5 kHz pseudorandom
hydrophone range	293 m.
measured results:	
difference frequency	10 kHz ± 5 kHz
acoustic level	171 dB re μPa
conversion efficiency	-51 dB re primaries

N.B. parameters taken from, or adapted from, Halsema (1992).

superposed, amplified and used to drive the sonar piston transducer. The pulse duration for both signals, driven simultaneously, was 51 milliseconds, a long duration required by the maximum length sequence used to create the PRMS.

I made a few slight modifications in my simulation. I use two cw waveforms purely out of convenience and due to array space limitations on the computer, and I use Q = 2.9 rather than the actual, Q = 13.7; this allows the waveforms to quickly reach steady state. The use of 184 kHz and 174 kHz cw signals, the primaries, allow a pulse duration of 0.6 millisecond, hence giving 110 and 104 full cycles respectively of the primaries, and eventually after nonlinear mixing, approximately 6 cycles at the difference frequency of 10 kHz. Fig. 5-1 shows the waveform 'launched' into the water. There is no distortion here, as this is the startup waveform. The figure is an acoustic pressure vs. time trace, which is then converted and 'flipped' to be viewed in a p'-x format. This was done purely out of convenience because it is easier to see nonlinear self distortion of the wave in a position format rather than in a time format (as viewed on an oscilloscope *e.g.*). In this type of view, which will be used throughout this thesis, the wave always travels to the right. The individual cycles are nearly impossible to see on this scale, but the interference of the two frequencies is clear, with the formation of deep amplitude nulls.

Figs. 5-2 and 5-3 show a pair of p'-x plots, taken at positions close to the transducer. The plots shown on the top are the actual p'-x trace that would be observed, while each bottom plot is a low pass filtered version of the accompanying plot above. Since we expect a difference frequency near 10 kHz, the filtering is low pass with a Hanning taper. The -3 dB limit was set at approximately 11 kHz, thereby placing a null at approximately 22 kHz. The Hanning taper provides a -32 dB peak sidelobe and a -18 dB per octave rolloff in the sidelobe response, to ensure that the primary waves will be -54 dB relative to any difference frequency wave. The plots were obtained at 2 and 4 meter distances which would technically place them in the near field of the transducer (near field limit is approx. 10.3 m). The model used here is a quasi-plane wave, so there is no appearance of near field minima and maxima.

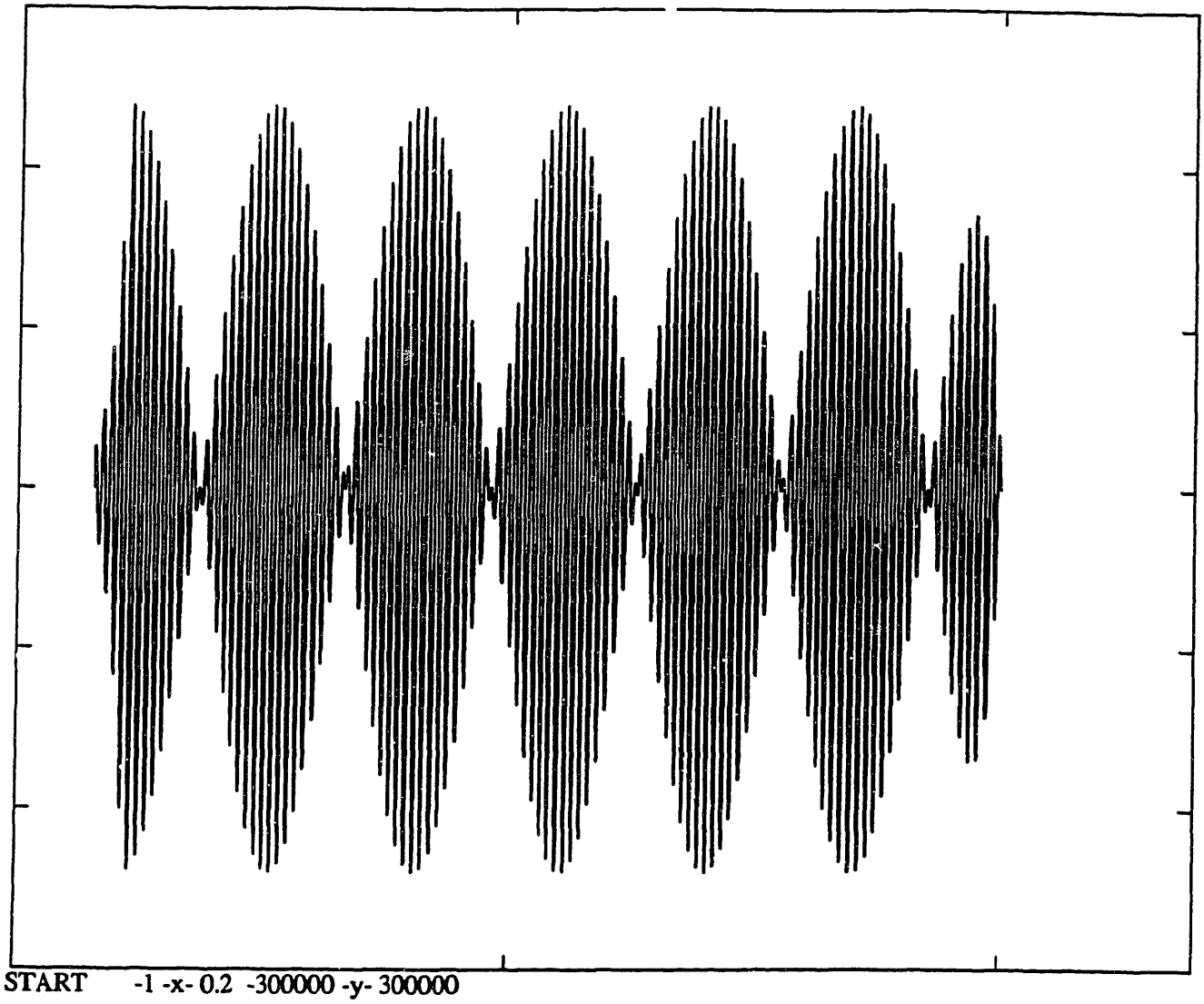

Fig. 5-1 Computational model of the Boston Harbor parametric sonar experiment. Startup waveform. Two cw tones, at 174 kHz and 184 kHz are transmitted simultaneously for 0.6 ms, giving about 104 and 110 cycles of each wave respectively. The interference between them gives rise to the amplitude modulation. Scales: p' in Pascals, x in meters.

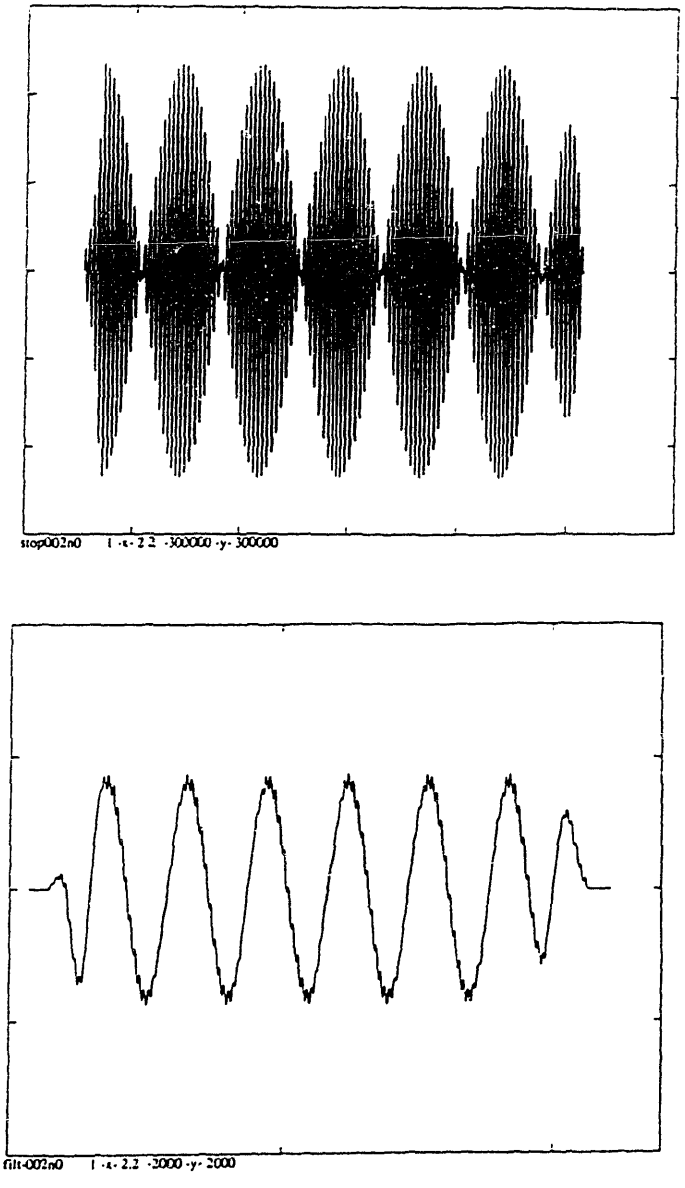

Fig. 5-2 Computational model of the Boston Harbor parametric sonar experiment. x = 2.0 m data. Upper: unfiltered; lower: filtered at 11 kHz low pass Hanning. Difference frequency wave at 10 kHz clearing visible in lower graph. Conversion efficiency approximately -49.5 dB. Scales: p' in Pascals, x in meters.

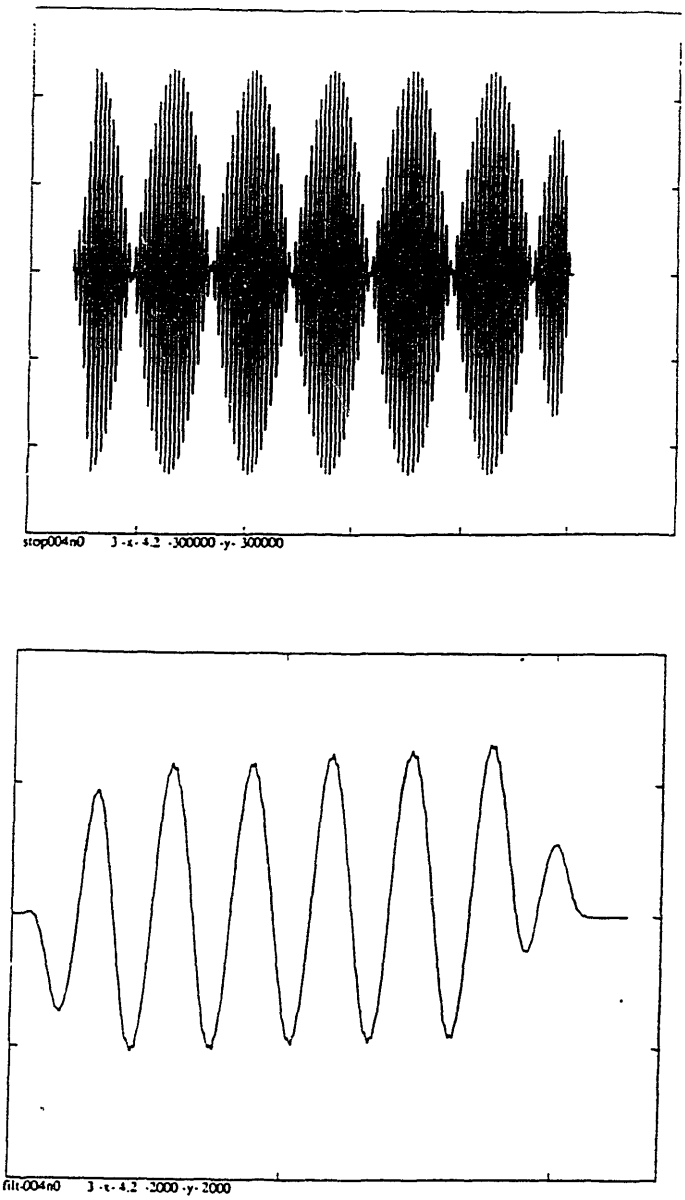

Fig. 5-3 Computational model of the Boston Harbor parametric sonar experiment. x = 4.0 m data. Upper: unfiltered; lower: filtered at 11 kHz low pass Hanning. Difference frequency wave at 10 kHz clearing visible in lower graph. Conversion efficiency approximately -48.9 dB. Scales: p' in Pascals, x in meters.

The filtered portions of each plot clearly show the emergence of the difference frequency wave, although it is not visible in the unfiltered versions. The much greater attenuation at 174 and 184 kHz, compared to the attenuation at 10 kHz, will tend to eventually strip the high frequency components from the pulse and leave only the low frequency parts. Thus taking measurements (or computational data in my case) close to the source, and using low pass filtering approximates the natural low pass filtering of acoustic wave propagation in a fluid like sea water.

There are both good and bad features to the filtered plots in Figs. 5-2 and 5-3. The good feature is that the effective conversion efficiency, 20 $\log_{10}(p/252e3)$, where p is the acoustic pressure at 10 kHz, varies from -49.5 dB to about -48.9 dB. These are on-par with the -51.2 dB measured results obtained by Halsema (1992) using the cw-PRMS experiments where the conversion was measured in a 10 kHz band. Note that in Halsema's experiment, the acoustic level was measured at 293 m, the component at 10 kHz was obtained by spectral analysis, and then extrapolated back to the source by accounting for spreading and absorption. Parametric sonars exhibit the property that the primary waveform(s) distort quickly, in a short distance, thereby forming the difference frequency components. Careful study of the parametric sonar papers in *Nonlinear Acoustics 1954 to 1983*, a series of published reprints bound together as a book, reveals this typical behavior where the parametric source strength eventually peaks and then decays thereafter as an ordinary sound wave.

The bad feature that is especially evident in Fig. 5-3 is the upward slant (left to right) in the difference frequency envelope. It is a consequence of the slight but consistent difference in the absorption of the compression and rarefaction sides of the primary waveforms. It's such a small difference that it isn't at all obvious on the large scale of the unfiltered plot, but it does emerge in the filtered versions. This is a wholly unphysical result, an outgrowth of a computational inconsistency and not of any underlying real physics. Since the center section of the primary sound pulse is steady, *i.e.* in a region well away from the turn-on and turn-off transients of the sonar transducer source, then the center section of the sound pulse will be symmetric about the

ambient pressure. Nonlinear effects will cause the wave to distort but in a symmetrical fashion, and likewise, because of the wave symmetry about the ambient pressure, the absorption will also be symmetric. That's reality. However, on the computer, where I calculate absorption directly from the wave shape, using $\nabla^2 u$, u and the associated constants of viscosity, heat conduction, and relaxation, there is room for slight differences in absorption from compression to rarefaction even when the wave is symmetrical. A fundamental problem as a result is that, in observing the wave at greater distances from the source, the offset in the waveform becomes more prominent. We can also observe by close-up inspection of the primaries that they have proceeded from being distorted in Fig. 5-2, to being saturated in Fig 5-3. The offset described above is probably related to the differences in absorption when the wave saturates, *i.e.* it is most shocked. In contrast, on the observation scale of the primary waves, this defect is not even noticeable. However, it does tend to contaminate some of the features of nonlinear acoustics and makes observation close to the source necessary. This suggests one of the aims of future research, to improve the computational algorithm so that it free of this defect.

To briefly summarize then for the case of the parametric sonar, the calculated value for conversion efficiency is slightly larger than found by Halsema (1992), but the differences are slight when considering the differences in the experiment parameters *vs.* the ones used here. Furthermore, considering that this approach is entirely novel, and that this scenario is the first attempt at verifying the theory and approach, the agreement is quite good. The modeled scenario also revealed some unphysical results which emerge more fully as the waveform proceeds.

5.2 Pulse Self-Demodulation

The self demodulation of a pulse is one of the most interesting features of nonlinear acoustic phenomena. An example is the best way to describe it, so I offer Fig. 5-4 as an example. The series of oscilloscope snapshots is taken from Moffett, Westervelt and Beyer (1970) and shows the transformation of a

sinusoidal pulse of 10 MHz into a pulse that doesn't at all resemble the initial pulse. The series of snapshots was obtained by increasing the separation between the source and the receiver. The explanation for this behavior, which only occurs in large amplitude waves, seems mystifying and is perhaps so since most investigators of the phenomenon haven't come up with a simple explanation for it. Until now. First I'll provide the simple explanation, which follows easily once space/time domain absorption is understood, and then I will show a computational example.

A simple explanation for pulse self demodulation

Turning again to Fig 5-4, we see the first snapshot in the upper-left corner, as received at x = 4.5 cm. This shows the usual characteristic of a mechanical oscillator (the acoustic transducer) that requires Q cycles to reach steady-state, a center region where the transducer vibrates at constant amplitude, and a trailing section where the transducer exhibits a decaying amplitude envelope after electrical shutdown. Note that these are oscilloscope traces, so the pulse acts as though it is moving to the left. The trailing edge disappears off the photo, so we never really see the end of the pulse. The next two snapshots, at x = 7.5 and 10.5 cm respectively, show the onset of distortion in the pulse envelope. The distortion occurs in a very deliberate manner and it is entirely related to both the nonlinear distortion of the large amplitude waves in the pulse, and the enhanced absorption for a distorted wave. The vertical scale also decreases by factors of 5 and 25 respectively.

Here's how it works. Mentally divide the pulse into three discrete regions: **A**. the rise-time region on the left; **B**. the steady-state constant-amplitude region in the center; and **C**. the decay region on the right. In the upper of **A** are the compression half cycles, which are amplitude weighted by the rise-time envelope of the transducer. This gives them the appearance, close-up, of skewed half-cycle sine waves, and their skew is in the backward direction (to the right). Because this is a large amplitude pulse, the nonlinear phase speed $c \approx c_0 + \beta v$ causes the compression half cycles in **A** to advance to the left, which makes them less distorted and more like pure sinusoidal half-cycles. By un-distorting them, they will absorb at the same rate as would an ordinary sine

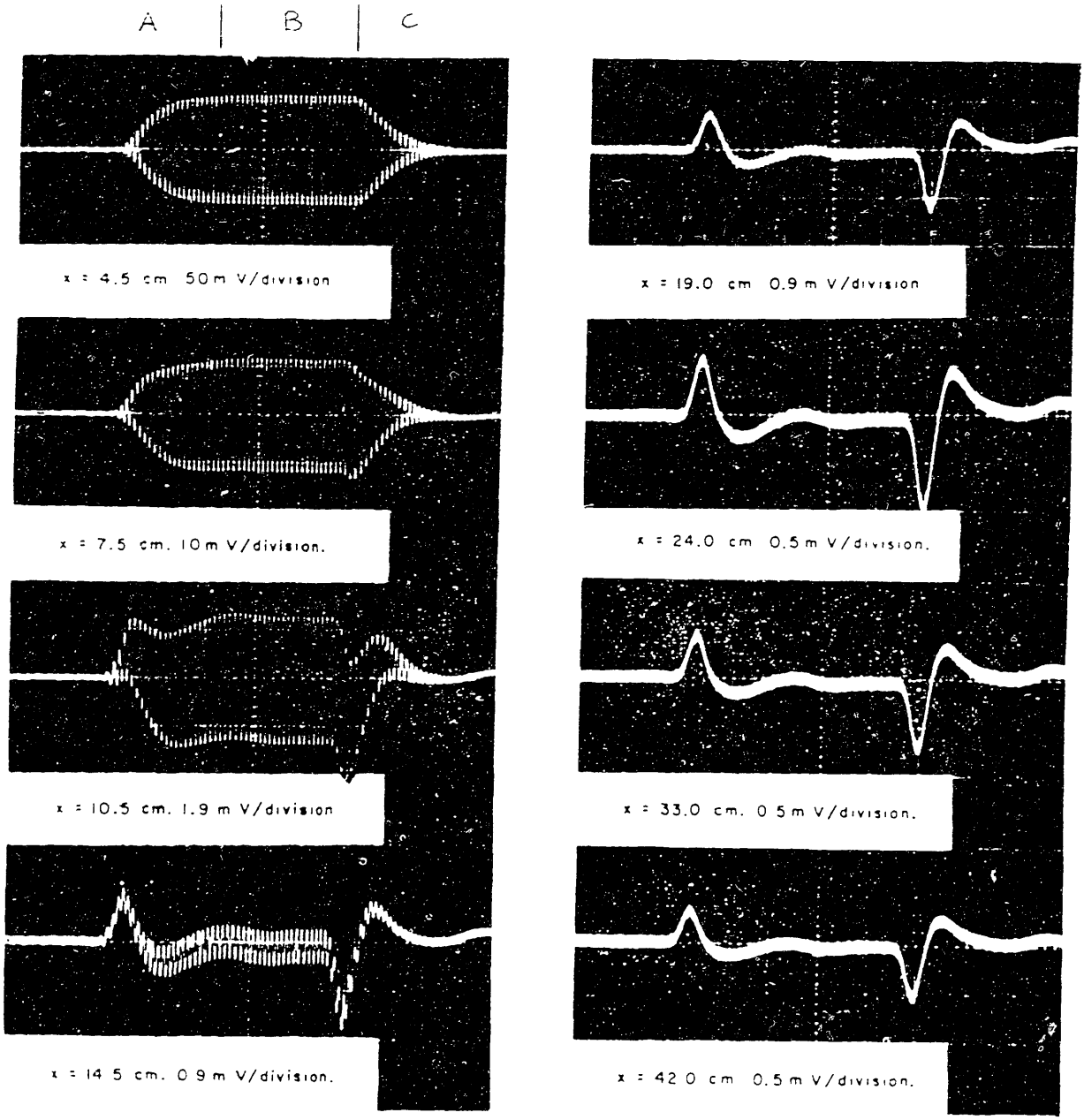

Fig. 5-4 Pulse self-demodulation example, from Moffett *et al* (1970).

wave of the same frequency. We can make a similar argument for the rarefaction half-cycles in region **C**. These half-cycles were pre-distorted in the forward direction (to the left) in the tail of the pulse and they will undistort due to nonlinear effects. Therefore as the wave pulse progresses, the compressions in **A** and the rarefactions in **C** will undistort, and hence absorb at a rate on-par with an ordinary sine wave of the same frequency. One the other hand, the rarefaction half-cycles in **A** and the compression half-cycles in **C** will distort even more than they were to begin with. This causes them to absorb at a greater rate than anything else in the problem. Last, the full cycles in the center section **B**, will distort in symmetrical fashion (the sine wave equally distorts in both compression and rarefaction half-cycles into a sawtooth wave). So the center section **B** will distort and hence be absorbed at a rate increasing with propagation distance.

The differential absorption in region **A** (bottom rarefaction absorbs faster than the top compression) causes the envelope to distort, and this causes a positive displacement of the local mean pressure of the wave pulse. In the opposite sense in region **C**, a negative displacement of the local mean pulse pressure occurs. These offsets are what eventually turn up as the transient self-demodulation witnessed in the further snapshots in the figure. It only remains for the propagation to occur, and the absorption to eliminate the original pulse carrier frequency. Eventually, only the much-lower frequency transients survive. Hence the entire process is due to the combined effects of nonlinear distortion, enhanced absorption for non-sinusoidal waves, and also because parts of the wave pulse were pre-distorted to begin with. It is worth stating, even if this is an obvious overstatement, that a large amplitude steady-state cw tone can never exhibit the behavior described above, because there is no predistortion offered by the leading and trailing edges of the sound pulse. The preceding argument, and the space/time domain view on absorption for that matter, can also be reconciled in the frequency domain, although the issue of windowing and the accompanying bandwidth for the window, tends to obscure things. That's all I wanted to say about the simple explanation. Now for the computational example.

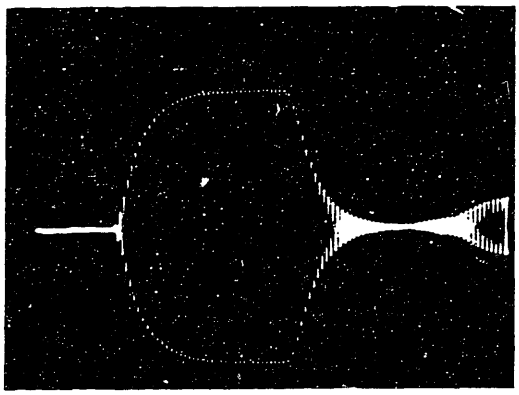

FIG. 3. Primary pulse (of reduced length), 5 μs/division. 15 V_{pp} applied to 2-MHz projector.

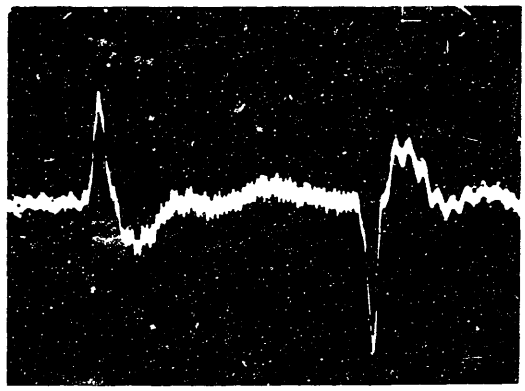

FIG. 4. Secondary signal received at 6.3 m. Scales: 0.044 mV/division, 5 μs/division.

Fig. 5-5 Oscilloscope snapshots from Moffett *et al.* (1979). The left figure is a representative sound pulse at 2 MHz in fresh water, with approximate pressure amplitude of 533 kPa. The right figure is a filtered (600 kHz low pass) snapshot received at 6.3 meters away. The transient self-demodulation from the transducer turn-on and turn-off is evident. The filtered pressure amplitude is approximately 70 Pa.

A computational example of pulse self demodulation

The computational example chosen follows an experiment of Moffett and Mello (1979). This one is more realistic than the one used in the preceding section since it was performed in fresh water rather than in carbon tetrachloride. All physical aspects of the experiment were approximately replicated in the computer model. The main difference was that they used a pulse duration of 30 μs and I only used 20 μs for computer economy. Two oscilloscope snapshots from their paper are shown here in Fig. 5-5. The computer model waveforms at startup, 0.2 m (unfiltered and filtered), and 1.0 m (unfiltered) are shown in Figs. 5-6, 5-7, and 5-8.

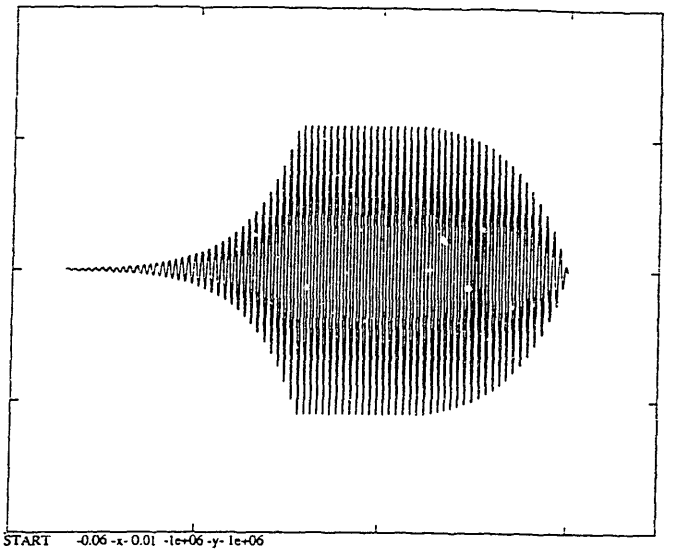

Fig. 5-6 Startup waveform for pulse self demodulation, in p'-x format. x-scale in meters, acoustic pressure p' scale in +/- 1e6 Pa.

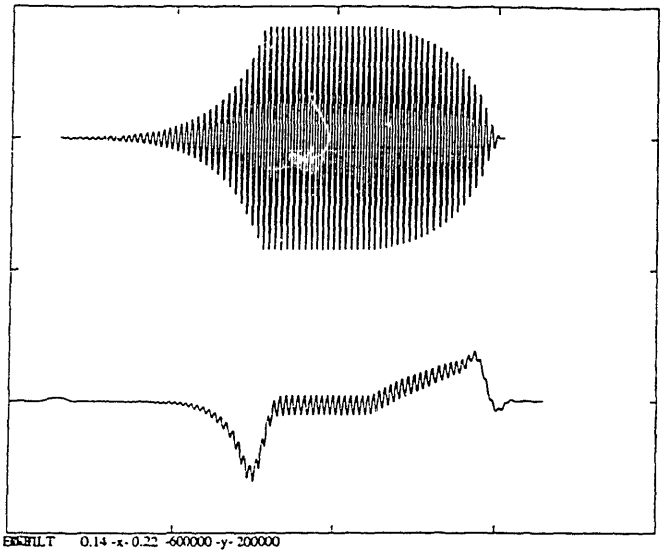

Fig. 5-7 Waveform for pulse self demodulation at 0.2 m distance, in p'-x format. x-scale in meters for both plots. Unfiltered upper plot: 200 kPa to -600 kPa; Filtered lower plot: -2000 to 6000 Pa.

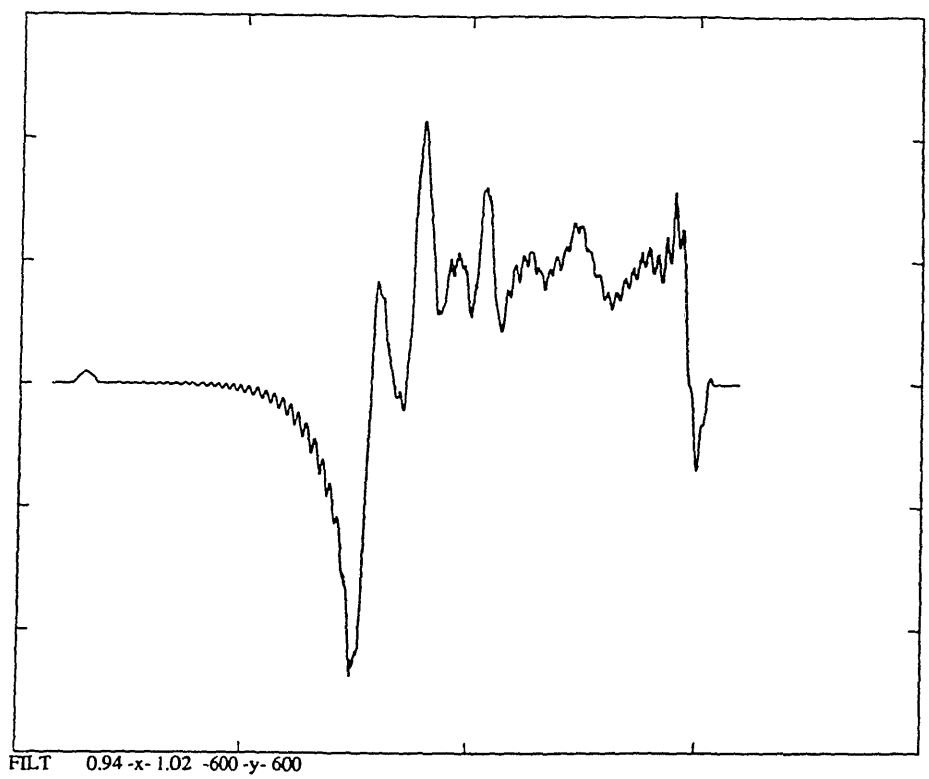

Fig. 5-8 Filtered Waveform for pulse self demodulation at 1.0 m distance, in p'-x format. x-scale in meters, p' scale +/- 600 Pa.

First, at 0.2 m distance (Fig. 5-7), the filtered plot shows the obvious emergence of the self demodulation that is too fine to be observed on the unfiltered version. If there were no further self distortion in this Figure, and the only remaining effects were geometrical spreading due to a finite beampattern and absorption of the 2 MHz carrier signal both out to 6.3 meters, then the self demodulation transients would have amplitudes of about 164 Pa, which is approximately a factor of two different from the experimental filtered data. This agreement is only crude at best, since the source levels used in the computer model were extrapolated from Moffett *et al.* Another reason for a lack for perfect agreement is that the E-27 hydrophone used to make the experimental measurements was non-ideal for the task. Consider that the E-27 is considerably larger than a wavelength in size at 2 MHz, has a very narrow beampattern at 2 MHz (which could easily cause misalignment problems), has a mounting baffle that could contribute diffraction ripples in the hydrophone response, is only rated for a uniform free-field voltage sensitivity from 100 kHz to 400 kHz, and has an unknown response above 700 kHz. In addition, the E-27 is a reversible transducer so it can operate as a transmitter as well as a receiver; when used as a transmitter, the E-27 at max power is not capable of transmitting the level it was receiving in the Moffett *et al.* experiment even at 6.3 meters distance. So there is every chance that the E-27 was contaminating the measurement in a host of ways, including its own nonlinear response. The E-27 hydrophone design and performance specifications are included as Appendix C.

Assuming (optimistically) that the E-27 did not greatly influence the results in Moffet *et al.*, we need an explanation for the discrepancy between the measured data (from Moffett *et al.*) and the computed data, especially concerning Fig. 5-8. The Fig. 5-8 result shows the same basic increase in the local pressure with increasing x-position in the pulse that was observed in the parametric sonar case.

To summarize then, the computational model, and hence the theory presented, gives early indications that pulse self demodulation approximately agrees with experiments, certainly on a qualitative level, and perhaps on a quantitative

level as well. The pulse self demodulation test is probably the toughest test for not only the wave packet theory because it requires a decent model for the nonlinearity, the absorption, and for their combined effects, but also for the computational model. The close-to-transmitter data is encouraging, but the far field results are poor.

5.3 Medical Ultrasound Heating

A series of two experiments were performed during 1989-1990, to demonstrated that intersecting large-amplitude beams of focused ultrasound would deposit more heat than the heat deposited separately by each focused beam. The complete report written at the end of the second experiment, which summarizes both, is included here as Appendix A. Only the salient features of the experiment will be introduced here.

Two confocal (coincident foci) ultrasound beams, one at 0.9 MHz and the other at 1.5 MHz, were first driven individually, and then simultaneously upon a thermocouple to see if the simultaneous drive generated more heat than would be deposited by ordinary superposition. The idea was to use the high intensity region of the coincident foci to enhance sound-sound interaction, with one wave helping to speed the saturation process for the other, and *vice versa*. The results showed an increase of about 1 degree Celsius extra heat when driven together than by the numerical superposition of the temperature gain in individual trials.

Numerical modeling of such an interaction process poses some difficulty, especially if one attempts to treat everything in the problem. To circumvent this potentially cumbersome enterprise, a first-cut simple approach was taken. The approach assumes that the two beams are uncorrelated with each other (a safe assumption since the frequencies are different), the mixing region was *nominally* a 1 cm cube, the wavelengths are all smaller than the intersection region, and the pulse durations were 0.1 seconds. Hence a great many waves passed through the interaction cell, so the whole process can be modeled by

treating the local acoustic pressure in an ergodic sense, both spatially and temporally. This allows the calculation of an effective v_e for the particle velocity. Since both waves had about the same particle velocity based on energy deposition from the thermocouple, then the effective increase in v_e is 1.4. To simplify further, this increase in acoustic particle velocity was instead attributed to the coefficient of nonlinearity β in the interaction region only.

The procedure was simple thereafter. Two separate runs of the propagation code gave the pressure wave for both the 0.9 and 1.5 MHz pulses. These were then used as inputs to the propagation code having a model for an elastomer (in which the thermocouple was encapsulated). The model treats only longitudinal wave propagation, shear waves not being considered; this is an assumption which may or may not be valid. A second, near-identical, propagation code was modified for the enhanced coefficient of nonlinearity β. Thus, using the 0.9 MHz wave input to both the modified and unmodified codes, the difference in the energies between the two exiting waveforms determines whether the interaction is present. One could argue that this type of approach is 'rigged' from the start to work; I agree, but the central issue is whether the resulting interaction is significant.

The simulation showed that the exit waveform energy for the interaction case (modified program) was about 97.7% of the exit waveform energy for the separate runs with the unmodified code. To cast that in terms of the parameters used to describe the actual experiments, $\sigma_{heat} = 1.02$, which is in the right direction, but underestimates the experimental value of 1.06. What does this mean, and what are the other possible sources of error? One error source not considered is the influence of the acoustic particle velocity on the thermocouple and attendant wires, as discussed by Handler (1976), which would tend to add friction to the problem. Another error source present in the experiment, but not present in the computer model is the heat conduction in the wires themselves. The absence of shear waves has already been mentioned as a possible error source.

Clearly, to really answer the question of the significance of the nonlinear interaction, a better model must be used that incorporates all these things and

in which they may be isolated to see their effect on the ensemble experiment. For now, there is qualitative agreement between the computed results and those from the experiments.

5.4 Shock Waves

This section explores the development of the shock layer, and includes a general discussion and explanation for weak shock theory and why it works. The model used is the same one used in demonstrating pulse self-demodulation. The approach is to choose one cycle of the wave pulse, and, for each propagation interval, identify the thickness of the shock based on 5% to 95% of the peak-to-peak amplitude. These measured shock thicknesses are also compared with a viscous calculation of the shock thickness based on a thermal-modified expression from Blackstock's notes (1993), which was in turn based on the theory of G.I. Taylor.

The workhorse for this example will be the same one used for pulse self demodulation. The computer model already incorporates the expression for the shock thickness given by Blackstock (1993) based on viscosity; the model also incorporates the effect of heat conduction in an *ad hoc* manner, since in the case of dissipation it can be shown that heat conduction losses take the same basic form as those for viscosity (see Chap. 3 for details).

To recap, the initial starter pulse was a 2 MHz pulse having a peak pressure amplitude of 553 kPa directly exiting the source transducer. The dissipationless shock formation distance for this problem is approximately 0.11 m. Fig. 5-9 shows one cycle in the steady-state region from the starter pulse, and the shock thickness (using the term loosely since it hasn't actually formed) is 26.2e-5 m, which is almost a half-wavelength. Note that by convention the shock thickness is arbitrarily measured from the 5% to 95% of the peak-to-peak values. Fig. 5-10 shows a similar single steady-state cycle after 0.1 m of propagation, a distance quite close to the dissipationless shock distance. Here the shock thickness is now 11.78e-5 m. Finally, Fig. 5-11 shows the single cycle after 0.32 m of propagation, with a shock thickness of 3.4e-5

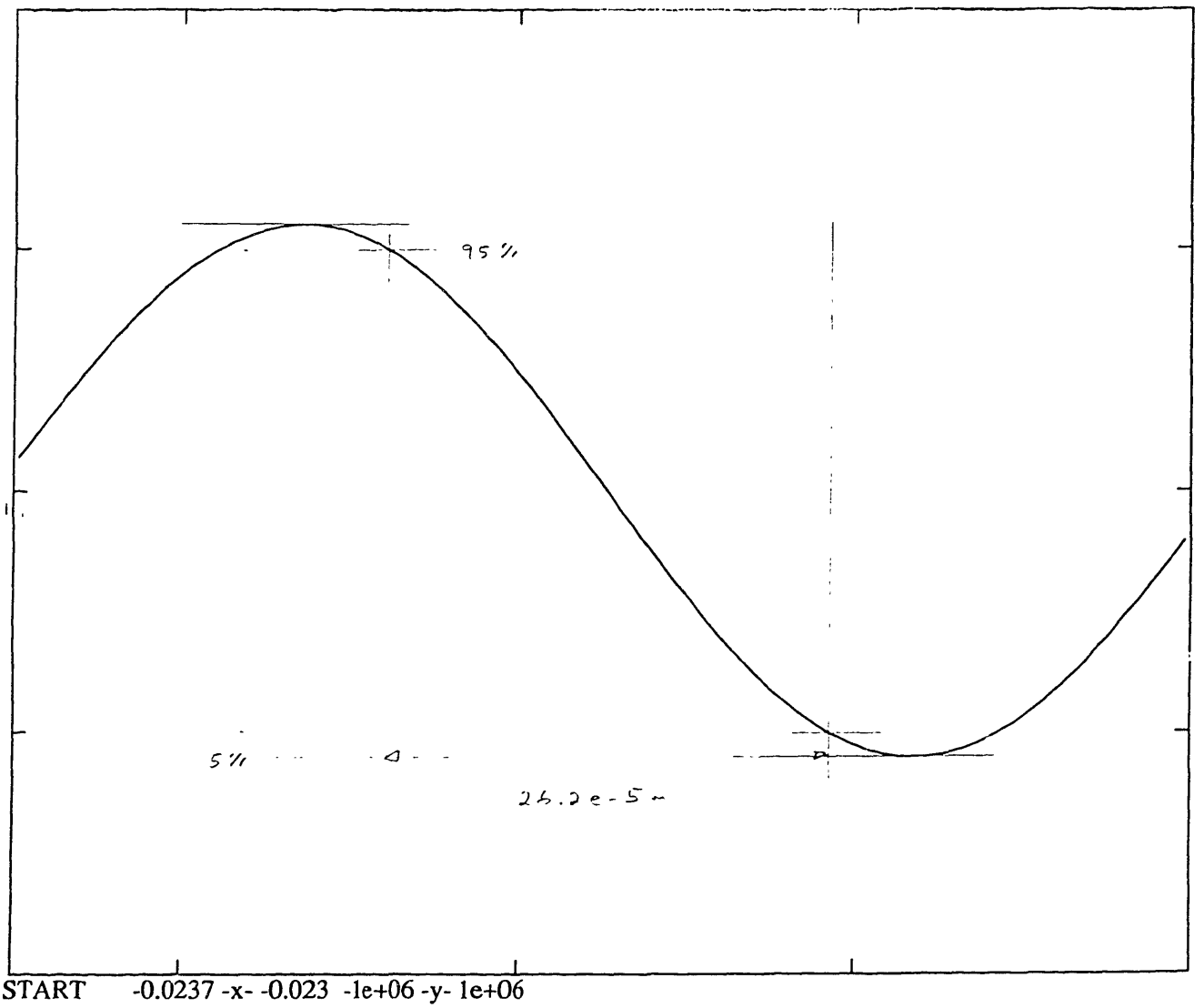

Fig 5-9 Startup waveform for shock study. Scale is p'-x, and wave travels to the right. p' = 553 kPa, f = 2 MHz, fresh water case with viscosity and heat conduction. 5% to 95% of peak-to-peak pressure amplitude locates the span of the shock.

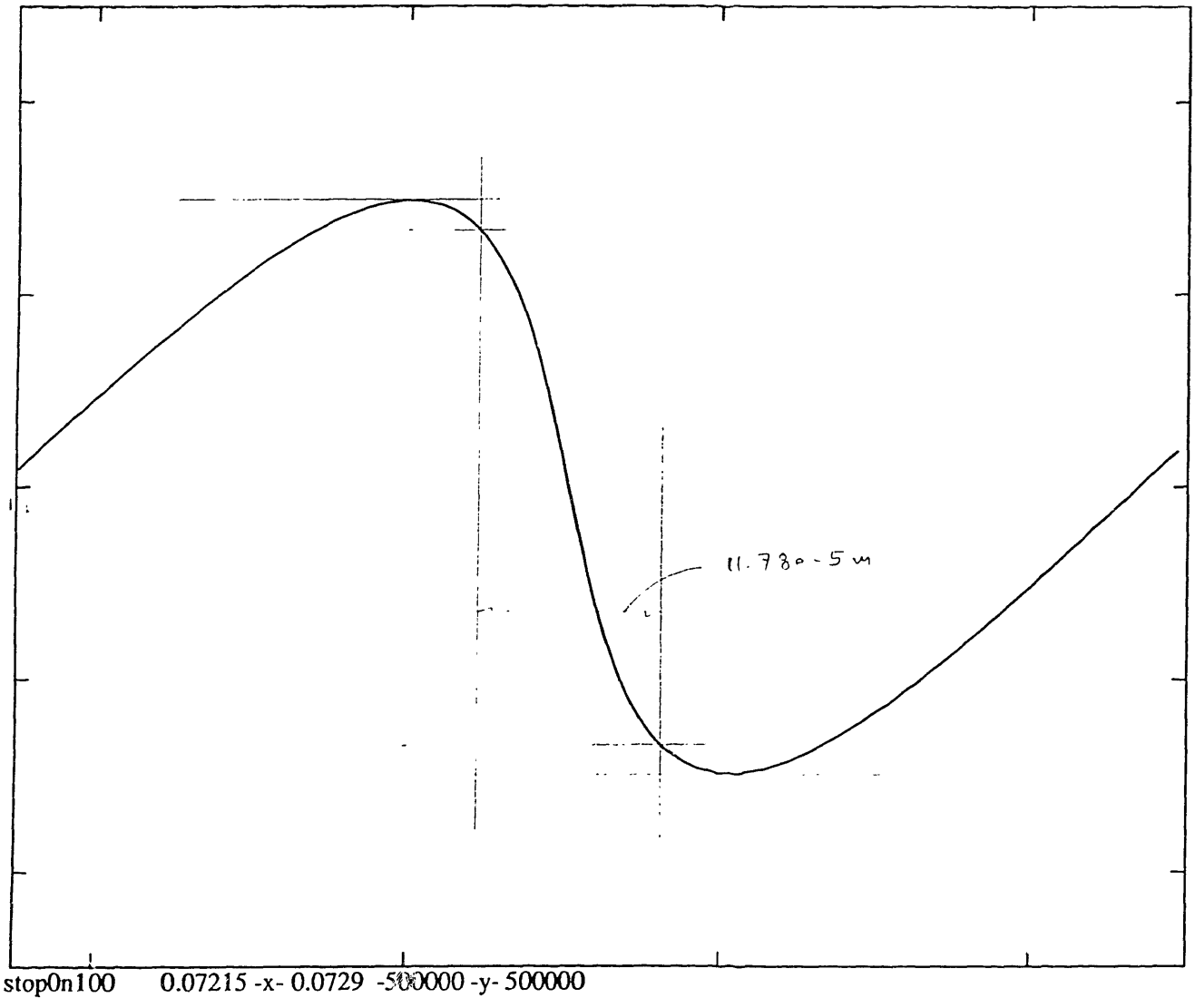

Fig 5-10 Shock study waveform at 0.1 m distance. Scale is p'-x, and wave travels to the right. f = 2 MHz, fresh water case with viscosity and heat conduction. 5% to 95% of peak-to-peak pressure amplitude locates the span of the shock. span = 11.78e-5 m.

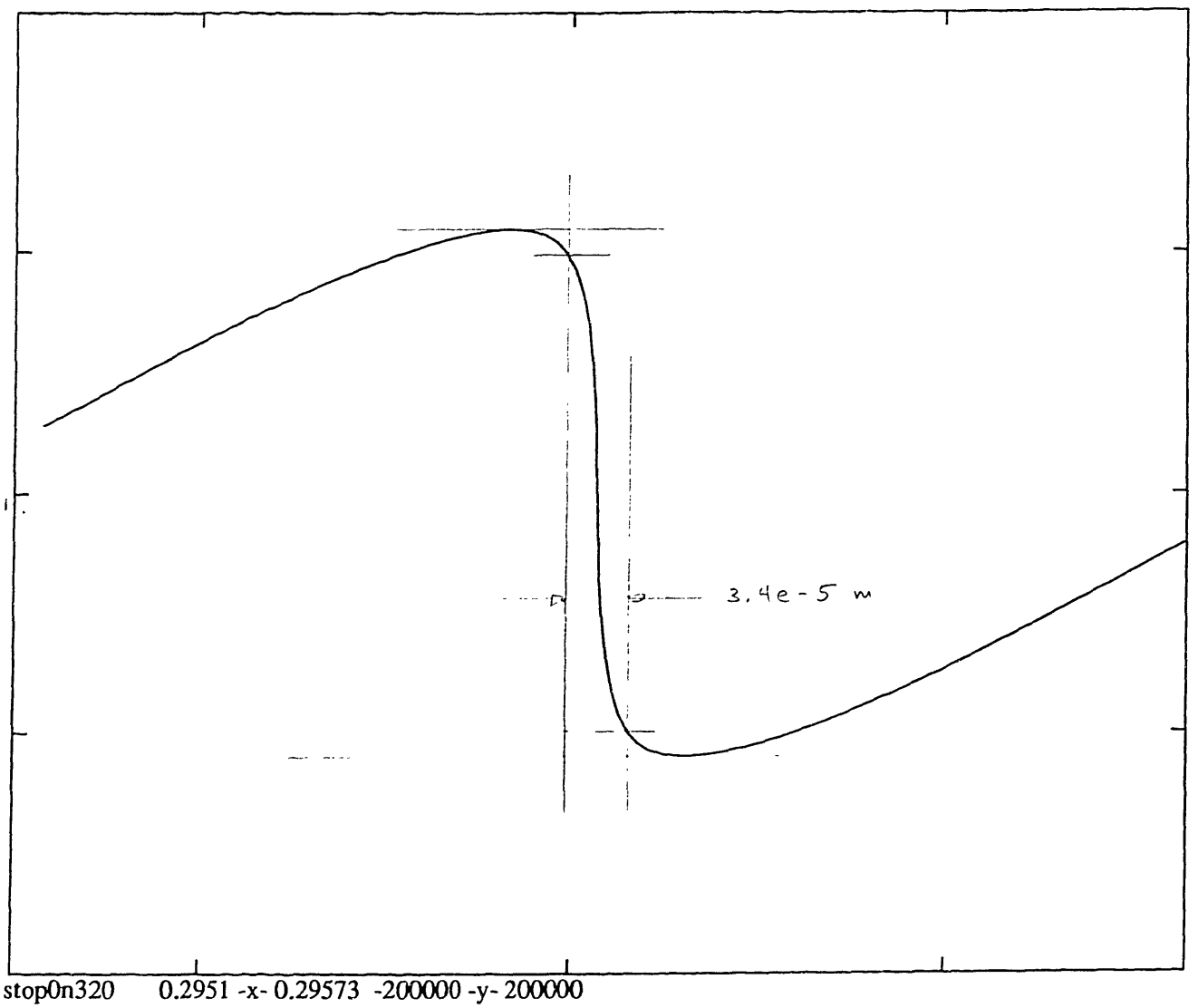

Fig 5-11 Shock study waveform at 0.32 m distance. Scale is p'-x, and wave travels to the right. f = 2 MHz, fresh water case with viscosity and heat conduction. 5% to 95% of peak-to-peak pressure amplitude locates the span of the shock. span = 3.4e-5 m.

Table 5-2 Shock Thickness vs. Propagation Distance

	travel dist. (m)	5% to 95% shock thk (m)
starter pulse	0.00	26.2 e-5
	0.10	11.8 e-5
	0.20	5.5 e-5
	0.26	3.6 e-5
	0.38	3.4 e-5
	0.44	3.5 e-5
	0.50	3.8 e-5
	0.60	4.6 e-5
	0.70	5.0 e-5
	0.80	5.7 e-5

notes:

1. initial undistorted half-wavelength = 36.5 e-5 m

2. theoretical calculation for 5% to 95% shock thickness based on Taylor's theory, per notes by D.T. Blackstock (1993, modified by K.D. Rolt for heat conduction): shock thickness = 2.02 e-5 m

3. dissipationless shock dististance = 0.12 m

   " " saturation dist = 0.36 m

4. end of nearfield = 0.035 m

m. Other shock thicknesses for various propagation distances are given in Table 5-2, along with accompanying notes. It may be noted that the shock thickness reaches a minimum, and then gradually increases. The increase is mostly due to the reduction in amplitude of the waves, and minimally due to the decrease in the slope of the p-x in the shock. The slope of the shock will "unwind" back to the slope on the parent undistorted pulse once the wave pressure amplitude returns to a level where energy can no longer be usefully convected into the shock region; *i.e.* the local problem then behaves in the manner of linear acoustics. When this occurs, the absorption doublet influences the wave faster than the energy can convect (and hence distort) into the shock region, and so the shocks become more rounded until they vanish. When this occurs, the remaining energy is merely an "old-age" linear acoustic sine wave of greatly reduced amplitude.

The shock layer, once stabilized, represents the ongoing battle between the energy dumped in by both the compression and rarefaction sides of the shock, and the dissipation forces at work. The significant observation to make, which Mendousse suggested in 1953 for viscosity, is that the $\nabla^2 u$ operator in all the dissipation terms prevents the wave from ever actually becoming multivalued. As multivalueness is approached, the $\nabla^2 u$ term merely changes into a sharper, more potent, doublet. Dissipation always wins at the shock front, because the doublet can keep pace with any energy the shock can provide, at least as far as the weak shock analysis here is concerned.

This brings me to the last point of discussion on shocks, the matter of weak shock theory and the equal-area rule. Weak shock theory is developed from the conservative equations of mass, momentum, and energy as applied across a shock boundary. The outgrowth is the equal-area rule, which allows shocks to form, become multivalued, and to then be quenched in a sensible manner by finding the place at which the areas swept out under the multivalue region are equal. One this vertical line is found, marking an equal area on the left, and the other on the right, the offending multivalue regions are merely chopped off, and the problem may proceed. Though this is a handy way to solve some problems, it does allow the multivalue wave to occur and it (at present) doesn't provide the ordinary attenuation of viscosity, heat

conduction, and relaxation. On the other hand, the work shown in this thesis provides these things, and if the step sizes are small enough, and the computational algorithm is clean, then the equal are rule need never be applied again. But is this a good idea? In a word, no. The beauty of the equal area rule is computation speed, at the expense of accuracy of the waveform at the shock region. The method also gives a very easy way to understand energy loss in a shock wave once the wave is fully saturated. The method of absorption introduced here provides the loss at the shock in a direct manner, without resorting to unphysical conditions, but it is also computationally much more demanding and work to smooth out the kinks remains to be done. The ultimate recourse would be to use some combination of both; the wave packet approach provides sensible p'-x or p'-t curvature at the shock region while the equal area rule cleans up any stray acoustic particles that might have sneaked through the shock barrier. This would be *extremely* helpful in problems where the shock is strong and the full propagation is desired out to great distances. The equal area rule easily handles large propagation step sizes, while the wave packet approach is much more severely limited. Hence, the methods introduced here augment weak shock theory, and provide a different viewpoint for explanations that can't be grasped as well by staring down a KZK or NPE equation.

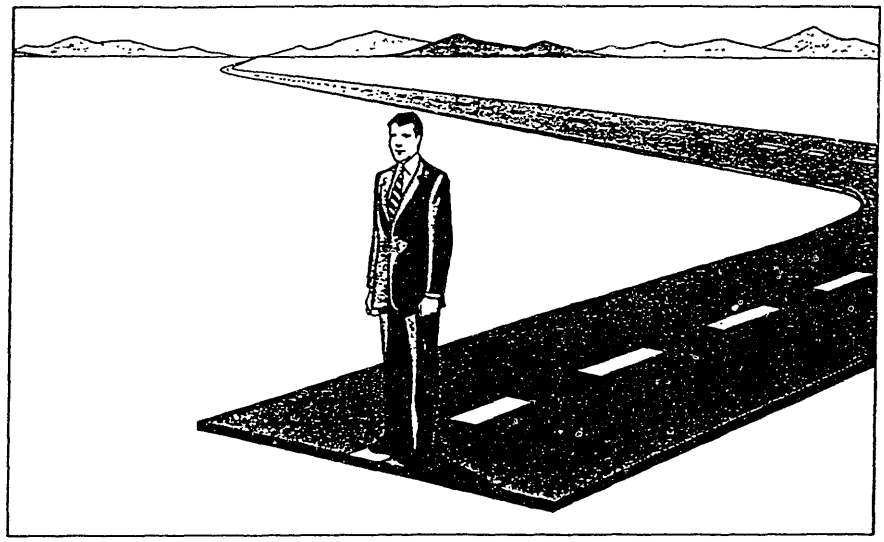

Chapter 6

Conclusions and Future Work

This thesis has attacked the broad problem of nonlinear sound waves, their propagation and their absorption, in a way that roughly combines ideas used by earlier workers using the phenomenological approach, and follows the thread idea furnished by Mendousse in (1953). Where Mendousse departed was in the high frequency approximation of the wave at the shock edges; this was probably a good idea since computers hadn't evolved to any great unclassified extent by that time, and the methods shown here demand significant computation to be useful.

A number of specific conclusion remarks have been made in the previous chapter, in conjunction with discussion of several case studies used to partially validate the model presented here. The comment/conclusion that I have to offer concerning my unified approach to solving nonlinear propagation problems in the way that I have attempted is that it appears to work, I believe it to be broadly correct, and I think there is enough validation among the examples in Chapter 5 to make the point. I find it both refreshing and scary, as I write this final Chapter, that I have attacked an old problem in fluids and acoustics in a relatively simple and unique way, but that I have not *fully* succeeded in proving my thesis by *bonafide* agreement with experiments from the literature. Instead, I have stretched out on a limb, so to speak, with an idea that is partially proven, and computationally still needs some housekeeping (or overhaul). To summarize the conclusions and contributions:

Conclusions

1. A simple propagate-absorb model for nonlinear acoustics does compare qualitatively with a variety of otherwise unrelated experiments.

2. In some cases, the agreement between experiment and the model used here is quantitative as well.

3. The agreement of shock thicknesses with theory is extremely good.

4. Use of nonlinear acoustics as a test of the wave packet time/space domain absorption model is probably the most severe one that could be used.

   The agreement (in 1 and 2 above) suggests that there is some truth to the absorption model.

5. More work needs to be done in cleaning up the long distance behavior of the solutions (*i.e.* at distances beyond those shown here).

   The problem has been isolated to errors in the absorption model, and <u>not</u> in the propagation model.

Contributions

1. Models for time/space domain absorption that agree with theory for pure tones, and provide absorption coefficients for wide-band signals.

   These models don't care if the problem is linear or nonlinear, only the shape of the wave (in a p'-x or p'-t format) is important.

2. The phenomenological propagation model for nonlinear acoustics, best represented by the thesis work of Pestorius, a model which omits conventional absorption and uses weak-shock theory (via the equal-area rule), has been joined by the wave packet approach which includes conventional absorption.

   Conventional absorption provides the mechanism for formation of stable, smooth, shocks without the use of weak shock theory.

Discussion of Sources of Error

There is always some merit in baring one's intellectual soul however, as it gets the ideas out on the street where others can view them, and add comments, criticism, or help. The reader will find that this work is a noble attempt to solve a tough problem, which if left to the theory alone, looks great. Ahhh, but then I made the ultimate mistake of trying to prove the theory by experiment.

The increase in the error of the computed results bears some discussion here, and will probably be something that I will spend some time on in the next few months, and perhaps the next few years as well. You could refer to these things self-criticism.

Local mean pressure, based on neighboring locations on a wave where $\nabla^2 u = 0$.

I think that the idea of some local mean pressure as the reference for defining a local energy density, is a correct one, especially if one tries to reconcile sound absorption in the time/space domain from the viewpoint of a wave packet that 'sees' only what its neighbors are doing, and has no knowledge of what the true ambient fluid pressure is. A possible problem question is: should the local reference be a straight line between neighboring $\nabla^2 u = 0$ points, or should it be some curve? I don't know the answer to this question; if I did, I would have presented the material in this thesis in a more direct manner, and I would have hidden or omitted the labor needed to get to the right answer.

This whole question is conveniently sidestepped if one opts for a Fourier approach, by taking a windowed transform of the wave, applying a sensible absorption law to the frequency bins (an ω^2 weighting for viscosity *e.g.*), and then inverse transforming. I readily acknowledge the utility, speed, and proven reliability of Fourier methods, but I'm not satisfied because they don't really explain to me why absorption works at all. The Fourier approach divides the waveform into a superposition of fundamental and harmonics, and the absorption acts in an independent manner on each of the fundamental and harmonics. This is troublesome, conceptually, because in a shock problem where the wave is sawtooth-like, the absorption acts almost exclusively in the shock front, and practically nil elsewhere. The Fourier approach would have us believe that the absorption acts everywhere, on each separate harmonic.

Another difficulty that I'm not happy with is that you need to window the waveform in some fashion. You could of course not window, assuming you had infinite computational resources and speed, but practically everyone needs a window. If I pose the question: what is the absorption of some arbitrary point Q on a waveform?, the Fourier-based method relies on taking a window in the region of my point Q, transforming it into the magnitude and phase spectrum, applying absorption, then inverse transforming. The calculation becomes more accurate the wider the window is. I counter this with still another question: why is it necessary to use a wider window when I am only interested in a point Q, or the neighborhood of point Q within the limits of continuum mechanics? The answer to this question is tied to the rules of the transform: the transform has no ability to resolve accurately unless it can grab enough of the wave. There are much more mathematical ways of stating this (go check a math or engineering book if you are really so inclined), but the result is that if the window is too small, the resulting spectrum will be wider and wider band. The transform is giving us an answer, and it's a correct answer, but it isn't the answer to our question. If the window is truly acting only in the neighborhood of my point Q, then the spectrum will be constant and uniform across all frequencies.

So using the transform method, to me, for finding acoustical absorption involves a paradox. This puzzle is partly responsible for the direction that I have taken in deriving space/time domain absorption. My approach involves

only looking at point Q and its neighborhood (necessary because $\nabla^2 u$ is needed to find the energy loss). So I have donned the physicist's hat in trying to explain how absorption works, no matter whether it is for a linear or nonlinear acoustic problem. I do this partly because the Fourier-based method doesn't really answer the question of how it works, and partly because Fourier methods have a tough time when the waveform forms a steep sharp-cornered shock. The absorption model I have introduced is hence interesting, it explains a lot especially when applied to a nonlinear acoustics problems like shock waves and pulse self-demodulation, but it isn't fully mature. So there is potential source of error because I don't have a firm answer for how to define the local reference for pressure (or particle velocity).

Numerical Issues

The numerical issues that could cause problems are the same ones that plague programmers everywhere. The two main ones are numerical stability, and the encroachment of roundoff error into the solution.

Because I am not using finite differences to propagate my waves, the Courant condition of making the time step small enough so that no node are overstepped doesn't apply. My reference frame is really a retarded coordinate frame, one that effectively follows the wave as it travels. Thus the wave really doesn't move, but it may distort depending on how nonlinear the problem is relative to absorption. Furthermore, the propagation part of the numerical code was tested for very long range propagation and the result was that linear acoustic problems didn't change shape, while nonlinear acoustic problems distorted, became multivalued, but remained smooth and symmetric.

Only when the absorption is applied do the numerical solutions become ragged or uneven. The unevenness has been shown to be especially related to nonuniform absorption of compression shock to rarefaction shock even though the parent undistorted wave was symmetric about the ambient pressure. This is a result of the inability to calculate a smooth even second derivative when the waveform forms a shock. It actually could be that there is a related form of the Courant condition hidden, that demands smaller step sizes in order to ensure smoothness in the solution. Intrinsically, because I am

implementing numerical versions of actual loss mechanisms (viscosity, heat conduction, and relaxation), the loss mechanisms should actually help stabilize the solution in the same way that they smooth a wave pulse in the real world. But the numerical implementation, if forced to work in too large steps, can upend the stability. In my case, my solutions don't blow up, they just absorb in an uneven fashion.

Roundoff error might also be a source of error here, but roundoff error in a numerical solution, especially one in performed with double machine precision, are usually related to making the step size excessively small.

Summary

Moving on to the future work department, the computational implementation needs attention, because it is not 100% consistent in calculating the local absorption. Once this task is met, then there are a whole host of other benchmarks in the acoustics community that could be brought to bear on the approach. A large raft of sanity checks will be needed. Comparisons with the NPE- and KZK-based methods would also be useful and likewise educational.

Last, the unconventional approach taken here is probably due to my lack of excessive exposure to the fine groups studying nonlinear acoustics in Austin Texas; Bergen, Norway; Rochester, NY; and in the FUSSR. Had I attended graduate school in one of these places, then I probably never would have gone this route. I hope that I have learned something here, that I have helped broaden the knowledge base for others, and that I can broaden my own scope in nonlinear acoustics by understanding more fully the works that have been done by others.

"An Experiment in Parametric Ultrasonic Heating, Part II"

for

MIT 2.77

Research in Biological Effects and Applications of Ultrasound and Other Non-Ionizing Radiations

Fall 1990

by

Kenneth D. Rolt

6 March 1991

INTRODUCTION

A previous paper [Rolt, 1988] suggested that the nonlinear interaction of sound with sound as issued from intersecting sound beams could be exploited to produce nonlinear heat generation. An experiment was later performed [Rolt, 1990] at the MIT Hyperthermia Laboratory to confirm or deny this suggestion. The concept posed by the 1988 paper and attempted in the 1990 experiment was simple: using two fixed-amplitude, focused ultrasound transducers (labeled B and Y respectively) arranged with coincident foci, transmit B with a pulse of duration τ seconds and frequency f_B and measure the temperature rise; then independently transmit Y with a τ duration pulse at frequency f_Y and measure the temperature rise. The temperature changes for these two trials are ΔT_B and ΔT_Y respectively, and the temperature rise may be measured with a small thermocouple probe; finally, simultaneously transmit a τ duration pulse from both B and Y and measure the temperature rise, which we call ΔT_{B+Y}. We then define the dimensionless ratio

$$\sigma_{heat} \equiv \frac{\Delta T_{B+Y}}{\Delta T_B + \Delta T_Y} ,$$

where σ_{heat} is, by definition, the measure of the nonlinear heat generation due to the intersection and interaction of two sound beams. If the process of two sound beams interacting is a linear process, then the principle of superposition should hold and σ_{heat} should equal 1.0. If the process is nonlinear, then $\sigma_{heat} > 1.0$ and the extra heat is due to sound energy transforming itself from the parent transmit frequencies for B and Y, into a spectrum of frequencies which are usually comprised of the original frequency and harmonics of that frequency. This has been called self-modulation of a finite amplitude (large amplitude) sound wave. [See: Beyer,

1974; Saito and Tanaka, 1990; Baker, Anastasiadis and Humphrey, 1987; and NUSC, 1983 for further reference].

The results of the first set of experiments [Rolt, 1990] were that:

- in 7 separate tests at different power levels and intermediate angles, 5 of 7 showed that $\sigma_{heat} > 1.0$ (average of the 7 tests was 1.02)
- in the 8th test, for repeatability, (7 B; 7 Y; and 13 B+Y) the average σ_{heat} was 1.05.
- for all trials σ_{heat} , on average, was about 1.036.

These results *suggested* that there was a nonlinear increase in heat generation in the confocal region of two simultaneously-pulsed focused ultrasound transducers as compared to the heat generation from two transducers working independently, and that the temperature increase is attributed to nonlinear interaction of sound with sound. However, the lack of sophistication in the experiment, the lack of simultaneous spectral analysis to identify cavitation, and the relatively small number of trials at different power settings, prevented the postulation of nonlinear heat generation from being *proved.*

The recommendation was to repeat the experiment under superior conditions (better control of transducer positioning), with simultaneous measurement of ambient spectrum to identify cavitation, and calibration of the thermocouple to give an absolute measurement of temperature. These recommendations led to the work described in this paper.

Finally, it should be noted that it has previously been recognized that the heating of materials or tissues by ultrasound may be enhanced by the nonlinear interaction of sound as it travels from a source to the intended target area. This has been discussed in some detail by Bacon and Carstensen, 1990, and Hynynen 1985. This is merely a consequence of the formation of

Table I - Transducer Systems

	B	Y
frequency	1.5 MHz	0.9 MHz
head	# 4	# 1
polystyrene lense	36/101	38/101
tuning box; cable	box # 1; E	box # 2; 9'
VCA	red (blue failed)	yellow
amplifier	IFI, 130 W	EIN, 200 W
pulse duration τ	0.1 seconds	

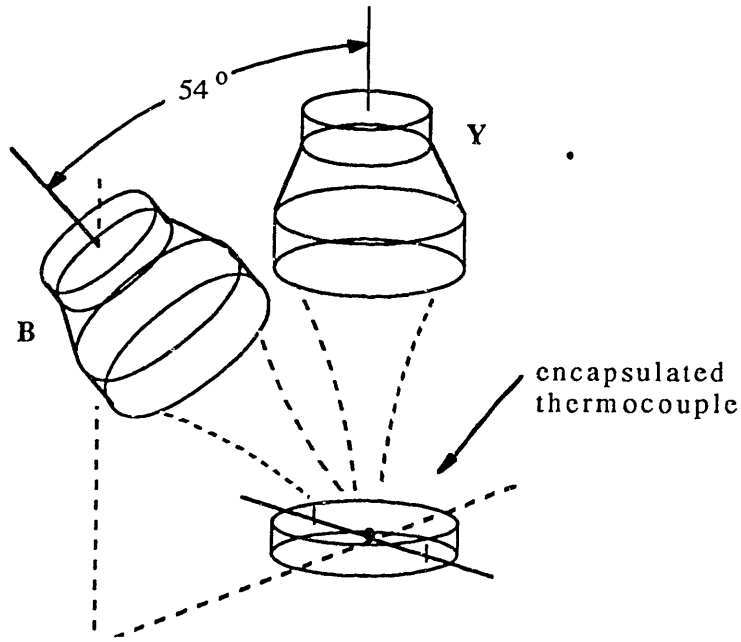

Figure 1 - Arrangement for Temperature Measurement of Intersecting Focused Ultrasound Transducers

higher spectral components during wavefront flight, and it is these higher spectral components which enhance the heating. This work allows for this sort of nonlinear increase, but still further proposes to divide the sound source into a plurality of separate sources, which then interact with each other at the confocal region.

OBJECTIVES AND EXPERIMENTAL DESIGN

As in the previous experiment, the objective was to determine if the heating within the confocal (intersecting) region of two focused sound beams generated heat in a nonlinear way.

The experimental set up was considerably more sophisticated and more reliable (no water tank leaks) than the previous experiment. A simplified illustration of the set up is shown in Figure 1. The same quartz ultrasound transducers, with attendant transducers heads, lenses, and water-sealing cones (flanges) from the 1990 experiment were used here. Each transducer head-cone combination contains degassed water, and the water is sealed into each unit by means of stretched Trojan™ latex condoms. Small air bubbles are removed from the sealed unit by the use of a syringe which is designed to attach to a special valve on the body of the water-seal cone. Thus each transducer assembly is ensured to be free of any air bubbles for the duration of the experiment.

Table I lists the components of each transducer and drive assembly, and identifies them as the color-coded B (blue) and Y (yellow) system, and the details of the entire apparatus are included in the Appendix. The general arrangement for the experiment is shown in Figure 1, and the schematic is shown in Figure 2.

Each transducer head is mounted on a separate positioning mechanism. The 1.5 MHz Blue head was mounted on a six degree-of-freedom, motorized computer controlled platform, and was inclined to about 54° from the vertical. The 0.9 MHz Yellow head was mounted on a five degree-of-freedom, manually

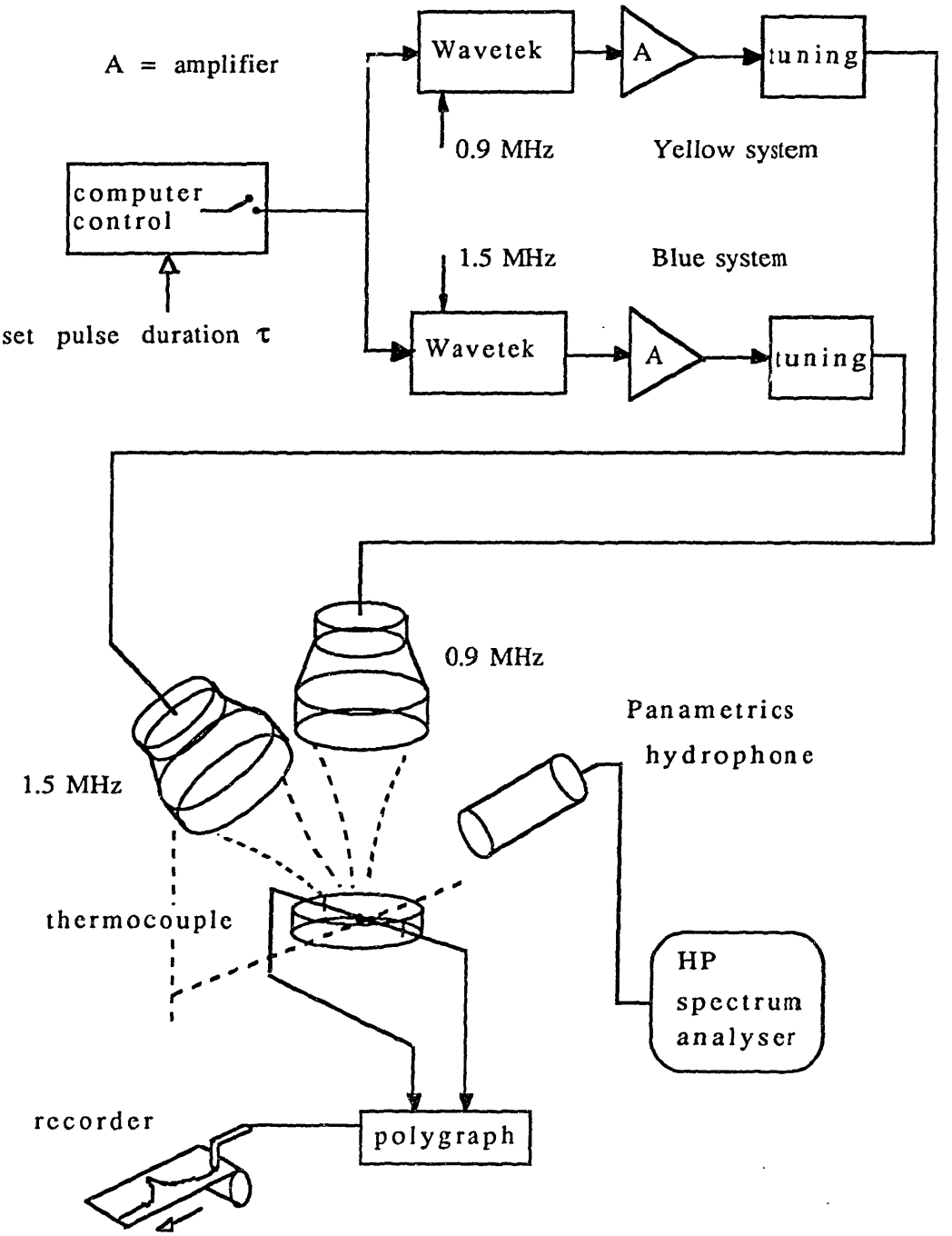

Figure 2 - Schematic of Experiment

controlled platform, with the transducer aimed straight down. Thus the intermediate angle between the transducers was 54°, which is about the same as the previous experiment. The position resolution of each platform was about 1 mm.

Each transducer was calibrated for voltage *vs.* radiation pressure (as measured in grams) using a Mettler PC 440 electronic scale. The calibration data are included in the Appendices.

The thermocouple used for the experiment was constructed in the MIT Hyperthermia Lab *via* a capacitive discharge butt weld technique. The thermocouple bead (the junction of the two dissimilar wires, in this case chromel and constantan) was observed under a microscope and found to be free of oxide, and the weld bead was not much larger than the wire diameter (.003 inches or .076 mm). This thermocouple was then encapsulated in a 5.5 cm diameter, .75 cm deep petri dish mold using GE RTV 615 silicone rubber. This encapsulant was chosen for it's reasonable match to the ρc of water, because it's transparent, and because of the relative ease to degas the two components after mixing by means of a laboratory vacuum. This encapsulant also absorbs ultrasound to the same order of magnitude, *per* unit thickness, as certain type of human tissue (see Appendix, and Goss *et al.*, 1978, 1980). The direct-current (DC) resistance across the thermocouple leads was checked after welding, after encapsulation, and after the experiment to verify electrical continuity.

The encapsulated thermocouple (hereafter referred to as the thermocouple) was mounted on a block of wedge-absorber polyethylene, similar to the glassfibre ones employed in air acoustic anechoic chambers. The polyethylene block was then placed at the bottom of an 8 gallon capacity acrylic-walled tank, and suitably weighted to prevent floatation and thermocouple movement. Several other polyethylene wedge absorbers were also randomly placed in the tank to enhance the absorption, and to reduce the quantity of degassed water needed to fill the tank.

The thermocouple was precalibrated using a cold reference ice bath, and the Grass polygraph was also precalibrated for operation from 20 to 60 °C.

With the thermocouple and transducers thus arranged and calibrated, a series of pulses were issued from each transducer, starting with the Yellow 0.9 MHz system, to align each transducer focus with the thermocouple. The separate positioning systems were found to be an improved arrangement over the previous experiment.

When the two transducers were suitably arranged with foci coincident with the thermocouple, the experiment could now commence. The initial protocol for the experiment was in two parts: the first was a low/medium power test involving 10 pulses for B only, 10 pulses for Y only, and then 10 pulses for simultaneous B and Y transmission. The second part of the experiment was to repeat the first part but now at a higher drive level. While both tests were being conducted, a small Panametrics transducer (f_r = 6 MHz) steered at the confocal region, would simultaneously measure the ambient noise by means of a Hewlett-Packard 8553 B spectrum analyzer. This was intended to identify finite amplitude harmonics, stable cavitation, and unstable cavitation.

The computer was programmed to give a 0.1 second duration pulse; this acted as a simultaneous trigger for the two voltage controlled amplifiers (VCAs). The VCAs were, in turn, connected to their respective color-coded Wavetek waveform generators. The Waveteks then were connected to respective color-coded tuning boxes, and then on to the B and Y transducers. The relatively long pulse duration, combined with the fast rise time of the electronics (capable of operation to at least 35 MHz) and the simultaneous triggering ensures overlap of the acoustic waves from the transducers as they travel through the confocal region and gives adequate opportunity for nonlinear effects to occur.

EXPERIMENT RESULTS

Low/Medium Power:

Blue (1.5 MHz)	trial	# boxes on polygraph paper
500 mV (12.8 W)	1	8.6
	2	8.8
	3	8.4
average = 8.58	4	8.5
σ = .166	5	8.6
	6	8.8
	7	8.8
	8	8.5
	9	8.5
	10	8.3
harmonics:	2nd	-20 dB from primary
	3rd	none observed above -35 dB

Yellow (0.9 MHz)	trial	# boxes on polygraph paper
400 mV (1.3 W)	1	7.6
	2	7.1
	3	7.1
average = 7.31	4	7.2
σ = .247	5	7.7
	6	7.4
	7	7.0
	8	7.0
	9	7.5
	10	7.5
harmonics:	2nd	none observed above -35 dB
	3rd	" " " " "

Blue (1.5 MHz, 500 mV, 12.8 W)
and & Yellow (0.9 MHz, 400 mV, 1.3 W)

	trial	# boxes on polygraph paper
	1	16.8
	2	16.8
	3	16.6
average = 16.93	4	16.8
σ = .369	5	16.8
	6	16.8
	7	17.0
	8	16.8
	9	18.0
	10	16.9

harmonics:	primaries	about 1 dB apart
	2nd	-22 dB from primaries
	3rd	none observed above -35 dB

High Power:

Blue (1.5 MHz)	trial	# boxes on polygraph paper
1000 mV (45.6 W)	1	31.8
	2	31.6
	3	30.6
average = 31.64	4	31.4
σ = .71	5	32.6
	6	31.4
	7	31.4
	8	31.0
	9	33.2
	10	31.4

harmonics:	2nd	-19 dB
	3rd	-30 dB

Yellow (0.9 MHz)	trial	# boxes on polygraph paper
800 mV (4.9 W)	1	29.4
	2	29.5
	3	29.4
average = 29.45	4	29.2
σ = .478	5	29.4
	6	29.1
	7	29.5
	8	30.8
	9	29.0
	10	29.2

harmonics: 2nd -26 dB
3rd none observed above -35 dB

Blue (1.5 MHz, 1000 mV, 45.6 W)
and & Yellow (0.9 MHz, 800 mV, 4.9 W)

	trial	# boxes on polygraph paper
	1 - 10	scale overload
average = 62.7	11	63.2
σ = .5	12	62.2

harmonics: 1.5 MHz about 3 dB below 0.9 MHz
2nd -25 dB re 1.5 MHz
3rd -30 dB re 1.5 MHz
4th -32 dB re 1.5 MHz

Calculations:

N.B. One box on the polygraph paper equals 0.8° C.

		boxes ± deviation	°C
Low/Medium Power:	B only	8.58 ± .17	6.86
	Y only	7.31 ± .25	5.85
	linear sum	15.89 ± .42	12.7
	B + Y	16.93 ± .37	13.5

$$\sigma_{heat} = \frac{16.93}{15.89} = 1.065$$

High Power:	B only	31.64 ± .71	25.3
	Y only	29.45 ± .48	23.6
	linear sum	61.09 ± 1.19	48.8
(2 trials only)	B + Y	62.7 ± .5	50.2

$$\sigma_{heat} = \frac{62.7}{61.09} = 1.026$$

DISCUSSION AND CONCLUSIONS

The discussion of the results, and the experiment conclusions are divided into four parts: first, the penetration of the ultrasound into the encapsulant are discussed; second, the results of the low/medium power tests are discussed; third, the results of the high power tests are discussed; and fourth, the conclusions are given.

I. Ultrasound Penetration into Encapsulant

The experiment set up, using the 0.9 MHz (yellow) transducer at normal incidence and inclining the 1.5 MHz transducer at an angle was done for convenience in aligning the focus of each transducer upon the thermocouple, since it was more difficult and time consuming to realize focal alignment with two transducers directed at angles not parallel to the x-, y-, and z-translation of the positioning mechanism (as in the 1990 experiment). Thus, the 0.9 MHz transducer was quickly aligned, while the 1.5 MHz transducer required more alignment time.

Figure 3 illustrates the geometry for the 1.5 MHz blue transducer. The main radiation axis is shown emanating from the lense into the water (layer 1) at a 54° angle from the normal, and it penetrates the silicone rubber (layer 2) at angle θ_2. Since $c_1 > c_2$, the waves will always propagate from the water and into the rubber. We observe this by assuming that any wavelength in layer 1 projects a trace wavelength at the 1-2 interface, and this trace wavelength must likewise match the projected wavelength in layer 2. This is merely Snell's law [Kinsler and Frey *et alia*, 1982], and thus

$$\text{projected trace wavelength} = \frac{\lambda_1}{\sin\theta_1} = \frac{\lambda_2}{\sin\theta_2} \qquad \lambda_n = \frac{c_n}{f}$$

$$\frac{c_1}{\sin\theta_1} = \frac{c_2}{\sin\theta_2}, \qquad \frac{1480}{\sin 54} = \frac{1025}{\sin\theta_2}, \qquad \theta_2 = 34.07°.$$

The inclination angle of a small streak of cavitation bubbles embedded in the rubber (about 1 cm from the thermocouple, and created during focal alignment but not during the actual measurements) was measured at 33.7° from the normal, experimentally confirming this result.

The propagation of the oblique 1.5 MHz waves may also be viewed using the SAFARI code [Schmidt, 1987], and this is shown as a contour plot of transmission loss in Figure 4. The focused transducer is replaced in the model by a similarly focused line array; at the extreme left side of the figure, note the dashed lines showing the focusing lense, and the dark solid line for the line array. The silicone rubber location is shown by the two parallel dashed lines at .1117 and .1187 meters depth. The air-water interface exists at zero

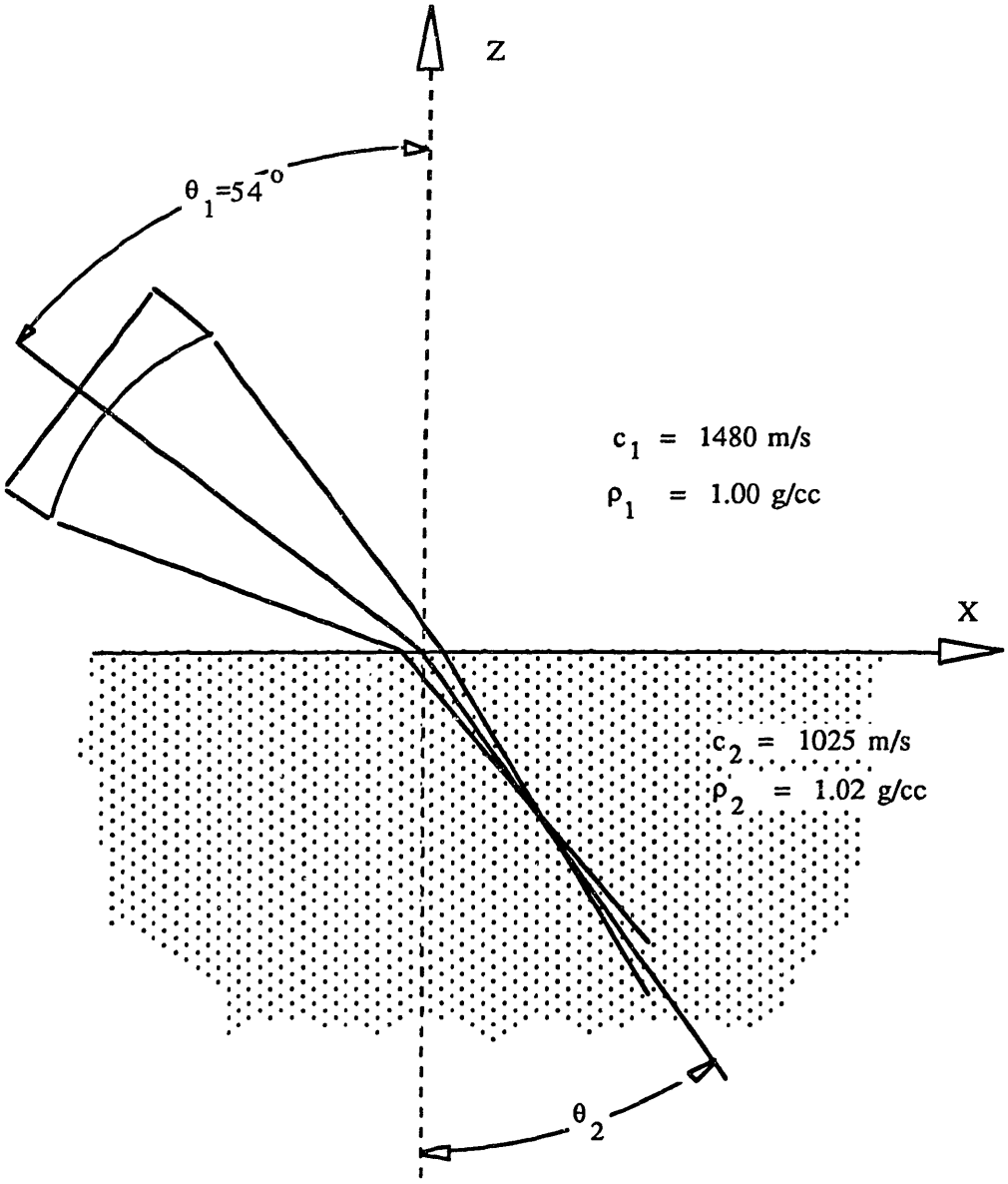

Figure 3 - Refraction of oblique focused waves

depth, and the remaining regions above and below the silicone rubber are water. The thermocouple location is shown by a small black triangle at depth = .1115 meters, and range = .0817 m. Note that the thermocouple is not exactly at the focus center due to the refraction of the silicone rubber. The SAFARI model creates full-wave solutions for two-dimensional wave propagation problems in layered media. In this case, the approximations made are that the circular-symmetry focused transducer is replaced by a similarly sized, 100-element focused line array ($\lambda/2$ spacing), and the model is 2-D (range and depth). The contours represent the sound field intensity in 6 dB increments, and absorption is included for both sound waves in the water, and for longitudinal (sound) and shear waves in the rubber. The input file for the model is included at the top of the figure.

II. Low/Medium Power Tests

The calculations on page 12 show that the linear sum for the B and Y systems resulted in a 12.7 °C temperature increase, whereas when B and Y were operated simultaneously the temperature increase was 13.5 °C. This resulted in a 0.8 °C higher temperature for the same electrical input power, and resulted

```
SAFARI FIP
P N C L
1.5E6
4
0 0 0 0 0 0 0
0 1480 0 0 0 1.0 0 0
0.1117 1025 287 0.1476 .4428 1.02 0 0
0.11873 1480 0 0 0 1.0 0 0
0.05587 100 .493E-3 35.9 3 .1152
0 0.20 50 1
240. 1E8
2048 1 1000
0 .00016 12 .00004
0 .16 12 .02
0 24 6
```

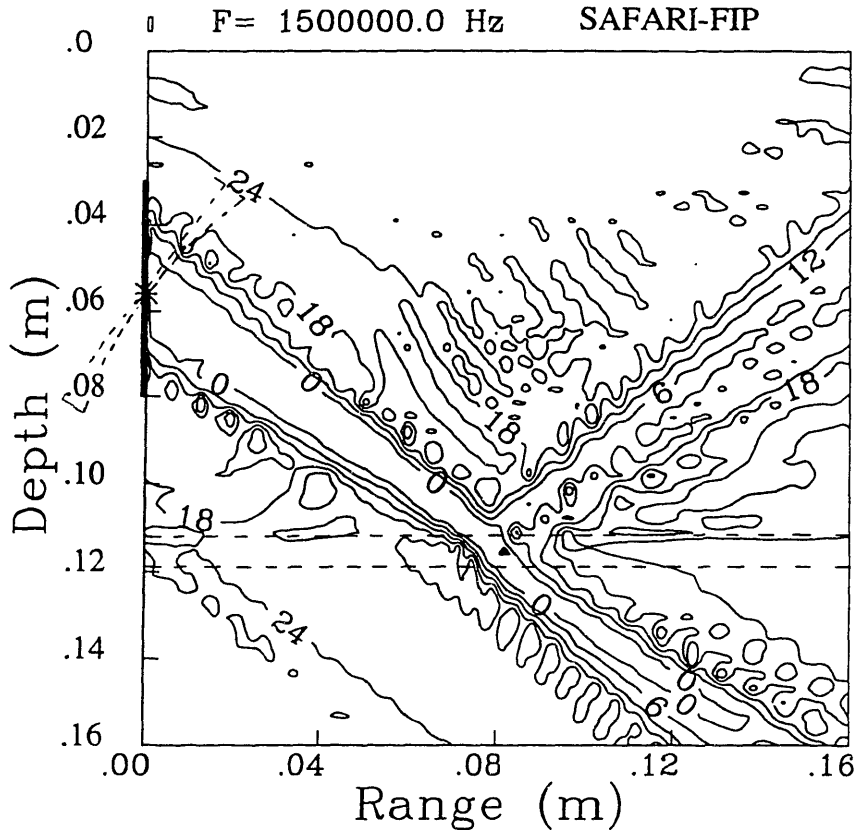

Figure 4 1.5 MHz Xmit Contour

in a σ_{heat} of 1.065, which favorably agrees with the results from the 1990 experiment.

A statistical analysis test of the null hypothesis [see Snedecor, 1950] shows that the evidence of the two sets of data (Blue only, and Yellow only) differentiates the ΔT for the Blue and Yellow systems into two populations with unequal means (see Appendices for calculation summary). Hypothesis tests were also done for B *vs.* B+Y, and for Y *vs.* B+Y with similar results. In layman's terms, this shows that the data are statistically independent and therefore good for our purposes.

The presence of ambient second harmonics during the B, Y, and B+Y tests strongly suggests the presence of nonlinear effects either from the drive levels themselves, or from interaction effects. The second harmonics could also be a consequence of stable cavitation, but this could not be confirmed due to the local oscillator spectral line of the analyzer interfering with the measurement of stable cavitation subharmonics. Third and fourth harmonics were not observed suggesting that the system could be driven harder, and there was no evidence of broadband impulsive noise suggesting that there was no unstable cavitation. Microscope inspection of the encapsulated thermocouple after the entire low/medium and high power tests showed no evidence of cavitation bubbles anywhere along the thermocouple wire.

To assess these remarks on cavitation, we may estimate the acoustical intensity in Watts/cm^2 at both the surface of the lense and at the focus for each of the Blue and Yellow transducers and compare them to established values for cavitation threshold in the literature. This is done by the following:

lense projected area $= \frac{\pi}{4}(6.2)^2 = 30.19$ cm^2

Blue (1.5 MHz): 12.8 W (input power from calibration)
Yellow (0.9 MHz): 1.3 W " " " "

lense surface intensity: Blue: 12.8/30.2 = 0.42 W/cm^2
Yellow: 1.3/30.2 = 0.043 W/cm^2

focal diameter $d_f = 1.22 \frac{\lambda f}{a}$, [Gooberman, 1968]

where λ = wavelength, f = focal length (101 mm),
a = lense radius (31 mm)

Blue (1.5 MHz): d_f = .321 cm
Yellow (0.9 MHz): d_f = .535 cm

focus section area $A_{focus} = \frac{\pi}{4}(d_f)^2$, cm^2

Blue (1.5 MHz): A_f = .0809 cm^2
Yellow (0.9 MHz): A_f = .2248 cm^2

focal intensity: Blue: 12.8/.0809 = 158 W/cm^2
Yellow: 1.3/.2248 = 5.78 W/cm^2

These estimates for focal intensity assume no absorption in either the water or in the silicone rubber.

To account for absorption we multiply the absorption-free intensity by the following {GE 615, per Appendix: μ = 1.44 dB cm^{-1} MHz^{-1}}:

Yellow (0.9 MHz):

$\mu_{0.9}$ = 1.296 dB/cm
$\alpha_{0.9}$ = $\mu_{0.9}$/8.686 = 0.149 Nepers/cm
power $\hat{\alpha}_{0.9} = 2\,\alpha_{0.9}$ = .298 Nepers/cm
coefficient of transmission at normal incidence = 0.95
[see Kinsler *et al.*, 1982]

$I_{Y\text{-focus}}$ = (5.78 W/cm^2) (0.95) $e^{-(.298 \cdot .35\ cm)}$ = 5 W/cm^2

Blue (1.5 MHz):

$\mu_{1.5}$ = 2.16 dB/cm
$\alpha_{1.5}$ = $\mu_{1.5}$/8.686 = 0.249 Nepers/cm
power $\hat{\alpha}_{1.5} = 2\,\alpha_{1.5}$ = .497 Nepers/cm

coefficient of transmission at oblique incidence = 0.48
(54°, or 36° grazing) [see Kinsler *et al.*, 1982]

$$I_{B\text{-focus}} = (158\ W/cm^2)\ (0.48)\ e^{-(.497\ \bullet\ .7\ cm)} = 54.3\ W/cm^2$$

These values suggest two things. First, the ΔT for the yellow and blue systems were both about 6 °C and yet the intensities at the focus were an order of magnitude different. This implies that the blue system (1.5 MHz) did not have it's true focus aligned with the thermocouple; instead a focal sidelobe was present. This is reasonable because the two transducers could not have been moved any closer to each other with the lenses and the 54° separation angle used. Noting the focal displacement due to refraction in Figure 4, it is entirely possible that the blue system was not adequately aligned. Thus, the theoretical peak focal intensity is 54 W/cm^2 for the 1.5 MHz system, however the actual intensity at the thermocouple was reduced by an order of magnitude because the temperature increases were about the same. If we assume that the yellow system was properly aligned with the thermocouple, then we may assume that the intensity for each of the systems was about 5 W/cm^2, and it is these intensities which are responsible for the heat generation.

The second feature is that the peak focal intensities in degassed water are well below the estimates for unstable cavitation, and below the levels considered for stable cavitation [Lele, 1987]. So the extra heat supplied by two transducers firing simultaneously cannot be attributed to either cavitation phenomena.

From the thermocouple data listed in the Appendices, the thermoelectric voltage change for the temperature range from 20 to 26 °C (for a pulse from either the Blue or the Yellow system) is:

26	1.556
20	1.192
6 °C	.364 mV

The thermoelectric voltage change for the temperature range 20 to 32 °C (for the simultaneous pulsing from both Blue and Yellow systems) is:

32	1.924
20	1.192
13 °C	.732 mV

From these two numbers we may estimate the dimensionless nonlinearity parameter $\sigma_{T/C}$ associated with the thermocouple by the same ratio used in finding σ_{heat}; that is:

$$\sigma_{T/C} = \frac{.732}{(.364 + .364)} = 1.0055$$

Likewise from the Appendices, we note that the amplitude linearity for the Grass polygraph oscilloscope is 2% full-scale. Since full-scale for this experiment was 40 °C, then a 12 °C temperature rise represents, at worst, 30% of the full-scale error, or .6%. The dimensionless nonlinearity parameter for the oscilloscope recorder is then 1.006. We note that the parameters for both the thermocouple and for the oscilloscope recorder are below the σ_{heat} parameter; the combined nonlinearity associated with the thermocouple and the recorder is the multiplication of the two, which gives 1.015. This is still too small to account for the σ_{heat} = 1.065 from the experimental data.

One final comment is that the contamination of the heat transfer between the B, Y, and B+Y experiments. The thermocouple wire and the encapsulant together provide the heat conduction path for the thermocouple bead. During the solo trials for B, and for Y, the temperature rise was about 6 °C. With both B and Y transmitting, the temperature rise was about 13 °C. Since the temperature rise was about twice as high during the B+Y trials as it was during the solo B, or solo Y trials, then the heat transfer rate would likewise be twice as fast. What this empirically suggests is that the heat conduction during the B+Y trials was more severe than in the B and Y trials, and so the B+Y trial was contaminated more than the B or the Y. The heat transfer mechanism reduces the maximum temperature that either the B+Y, the B, or the Y could reach, but it influences the B+Y about twice as much as the B, or the Y trials. This means

that *the heat transfer mechanism actually reduces the value of* σ_{heat}. A heat transfer model could estimate the amount of the reduction, but for the purposes of this report, it is sufficient to note that the heat transfer comparison between the solo trials, and the simultaneous trials, is a source of experimental error that reduces σ_{heat}. This is in contrast to the errors associated with the thermocouple and the recorder.

The lack of unstable cavitation at the thermocouple site, the statistical goodness of the low/medium power data, the lack of sufficient nonlinearity in the thermocouple and in the chart recorder, and the general agreement with the results from the 1990 experiment strongly support the existence of nonlinear heat generation from confocal ultrasound transducers.

III. High Power Tests

The high power tests were inconclusive because the polygraph pen plotter exceeded its range, which gave identical maximum temperature values for each B+Y pulse. This was avoided by offsetting the scale on the polygraph thus allowing the pen to freely travel, but the linear range for the pen was still overwhelmed and the measurements were therefore of no use. It is expected that the nonlinear heat generation at the confocal region should be improved, and that σ_{heat} would exceed the value of 1.065 from the low/medium power test; this is suggested on the basis that nonlinearities found in parametric sonar (the creation of sum and difference frequencies) are enhanced at higher drive levels, but below the level where the shock threshold is reached.

IV. Conclusions

This experiment confirmed the results of the 1990 experiment, and appear to prove the notion of nonlinear heat generation from a plurality of confocal, independent transducers. The experiment was improved over the 1990 experiment by having the two transducers on separate positioning

mechanisms, by using a transparent encapsulant having absorption close to that for mammalian tissue, by calibrating the thermocouple, and by using a spectrum analyzer to monitor harmonics and (potential) cavitation. The main defect in the experiment, the difficulty in aligning the angled transducer (in this case, the 1.5 MHz), was largely due to the 101 mm focal length. This prevented the two transducer from being closer than 54° apart; placing them even this close created the alignment problem. This may be overcome by using any one of the lenses available having longer focal lengths. Long focal lengths were originally avoided because it was thought that there would be too much wave attenuation, and thus hampering the possible nonlinear effects due to reduced amplitudes at the confocal region.

The 1990 and 1991 experiments both show considerable promise in the nonlinear heat generation; the next experiment should improve still further on the experimental set up (longer focal length lenses), and should also be conducted at three power settings: low power (to establish a linear threshold), medium power, and high power. The last two settings would prove whether the effect improves at higher amplitudes, as it does in parametric sonar [NUSC, 1983].

ACKNOWLEDGEMENTS

The author gratefully acknowledges the help of Tony Pangan and Charles Welch in setting up and performing the experiment.

APPENDICES

EQUIPMENT DATA

encapsulant: GE RTV 615 silicone rubber compound
$\rho \approx 1.02$ g/cc, $c_p = 1027$ m/s @ 20 °C, [Folds, 1974].
$\rho c_p = 1.048 \times 10^6$ kg $m^{-2}s^{-1}$ (water $\rho c_p = 1.48 \times 10^6$,

ratio =.708).
DC resistance before/after experiment: 108 Ω

signal generator two Wavetek Model 278 (Blue and Yellow systems)

amplifiers Yellow: EIN RF Power Amp., Model 3100 L , ≈ 200W into 50 Ω, 250 kHz to 105 MHz.

Blue: IFI, Inc. Farmingdale NY. Model M2600, ≈ 130 W, 500 kHz to 35 MHz.

spectrum analyzer Hewlett -Packard 8553 B, 1 to 110 MHz

polygraph GRASS polygraph, model 7, Grass Instrument, Quincy MA (for thermocouple monitoring)

oscilloscope amplitude linearity = 2% full scale deflection

VCA (voltage-controlled amplifiers), MIT Hyperthermia Lab.

transducers Yellow: 0.9 MHz, head 1
polystyrene spherical lense 38/101
{*i.e.* #38, *f* = 101 mm}
slight melt distortion noticed on concave lense surface.
acrylic cone 20/51 {*i.e.* 51 mm}

Blue: 1.5 MHz, head 4
polystyrene spherical lense 36/101, no label on cone

B and Y transducer cones sealed with Trojan™ latex condom

Panametrics V 3026, 6 MHz/0.5" diameter (for harmonics and cavitation measurements.)

thermocouple: Omega Engineering, Inc., P.O. Box 4047,
Stamford, CT 06907-0047

butt-welded .003" (.076 mm) diameter chromel-constantan both having Teflon-coated wire; ANSI code E
max range -200 to 900 °C; emf: -8.824 to 68.783 mV
limits of error: ± 1.7 °C or 0.5% error above 0 °C

linearity (from: *The Temperature Handbook*, Omega Engineering 1990; type E, pp. Z-52, -53)

°C	thermoelectric voltage, mV	
0	0.000	
		delta, mV
20.	1.192	-
21	1.252	.060
22	1.313	.061
23	1.373	.060
24	1.434	.061
25	1.495	.061
26	1.556	.061
27	1.617	.061
28	1.678	.061
29	1.739	.061
30	1.801	.062
31	1.862	.061
32	1.924	.062
33	1.985	.061

TRANSDUCER CALIBRATION

Each transducer system is precalibrated so that the relation between input voltage for a continuous wave (cw) drive and radiation pressure (as measured by an electronic scale) is known. Since .069 grams is roughly equivalent to 1 electrical Watt for these quartz transducers, a maximum voltage may be specified so as not to overdrive the transducer.

The blue VCA failed just prior to the test (after we had aligned the foci of the two transducer systems), and so we were forced to substitute the red VCA. The calibration for the blue system (using the red VCA) was then performed after experiment. The calibration differed by about a factor of 2, giving about 45 Watts input power at maximum input voltage on the blue system, but this was done only in single-shots during the experiment (the pulse duration was always 0.1 seconds for all tests, and the duty cycle was less than 1%.)

Yellow 0.9 MHz system:

head 1, 9-foot cable, yellow Wavetek, yellow amp., yellow VCA
tuning box #2: tap 34, cap right .63, L2 left 34.25, L1 top 3.38

millivolts,	grams	
200	.021	
300	.054	
400	.092,	.091 check
600	.198	
800	.336	
1000	.525	
1200	.722,	.735 check
1400	.945	
1600	1.208	
1800	1.527	
2000	1.770	
2200	2.062	(29.88 W)

Blue 1.5 MHz system:

head 4, cable E, blue Wavetek, blue amp., blue VCA
tuning box #1: 15.41 left dial, 1.11 right dial

millivolts,	grams	
200	.084	
300	.172	
400	.291	
500	.436	
600	.614	
700	.817	
800	1.054	
900	1.303	
1000	1.580	
1100	1.931	
1200	2.290	(33.19 W)

Blue 1.5 MHz system *recalibration* after blue VCA failure:
head 4, cable E, blue Wavetek, blue amp., red VCA
tuning box #1: 15.41 left dial, 1.11 right dial

millivolts	grams	
200	.150	
300	.346	
400	.580	
500	.880	
600	1.230	
700	1.637	
800	2.106	
900	2.600	
1000	3.148	(45.6 W)

N.B. .069 g ≈ 1 Watt; radiation pressure measured with Mettler PC 440 electronic scale.

ENCAPSULANT PROPERTIES

General Elcctric RTV-615 two part silicone rubber.

ρ = 1.02 g/cc
optical refractive index 1.406
thermal range -60 to 204 °C
conductivity 0.00045 gm-cal/sec, cm^2, °C/cm;
or 0.11 BTU/hr, ft^2, °F/ft.
specific heat 0.3 cal/gram, °C.
mixing ratio: 10 parts A, 1 part B

measured ultrasonic properties [Folds, 1974]:

ρ = 1.02 g/cc c_p = 1083 m/s @ 0 °C $dc_p/dT = -2.9\ ^\circ C^{-1} ms^{-1}$
c_p = 1025 m/s @ 20 °C

for a 2.5 cm thick sample:
@ 500 kHz, transmission loss TL = 1.4 dB; @ 1 MHz, TL = 3.2 dB

so $\Delta TL/(\Delta F \bullet thk) = \alpha = 1.44$ dB $cm^{-1} MHz^{-1}$

This value compares to the same order of magnitude with those printed in Goss *et alia* 1978, 1980 for mammalian tissue.

STATISTICAL ANALYSIS SUMMARY

	# trials	D.O.F.	mean	sum of squares
Blue only:	10	9	8.58	.0276
Yellow only:	10	9	7.31	.0609

$\Sigma = 18$ $\quad \bar{x} = 1.27$ $\quad Sx^2 = .0885$

pooled variance $S^2 = .0885/18 = .004916$

$$S_{\bar{x}} = \sqrt{\frac{S^2(n_1 + n_2)}{n_1 n_2}} = \sqrt{\frac{.004917\ (10 + 10)}{(10)(10)}} = .0313$$

$$t = \frac{\bar{x}}{S_{\bar{x}}} = \frac{1.27}{.0313} = 40.5$$

d.o.f. = 18, and using Table 3.8, p. 65 in Snedecor (1950)

$P < .01$

	# trials	D.O.F.	mean	sum of squares
Blue only:	10	9	8.58	.0276
B + Y:	10	9	16.93	.1361

$\Sigma = 18$ $\quad \bar{x} = 8.35$ $\quad Sx^2 = .1637$

pooled variance $S^2 = .1637/18 = 9.09e\text{-}3$

$$S_{\bar{x}} = \sqrt{\frac{S^2(n_1 + n_2)}{n_1 n_2}} = \sqrt{\frac{.00909\ (10 + 10)}{(10)(10)}} = .0426$$

$$t = \frac{\bar{x}}{S_{\bar{x}}} = \frac{8.35}{.0426} = 195$$

d.o.f. = 18, and using Table 3.8, p. 65 in Snedecor (1950)

$P < .01$

	# trials	D.O.F.	mean	sum of squares
Yellow only:	10	9	7.31	.0609
B + Y:	10	9	16.93	.1361

$\Sigma = 18 \qquad \bar{x} = 9.62 \qquad Sx^2 = .197$

pooled variance $S^2 = .197/18 = .0109$

$$S_{\bar{x}} = \sqrt{\frac{S^2 (n_1 + n_2)}{n_1 n_2}} = \sqrt{\frac{.0109\ (10 + 10)}{(10)(10)}} = .0468$$

$$t = \frac{\bar{x}}{S_{\bar{x}}} = \frac{9.62}{.0468} = 205$$

d.o.f. = 18, and using Table 3.8, p. 65 in Snedecor (1950)

$P < .01$

BIBLIOGRAPHY

Bacon, D.R., and Carstensen, E.L. (July, 1990). "Increased Heating by Diagnostic Ultrasound due to Nonlinear Propagation" *J. Acoust. Soc. Am.* **88**(1), 27-34.

Baker, A.C., K. Anastasiadis, and V.F. Humphrey (1987). "Nonlinear Propagation in Focused Fields: Experiment and Theory" (**Ultrasonics International 87 Conf. Proc.**, Butterworth & Company Ltd., UK. ISBN 408023 481).

Beyer, R.T. (1975). **Nonlinear Acoustics**, (U.S. Govt. Printing Office for the U.S. Naval Sea Systems Command).

De Witz, G.H. and B.W. Yaeger, (1984). "Ultrasonic Subsurface Cleaning" U.S. Patent 4,444,146; 24 April 1984. Reviewed in *J. Acoust. Soc. Am.* **76**(5), 1600, Nov. 1984.

Fessenden, P., *et alia* (1984). "Experience with a Multitransducer Ultrasound System for Localized Hyperthermia of Deep Tissues" *IEEE Trans. Biomed. Engr.* **BME-31**(1), 126-135.

Folds, D.L. (1974). "Speed of Sound and Transmission Loss in Silicone Rubbers at Ultrasonic Frequencies" *J. Acoust. Soc. Am.* **56**(4), 1295-1296(L).

Gooberman, G.L. (1968). **Ultrasonics, Theory and Application** (Hart Publ. Co., N.Y.).

Goss, S.A., R.L. Johnston, and F. Dunn (1978). "Comprehensive Compilation of Empirical Ultrasonic Properties of Mammalian Tissues" *J. Acoust. Soc. Am.* **64**(2), 423-457.

Goss, S.A., R.L. Johnston, and F. Dunn (1980). "Compilation of Empirical Ultrasonic Properties of Mammalian Tissues. II" *J. Acoust. Soc. Am.* **68**(1), 93-108.

Hynynen, K. (1985). "Nonlinear Absorption During Scanned Focused Ultrasound Hyperthermia" **1985 IEEE Ultrasonics Symposium**, 925-929, IEEE NY.

Kinsler, L.E., A.R. Frey, A.B. Coppens, and J.V. Sanders (1982). **Fundamentals of Acoustics** (3rd edition, John Wiley & Sons, NY; ISBN 0-471-02933-5).

Lele, P.P. (1987). "Effects of Ultrasound on 'Solid' Mammalian Tissues and Tumors *in Vivo*" in **Ultrasound: Medical Applications, Biological Effects and Hazard Potential**, edited by Repacholi, M.H., Grondolfo, M, and Rindi, A.; Plenum Publ., N.Y., 275-306.

Lele, P.P. and K.J. Parker (1982). "Temperature Distributions in Tissues During Local Hyperthermia by Stationary or Steered Beams of Unfocused or Focused Ultrasound" in *Br. J. Cancer* **45**, Suppl. V, 108-121, C.R. Hill, Suppl. editor, H.K. Lewis & Co. Ltd., London.

NUSC, (1983). **Experiments in Nonlinear Acoustics, 1954 to 1983.** U.S. Naval Underwater Systems Center, Newport RI and New London CT.

The Temperature Handbook, Omega Engineering, Inc., P.O. Box 4047, Stamford, CT 06907-0047.

Rolt, K.D. (1988). "Parametric Sound Generation and Applications in Ultrasonic Scanning and Hyperthermia" for MIT course 6.562J, Fall 1988; (15 Dec. 1988).

Rolt, K.D. (1990). "An Experiment in Parametric Ultrasonic Heating" for MIT course 2.77, Spring 1990; (15 May 1990).

Saito, S. and H. Tanaka (1990). "Harmonic Components of Finite-Amplitude Sound in a Focused Gaussian Beam" *J. Acoust. Soc. Jpn.* (E)**11**, 225-233.

Schmidt, H. (1987). *SAFARI: Seismo-Acoustic Fast Field Algorithm for Range Independent Environments. User's Guide.* (SR 113, SACLANT ASW Research Centre, La Spezia, Italy).

Snedecor, G.W. (1950). **Statistical Methods**, (Iowa State College Press, Ames IA).

Appendix B

Exponential Decay of Acoustic Waves: an Alternate Approach

In Chapter 3, the exponential decay of acoustic waves was established by an *ad hoc* approach. This Appendix provides the same result in a more direct manner. The following will show the emergence of the exponential decay from a time domain viewpoint by considering only the loss due to viscosity. The math steps could likewise be duplicated for the contributions by heat conduction and by relaxation, but it is sufficient to show the basic steps here. We start with the intensity dissipation term (3.6)

$$\Delta I = U_o \cdot \Delta x \cdot (\tfrac{4}{3}\eta + \eta_b) \, |(\nabla^2 u)|_{x_o}| \, , \tag{B.1}$$

and we write the intensity loss in a slab of an acoustic wave as

$$I = I_o - \Delta I \, . \tag{B.2}$$

Using various substitutions from Chapter 3, we can write this strictly in terms of the acoustic particle velocity:

$$u^2 = u_o^2 \, [\, 1 - \Delta x \cdot \frac{(\tfrac{4}{3}\eta + \eta_b)}{\rho_o \, c \, |U_o|} \, |\nabla^2 u|_{x_o}|] \, . \tag{B.3}$$

Now let

$$\varepsilon = \frac{(\tfrac{4}{3}\eta + \eta_b)}{\rho_o \, c \, |U_o|} \, |\nabla^2 u_{|x_o}| \, , \tag{B.4}$$

so that (B.3) becomes

$$u^2 = u_o^2 [\, 1 - \varepsilon \cdot \Delta x] \,. \qquad \text{(B.5)}$$

Since acoustic intensity is directly proportional to u^2, we can then write:

$$I = I_o [\, 1 - \varepsilon \cdot \Delta x] \,, \qquad \text{(B.6)}$$

where $\varepsilon \cdot \Delta x$ is always much smaller than 1. We can now write a number of serial equations like (B.6), using one for each small Δx-thick slab the wave propagates through:

$$I_1 = I_o [\, 1 - \varepsilon \cdot \Delta x] \,, \qquad \text{(B.7a)}$$

$$I_2 = I_1 [\, 1 - \varepsilon \cdot \Delta x] \,, \qquad \text{(B.7b)}$$

$$I_3 = I_2 [\, 1 - \varepsilon \cdot \Delta x] \,, \qquad \text{(B.7c)}$$

$$\vdots$$

$$\text{and} \quad I_n = I_{n-1} [\, 1 - \varepsilon \cdot \Delta x] \,. \qquad \text{(B.7n)}$$

An implicit assumption made is that ε is the same in each equation; this is a reasonable assumption because each step Δx is assumed small enough that the spectral content, and hence $\nabla^2 u$ in each slab, is approximately the same. Combining equations (B.7) together so eliminate all I-terms except I_o and I_n we have:

$$I_n = I_o [\, 1 - \varepsilon \cdot \Delta x]^n \,, \qquad \text{(B.8)}$$

Expanding the terms in (B.8) we obtain:

$$I_n = I_o [\, 1 - \varepsilon \cdot n \cdot \Delta x + \varepsilon^2 \cdot \binom{n}{2} (\Delta x)^2 - \varepsilon^3 \cdot \binom{n}{3} (\Delta x)^3 \cdots] \,. \qquad \text{(B.9)}$$

Let's also assume that $n \cdot \Delta x = x$, so $\Delta x = x/n$. This allows us to assume that we have many thin slabs, and we can further assume that x is some finite

distance, so as the number n increases, Δx decreases. Making the substitution that $\Delta x = x/n$:

$$I_n = I_o \left[1 - \varepsilon \cdot x + \varepsilon^2 \cdot \binom{n}{2} (x/n)^2 - \varepsilon^3 \cdot \binom{n}{3} (x/n)^3 \cdots \right] . \qquad (B.10)$$

The last assumption is to let n become large in the limit for a given finite value of x, or $I_n \Rightarrow I(x)$ for large n, hence

$$I(x) = I_o \left[1 - \frac{\varepsilon x}{1!} + \frac{\varepsilon^2 x^2}{2!} - \frac{\varepsilon^3 x^3}{3!} \cdots \right] , \qquad (B.11)$$

or

$$I(x) = I_o \cdot e^{-\varepsilon x} , \qquad (B.12)$$

where recall that $\varepsilon = \dfrac{(\frac{4}{3}\eta + \eta_b)}{\rho_o c \, |U_o|} \, | \nabla^2 u |_{x_o} | \, .$

Eqn. (B.12) may also be rewritten for either the acoustic particle velocity u' or for the acoustic pressure p', rather than for intensity as shown. In both of these cases, the more familiar pressure absorption coefficient variable α is used, where $\varepsilon/2 = \alpha$. The coefficient α applies in both of these cases because the acoustic pressure and particle velocity are accurately related by the approximate impedance relation $p' = \rho c_o u'$.

As a last note in this appendix, and recalling from Chapter 3, it was stated that the absorption coefficient must always be negative by virtue of the local ratio of $\nabla^2 u$ to u_{loc} which is always negative. This would seem to confound the preceding analysis, since there's already a negative sign in the exponent of Eq. (B.12). An added negative sign would make Eq. (B.12) into an exponentially increasing function. The paradox is solved by recalling that this 'problem' was created artificially by assuming that

$$I = I_o - \Delta I$$

in Eq. (B.2) and thereby assuming the form of Eq. (B.3) as:

$$u^2 = u_o^2 \left[1 - \Delta x \cdot \frac{(\frac{4}{3}\eta + \eta_b)}{\rho_o c \, |U_o|} \, | \nabla^2 u |_{x_o} | \right] ;$$

note the negative signs in both of these Eqns. The use of the negative sign was an *a priori* assumption that energy is lost in the wave, in Eq. (B.2), and that the actual sign of $\nabla^2 u$ and u_{loc} was unimportant since the absolute values took care of them in Eq. (B.3). The confusion is removed entirely now by saying that Eq. (B.2) may be left alone, but that Eq. (B.3) must be written with a + sign if the absolute values are entirely removed. Finally, the absolute values are really unecessary in the analysis, as stated in the end of Chapter 3, but they are useful in the beginning of Chapter 3 in the development of time domain absorption, and they are extremely useful in the computational world especially if sign errors plague the programmer. *Res ipsa loquitur.*

Appendix C

E-27 Hydrophone Data

Type E27 Transducer

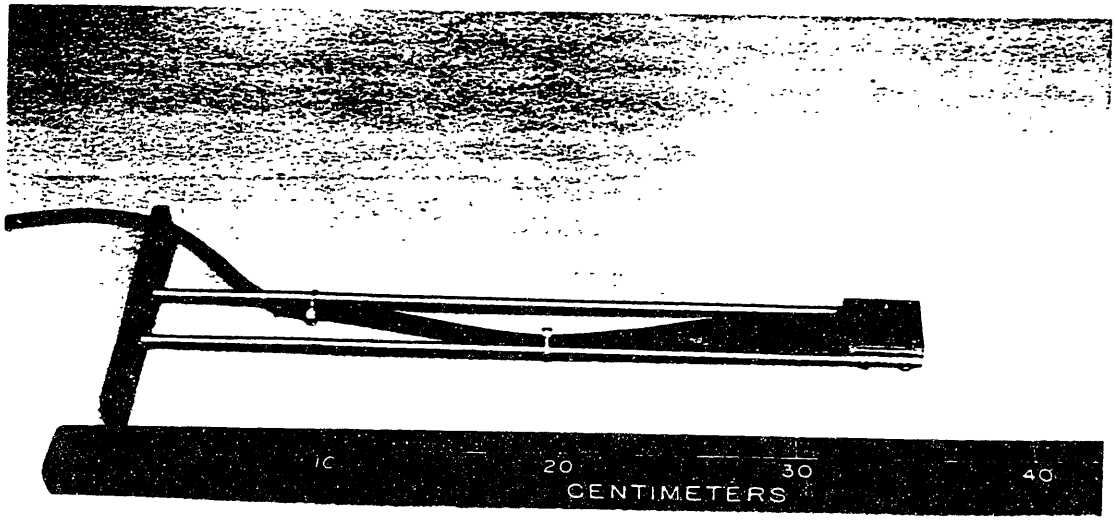

Fig. E27-1 - Type E27 transducer

FUNCTION: A reciprocal transducer and a standard hydrophone for ultrasonic frequencies.

DESIGN: An array of seven PZT disks in a hexagon configuration and cemented directly to a butyl rubber acoustic window.

FREQUENCY RANGE: 80 to 700 kHz
FFVS: See Fig. E27-2
TVR: See Fig. E27-3
MAXIMUM DEPTH: 17 m
TEMPERATURE RANGE: 0 to 35°C
MAXIMUM DRIVING SIGNAL: ~~2 V~~ 200 V
ELECTRICAL IMPEDANCE: See Fig. E27-4
DIRECTIVITY: Same in the horizontal (XY) and vertical (XZ) planes (see Fig. E27-5)
WEIGHT: 1.8 kg (4 lbs)
SHIPPING WEIGHT: 4.5 kg (10 lbs)
NORMAL CABLE LENGTH: 30 m
CABLE CODE: coaxial center — high signal
coaxial shield — low signal

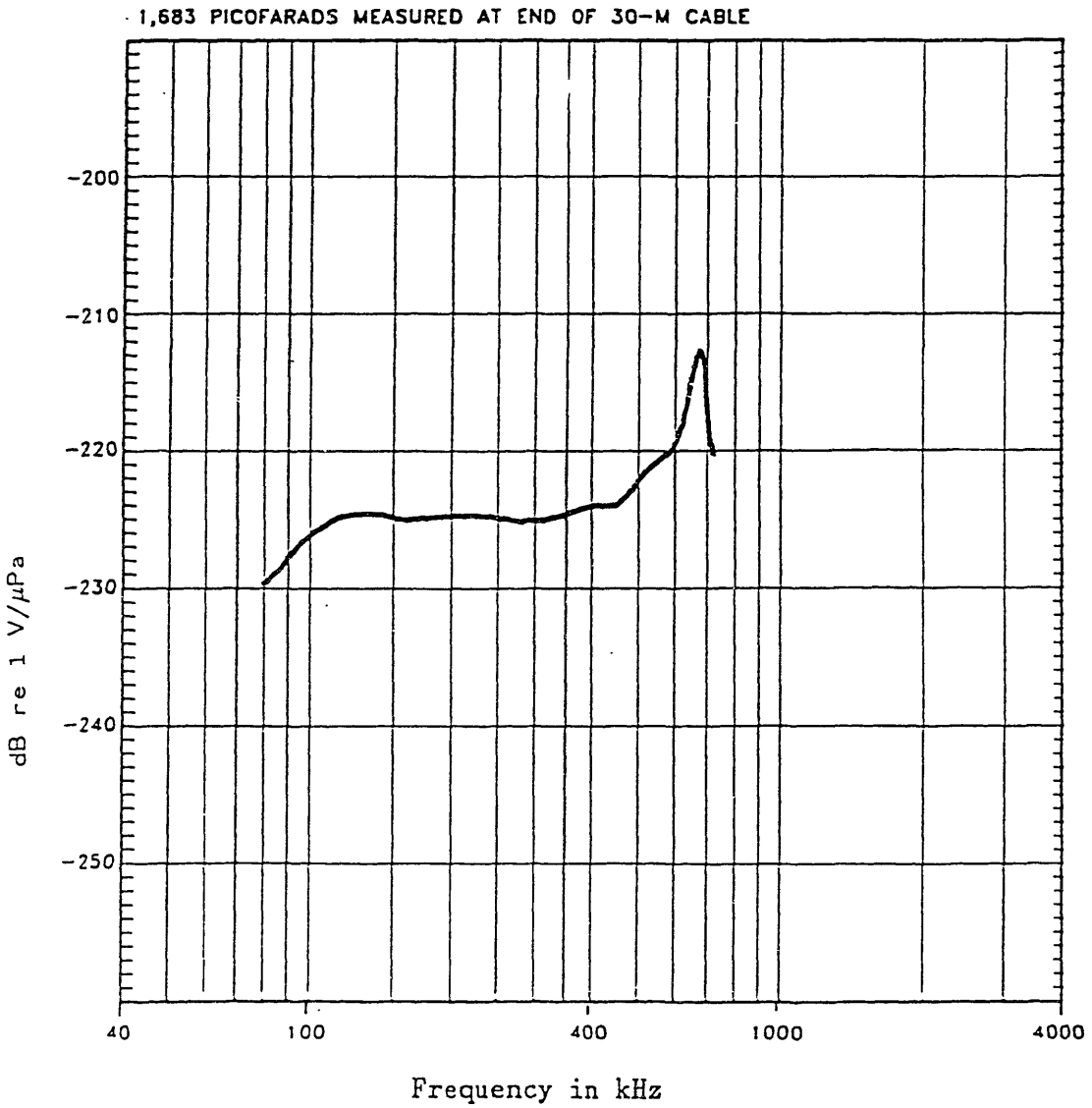

Fig. E27-2 - Typical FFVS for Type E27 transducer with 30-m cable.

Bibliography

Abramowitz, M. and I.A. Stegun, editors (1972). *Handbook of Mathematical Functions*, ninth Dover edition, Dover Publ., NY. See page 914 for coefficients for differentiation on sampled data.

Averkiou, M.A., Y.-S. Lee and M.F. Hamilton (1993). "Self-demodulation of amplitude and frequency modulated pulses in a viscous fluid" *J. Acoust. Soc. Am.* 94(5), 2876-2883.

Bacon, D.R. and E.L. Carstensen (1990). "Increased heating by siagnostic ultrasound due to nonlinear propagation" *J. Acoust. Soc. Am.* 88(1), 26-34.

Baker, A.C., K. Anastasiadis, and V.F. Humphrey (1987). "Nonlinear propagation in focused fields: Experiments and theory" in *Ultrasonics International 1987 Conference Proceedings*, Butterworth & Co., UK.

Bakhvalov, N.S., Y.M. Zhileikin, E.A. Zablotskaya and R.V. Khokhlov (1978). "Focused high-amplitude sound beams" *Sov. Phys. Acoust.* 24(1), 10-15.

Berktay, H.O. (1965). "Possible exploitation of nonlinear acoustics in underwater transmitting applications" *J. Sound and Vib.* 2, 435-461.

Bethe, H. and E. Teller (1941). *Deviations from Thermal Equilibrium in Shock Waves*, Cornell University, Ithaca NY.

Beyer, R.T. (1960). "Parameter of nonlinearity in fluids" *J. Acoust. Soc. Am.* 32(6), 719-721.

Beyer, R.T. and S.V. Letcher (1969). *Physical Ultrasonics*, Vol. 32 in the series on PURE AND APPLIED PHYSICS, Academic Press, NY.

Beyer, R.T. (1972). "Nonlinear Acoustics (Experimental)" in the *AIP Handbook*, McGraw-Hill, NY. pp. 3-206 to 3-210.

Beyer, R.T. (1975). *Nonlinear Acoustics*. First edition: Naval Sea Systems Command by the U.S. Government printing office; reprinting planned by the American Institute of Physics *c.* 1993.

Blackstock, D.T. (1962). "Propagation of plane sound waves of finite amplitude in nondissipative fluids" *J. Acoust. Soc. Am.* **34**(1), 9-30.

Blackstock, D.T. (1964). "Thermoviscous attenuation of plane, periodic, finite-amplitude sound waves" *J. Acoust. Soc. Am.* **36**(3), 534-542.

Blackstock, D.T. (1966). "Connection between the Fay and Fubini solutions for plane sound waves of finite amplitude" *J. Acoust. Soc. Am.* **39**, 1019-1026.

Blackstock, D.T. (1969). "History of nonlinear acoustics and a survey of Burgers' and related equations" in *Nonlinear Acoustics*, Conference Proceedings, DTIC No: AD 719 936. See ISNA, in this bibliography, for full citation.

Blackstock, D.T. (1979). *High Intensity Sound Research, 1961-1978*, (AFOSR Final Report 1 Nov. 75 - 31 Oct. 1978), Applied Research Lab., University of Texas (ARL:UT), ARL-TR-79-36. Also DTIC No.: AD-A 072 550; 21 June 1979.

Blackstock, D.T. (1986). *Research in Nonlinear Acoustics, ONR Final Report (1975-1984)*, Applied Research Lab., University of Texas (ARL:UT), ARL-TR-86-19. Also DTIC No.: AD-A 172 634; 2 July 1986.

Blackstock, D.T. (1988). "Calculation of the intensity and absorption of a finite-amplitude sound wave" *J. Acoust. Soc. Am.* **83**(S1), S5.

Blackstock, D.T. and Hamilton, M.F. (1993). Lecture notes, *Short Course in Nonlinear Acoustics*, Spring Meeting of the Acoustical Society of America, Ottawa Canada, 16-17 May 1993.

Bradley, J.N. (1962). *Shock Waves in Chemistry and Physics*, John Wiley & Sons.

Burgers, J.M. (1939). "Mathematical examples illustrating relations occurring in the theory of turbulent fluid motion" *Verhandel. Kon. Nederl. Akad. Wentenchappen Amsterdam, Afdeel Natuurkunde* **17**(2) (1st section), 1-53.

Carstensen, E.L., N.D. McKay, D. Delecki and T.G. Muir (1982). "Absorption of finite amplitude ultrasound in tissues" *Acustica* **51**(2), 116-123.

Christopher, P.T. and K.J. Parker (1988). "Shock wave production in medical ultrasound" *J. Acoust. Soc. Am.* **84**(1), S164(A).

Cole, R.H. (1948). *Underwater Explosions.* Princeton University Press. Republished by Dover Publications, NY (1965).

Cook, B.D. (1962). "New procedure for computing finite-amplitude distortion" *J. Acoust. Soc. Am.* **34**(7), 941-946.

Cotaras, F.D. and C.L. Morfey (1993). "Polynomial expressions for the coefficient of nonlinearity β and $\beta/(\rho c^5)^{1/2}$ for fresh water and seawater" *J. Acoust. Soc. Am.* **94**(1), 585-588.

Crighton, D.G. (1986). "The Taylor internal structure of weak shock waves" *J. Fluid Mech.* **173**, 625-642. This volume, No. 173 from Dec. 1986, contains papers presented at the IUTAM Symposium on *Fluid Mechanics in the Spirit of G.I. Taylor* held on the centenary of his birth.

Davis, B.J. (1990). *A Method of Rapid Hyperthermia for Treatment of Localized Malignancies by Scanned, Focused Ultrasound.* Ph.D. thesis, Dept. of Mech. Eng., MIT, Cambridge, MA, Sept. 1990.

Dean III, L. Wallace (1962). "Interactions between sound waves" *J. Acoust. Soc. Am.* **34**(8), 1039-1044.

Dunn, F. and W.D. O'Brien Jr. editors (1976). *Ultrasonic Biophysics.* Dowden, Hutchinson& Ross, Inc. publishers, Benchmark Papers in Acoustics, Vol. 7. ISBN 0-87933-206-9.

Earnshaw, Rev. S. (1858). "On the mathematical theory of sound" *Phil. Trans. Roy. Soc.* **150**, 133-148.

Euler, L. (1755). *Mem. acad. sci. Berlin* **11**, 274-315. See Blackstock (1969), p. 25 for several other citations of Euler's work.

Fay, R.D. (1931). "Plane sound waves of finite amplitude" *J. Acoust. Soc. Am.* **3**(2), 222-241.

Fay, R.D. (1956). *J. Acoust. Soc. Am.* **28**, 910.

Fay, R.D. (1962). "Corrected analysis of plane finite waves" *J. Acoust. Soc. Am.* **34**(9), 1269-1271.

Frey, H.G., *et alia* (1980). "A low frequency, broadband acoustic source for ocean research" in *EASCON '80 Record*, 275-280, IEEE, NY.

Fry, W.J. (1952). "Mechanism of acoustic absorption in tissue" *J. Acoust. Soc. Am.* **24**(4), 412-415.

Fox, F.E. and W.A. Wallace (1954). "Absorption of finite amplitude sound waves" *J. Acoust. Soc. Am.* **26**(6), 994-1006.

Fubini-Ghiron, E. (1935). "Anomalies in the propagation of acoustic waves of great amplitude" *Alta Frequenza* **4**, 530-581.

Gol'dberg, Z.A. (1957). *Soviet Phys. Acoust.* **3**, 340.

Goss, S.A., R.L. Johnston and F. Dunn (1978). "Comprehensive compilation of empirical ultrasonic properties of mammalian tissues" *J. Acoust. Soc. Am.* **64**(2), 423-457.

Goss, S.A., R.L. Johnston and F. Dunn (1980). "Compilation of empirical ultrasonic properties of mammalian tissues. II" *J. Acoust. Soc. Am.* **68**(1), 93-108.

Gradshteyn, I.S. and I.M. Ryzhik (1965). *Table of Integrals, Series, and Products*, Academic Press, NY.

Halsema, J.A. (1992). *A High Resolution Wide-Band Sonar Using Coded Noise-Like Waveforms and a Parametric Transmit Array.* Ocean Engineer thesis, Dept. of Ocean Engr., MIT, Cambridge, MA. Also C.S. Draper Lab. CSDL-T-1107, Feb. 1992.

Handler, R.A. (1976). *Nonlinear Absorption of Ultrasound in Biological Media.* M.S. thesis, Dept. of Mech. Eng., MIT, Cambridge, MA, Sept. 1976.

Hanish, S. (1988). *A Treatise on Acoustic Radiation: Volume V - Large Amplitude Radiation*, Naval Research Laboratory (U.S. Navy).

Harkrider, D. and F. Press (1967). "The Krakatoa air-sea waves: an example of pulse propagation in coupled systems" *Geophysical J. Royal Astronomical Soc.* **13**, 149-159.

Hartmann, B., G.F. Lee and J.D. Lee (1994). "Loss factor height and width limits for polymer relaxations" J. *Acoust. Soc. Am.* **95**(1), 226-233.

Hynynen, K. (1985). "Nonlinear absorption during scanned focused ultrasound hyperthermia" in *1985 Ultrasonics Symposium*, IEEE Press, NY, 925-929.

Ingard, K.U and D.C. Pridmore-Brown (1955). "Scattering of sound by sound" *J. Acoust. Soc. Am.* **27**(5), 1002(A).

Ingard, K.U and D.C. Pridmore-Brown (1956). "Scattering of sound by sound" *J. Acoust. Soc. Am.* **28**, 367-369.

Institute of Acoustics, Underwater Acoustics Group (1979). *Proceedings of the Institute of Acoustics: Underwater Applications of Non-Linear Acoustics*, Univ. of Bath, England, 10-11 Sept. 1979.

ISNA (International Symposium on Nonlinear Acoustics):

Nonlinear Acoustics, Conference Proceedings, T.G. Muir and D.S. Davis eds., held at Applied Research Laboratory, University of Texas at Austin, 10-11 Nov. 1969. *N.B.* - this is the second ISNA mtg. DTIC No: AD 719 936.

Frontiers of Nonlinear Acoustics, 12th ISNA. M.F. Hamilton and D.T. Blackstock, eds., Elsevier Applied Science, NY. (1990). ISBN 1-85166-537-4.

Ivey, L.E. (1991). *Underwater Electroacoustic Transducers.* the USRD Transducer Catalog, Naval Research Laboratory, Underwater Sound References Detachment. April 1991.

Jensen, F., W.A. Kuperman, M. Porter and H. Schmidt (1994). *Computational Acoustics.* American Institute of Physics for the Acoustical Society of America. ISBN 1-56396-209-8.

Keck, W. and R.T. Beyer (1960). "Frequency spectrum of finite amplitude ultrasonic waves in liquids" *Phys. of Fluids* 3(3), 346-352.

Kinsler, L.E., A.R. Frey, *et alia* (1982). *Fundamentals of Acoustics.* John Wiley & Sons, NY. ISBN 0-471-02933-5.

Kuznetsov, V.P. (1971). "Equations of nonlinear acoustics" *Sov. Phys. Acoust.* **16**, 467-470.

Laplace, P.S. (1816). See notes pp. 11-12 in Pierce (1989).

Lele, P.P. (1986). "Scanned, focused, ultrasound for controlled, localized heating of deep tumors" in *Hyperthermia in Cancer Treatment*, Anghileri, L. and J. Robert eds., CRC Press Inc, Boca Raton FL.

Li, Ping-Wa and D.T. Blackstock (1993). "Absorption of finite-amplitude ultrasound in biomedical tissue" *J. Acoust. Soc. Am.* **94**(3, Part 2), 1793, 126th meeting, Denver, Colorado, 4-8 October.

Lighthill, M.J. (1956). "Viscosity effects in sound waves of finite amplitude" in *Surveys in Mechanics*, Batchelor, G.K. and R.M. Davies, eds., Cambridge University Press, 250-351.

Lind, S.J. and M.F. Hamilton (1991). "Noncollinear interaction of a tone with noise" *J. Acoust. Soc. Am.* **89**(2), 583-591.

Lindsay, R.B. (1960). *Mechanical Radiation.* McGraw-Hill, NY.

Litzenberger, L.N. (1969). *Linear and Nonlinear Ion Acoustic Waves in Highly Ionized Plasmas in a Magnetic Field*, S.M. thesis, Dept. of Physics, MIT.

Litzenberger, L.N. (1971). *Nonlinear Coupling of Ion Acoustic Waves in Plasmas*, Ph.D. thesis, Dept. of Physics, MIT.

Lucas, B.G. and T.G. Muir (1982). "The field of a focusing source" *J. Acoust. Soc. Am.* **72**(4), 1289-1296.

McDonald, B.E. and W.A. Kuperman (1987). "Time domain formulation for pulse propagation including nonlinear behavior at a caustic" *J. Acoust. Soc. Am.* **81**(5), 1406-1417.

McLachlan, N.W. (1960). *Loud Speakers.* Dover Publ., NY.

Mellen, R.H., V.P. Simmons, and D.G. Browning (1979). "Sound absorption in sea water: A third chemical relaxation" *J. Acoust. Soc. Am.* **65**(4), 923-925.

Mendousse, J.S. (1953). "Nonlinear dissipative distortion of progressive sound waves at moderate amplitudes" *J. Acoust. Soc. Am.* **25**(1), 51-54.

Mitome, H. (1989). "An exact solution for finite-amplitude plane sound waves in a dissipative fluid" *J. Acoust. Soc. Am.* **86**(6), 2334-2338.

Mitome, H. (1991). "Absorption of one-cycle finite-amplitude soundin a dissipative fluid" in *Ultrasonics International 1991 Conf. Proc.*, Butterworths, 295-298.

Mix, L.P. (1971). *The Linear and Nonlinear Propagation of Ion Acoustic Waves in a Highly Ionized Plasma*, Ph.D. thesis, Dept. of Physics, MIT.

Moffett, M.B., P.J. Westervelt and R.T. Beyer (1970). "Large-amplitude pulse propagation -- a transient effect" *J. Acoust. Soc. Am.* 47(5), 1473-1474.

Moffett, M.B. and P.J. Mello (1979). "Parametric acoustic sources of transient signals" *J. Acoust. Soc. Am.* 66(4), 1182-1187.

Morse, P.M. and K.U. Ingard (1968). *Theoretical Acoustics*, McGraw-Hill Book Company, NY. ISBN: 07-043330-5.

Muir, T.G. and J.E. Blue (1969). "Experiments on the modulation of large-amplitude waves" *J. Acoust. Soc. Am.* 46(1, Part 2), 227-232.

Newton, I. (1686). See translation from the Latin in: *Newton's Principia: Motte's Translation Revised*, University of California Press, Berkeley, 1934; reprinted 1947. orig. translation by Andrew Motte (1729). See Pierce (1989), pp. 4-5, for notes on the editions and translations.

Nonlinear Acoustics 1954 to 1983. U.S. Naval Underwater Systems Center, Newport, RI and New London, CT.

Nonlinear Acoustics in Fluids, R.T. Beyer ed., Van Nostrand Reinhold Co., NY. ISBN: 0-442-21182-1.

Novikov, B.K., O.V. Rudenko and V.I. Timoshenko (1987). *Nonlinear Underwater Acoustics*. American Institute of Physics for the Acoustical Society of America, NY. ISBN 0-88318-522-9.

Parker, K.J. (1983). "The thermal pulse decay technique for measuring ultrasonic absorption coefficients" *J. Acoust. Soc. Am.* 74(5), 1356-1361.

Pekeris, C.L. (1939). "The propagation of a pulse in the atmosphere" *Proc. Royal Soc. London*, series A, 171:434-449.

Pestorius, F.M. (1973). "Propagation of plane acoustic noise of finite amplitude" Ph.D. thesis, University of Texas at Austin; also issued as a technical memorandum: ARL-TR-73-23, Applied Research Laboratories, the University of Texas at Austin (Aug. 1973); also AFOSR-TR-74-0711; DTIC No. AD-778 868.

Pierce, A.D. (1989). *Acoustics: An Introduction to Its Physical Principles and Applications*. 1989 edition published by the American Institute of Physics for the Acoustical Society of America, NY. ISBN 0-88318-522-9. Orig. edition 1981 by McGraw-Hill, Inc.

Poché Jr., L.B. (1971). "Underwater shock-wave pressures from small detonators" *J. Acoust. Soc. Am.* **51**(5), 1733-1737.

Press, W.H., *et al.* (1986). *Numerical Recipies*, Cambridge University Press.

Rolt, K.D. (1988). "Parametric sound generation and applications in Ultrasonic scanning and hyperthermia" a final report for M.I.T. course 6.562, 15 Dec. 1988.

Rolt, K.D. (1990). "An experiment in parametric ultrasonic heating" a final report for M.I.T. research course 2.77, 15 May 1990.

Rolt, K.D. (1990). *Ocean, Platform, and Signal Processing Effects on Synthetic Aperture Sonar Performance, S.M.* thesis, Massachusetts Institute of Technology, 28 Nov. 1990. Abstract in *J. Acoust. Soc. Am.* **89**(6), 3018(T), June 1991.

Rolt, K.D. (1991). "An experiment in parametric ultrasonic heating, part II" a final report for M.I.T. research course 2.77, 6 March 1991.

Rolt, K.D. and P.P. Lele (1992). "Apparatus and method for acoustic heat generation and hyperthermia" U.S. Patent Application, MIT docket No. MIT-5544, March 1992.

Rolt, K.D. and H. Schmidt (1992). "Parametric ultrasound heating: theory and modeling" *J. Acoust. Soc. Am.* **91**(4, Pt. 2), 2353(A), April 1992.

Rolt, K.D. (1992). "Parametric ultrasound heating: experiments" *J. Acoust. Soc. Am.* **91**(4, Pt. 2), 2353(A), April 1992.

Rolt, K.D. (1994). "Time domain acoustic absorption: a unified model for linear and nonlinear acoustics" *J. Acoust. Soc. Am.* **95**(6, Pt. 2), June 1994.

Roy, R.A. and J. Wu (1993). "An experimental investigation of the nonlinear interaction of noncollinear sound beams" *J. Acoust. Soc. Am.* **93**(4), part 2, 2383(A), April 1993.

Rudenko, O.V. and S.I. Soluyan (1977). *Theoretical Foundations of Nonlinear Underwater Acoustics.* Translated by R.T. Beyer, Consultants Bureau, NY. ISBN 0-306-10933-6.

Rudnick, I. (1958). "On the attenuation of finite amplitude waves in a liquid" *J. Acoust. Soc. Am.* **30**(6), 564-567.

Senapati, N. (1973). *A Study of Ultrasonic Cavitation in Biological Tissues and its Possible Damaging Effects. Sc.D.* thesis, MIT, Cambridge, MA, Dec. 1973.

Simkin, T. and R.S. Fiske (1983). *Krakatau, 1883.* Smithsonian Institute Press, Washington, D.C. ISBN 0-87474-841-0.

Stanton, T.K. and R.T. Beyer (1978). "The interaction of sound with noise in water" *J. Acoust. Soc. Am.* **64**(6), 1667-1670.

Stanton, T.K. and R.T. Beyer (1981). "Interaction of sound with noise in water II" *J. Acoust. Soc. Am.* **69**(4), 989-992.

Stepanishen, P.R. and P. Koenigs (1987). "A time domain formulation of the absorption limited transient parametric array" *J. Acoust. Soc. Am.* **82**(2), 629-634.

Stephens, R.W.B. and A.E. Bate (1966). *Acoustics and Vibrational Physics*, 2nd ed., St. Martins Press. See 485-486 for development of distance to (dissipationless) shock.

Stokes, G.G. (1845). "Sound attenuation due to viscosity" *Trans. Camb. Phil. Soc.* **8**, 75-102.

Stokes, G.G. (1851). "An examination of the possible effect of radiation of heat on the propagation of sound" *Phil. Mag.* **1**(4), 305-317.

Sutin, A.M. (1978). "Influence of nonlinear effects on the propagation of acoustic focusing systems" *Sov. Phys. Acoust.* **24**(4), 334-339.

Temkin, S. (1981). *Elements of Acoustics*, John Wiley & Sons, NY. ISBN 0-471-05990-0. See pp. 396-400 for the energy-dissipation method.

Tjøtta, J. Naza and S. Tjøtta (1981). "Nonlinear equations of acoustics with applications to parametric arrays" *J. Acoust. Soc. Am.* **69**, 1644-1652.

Too, G.P.J. and J.H. Ginsberg (1992). "Nonlinear progressive wave equation model for transient and steady-state sound beams" *J. Acoust. Soc. Am.* **91**(1), 59-68.

Trivett, D.H. and A.L. Van Buren (1981). "A FORTRAN computer program for calculating the propagation of plane, cylindrical, or spherical finite amplitude waves" USRD/NRL Memo. Report 4413, 19 Feb. 1981. See also Trivett, D.H. and A.L. Van Buren (1984). "Comments on 'Distortion of finite amplitude ultrasound in lossy media' by M.E. Haran and B.D. Cook [J.Acoust.Soc.Am. 73,774-779 (1983)]" *J. Acoust. Soc. Am.* **76**(4), 1257-1258.

Van Buren, A.L. and M.A. Breazeale (1968a). "Reflection of finite-amplitude ultrasonic waves. I. Phase Shift" *J. Acoust. Soc. Am.* **44**(4), 1014-1020.

Van Buren, A.L. and M.A. Breazeale (1968b). "Reflection of finite-amplitude ultrasonic waves. II. Propagation" *J. Acoust. Soc. Am.* **44**(4), 1021-1027.

Van Buren, A.L. (1975). "Mathematical model for non-linear standing waves in a tube" *J. Sound Vib.* **42**(3), 273-280.

Van Wylen, G.J. and R.E. Sonntag (1978). *Fundamentals of Classical Thermodynamics*, 2nd edition, John Wiley & Sons, NY. ISBN 0-471-04188-2.

Webster, D.A. and D.T. Blackstock (1977). "Finite-amplitude saturation of plane sound waves in air" *J. Acoust. Soc. Am.* **62**, 518-523.

Westervelt, P.J. (1957a). "Scattering of sound by sound" *J. Acoust. Soc. Am.* **29**, 199-203.

Westervelt, P.J. (1957b). "Scattering of sound by sound" *J. Acoust. Soc. Am.* **29**, 934-935.

Westervelt, P.J. (1963). "Parametric acoustic array" *J. Acoust. Soc. Am.* **35**(4), 535-537.

Westervelt, P.J. (1973). "Absorption of sound by sound" *J. Acoust. Soc. Am.* **53**(1), 384(A).

Westervelt, P.J. (1976). "Absorption of sound by sound" *J. Acoust. Soc. Am.* **59**(7), 760-764.

Westervelt, P.J. (1993). Personal communication.

White, F.M. (1984). *Heat Transfer*, Addison-Wesley Publ., Reading MA.

Wu, J. and G. Du (1990). *J. Acoust. Soc. Am.* 88(3), 1562-1577.

Yokoyama, I. (1981). "A Geophysical interpretation of the 1883 Krakatau eruption" *J. Volcanology and Geotherm. Res.* **9**, 359-378.

Zabolotskaya, E.A. and R.V. Khokhlov (1969). "Quasiplane waves in the nonlinear acoustics of confined beams" *Sov. Phys. Acoust.* **15**, 35-40.

Zavadil, S.W. (1976). *An Investigation of the Propagation of Non-Linear Acoustic Waves in a Viscous Fluid.* O.E. and M.S. thesis, Dept. of Ocean Engineering, MIT, Cambridge, MA, Jan. 1976.